POLITECNICO DI TORINO

SCUOLA DI DOTTORATO

Dottorato in Meccatronica – XXVII Ciclo

Tesi di Dottorato

Robust Techniques for the Optimal Operation of Photovoltaic Systems

Tutoro

Prof. Marcello Chiaberge

Coordinatore del corso di dottorato

Prof. Giancarlo Genta

Candidato

Ali Faisal Murtaza

Aprile, 2015

ANNO ACCADEMICO 2012 – 2014

This page intentionally left blank.

Acknowledgments

I would like to convey special thanks to my supervisor Prof. Dr. Marcello Chiaberge, who is always a source of guidance for me during the course of my Ph.D work. Because of his vision and efforts, I am grown from student to a competent researcher.

I would pay my compliments to Prof. Dr. Giancarlo Genta, who co-ordinated my Ph.D research for three years. He is always helpful, kind and takes necessary administrative measures whenever needed.

I would also appreciate my Research Group Fellows, especially Diego Boero and Dr. Mirko De- Giuseppe to make me feel Italy, a home away from home. I always thoroughly enjoyed their company not only during parties, farewells etc, but also their approach towards research. They never let me down and always helped me with their special skills whenever I face difficulties during my Ph.D research.

Finally, I must thank to my family members, especially my Mother, Father and Wife. These people are always source of motivation for me.

Abstract

Photovoltaic (PV) energy has witnessed tremendous growth in the recent past to meet the growing energy demands. PV system exhibits the (current-voltage) I-V curve, which varies non-linearly according to immediate weather conditions. Considering the high initial capital cost of PV system and its low conversion efficiency, it is imperative to operate the PV array under optimal condition on consistent basis. For this purpose, maximum power point tracking (MPPT) technique plays a pivotal role in the PV system. The main role of the MPPT is to track the unique maximum power point (MPP) on the I-V curve, when PV array is under uniform condition. On the other hand, during partial shading, the matter is further complicated as the I-V curve of PV array is transformed in to the shape containing multiple local maxima, one of them is global maximum. In that scenario, a specialized MPPT is required to search the global maximum.

The main aim of this thesis is to design the robust MPPT techniques for PV systems in order to harvest the maximum energy from PV plants. In this work, two novel techniques are designed: one is specialized for uniform conditions and other one for non-uniform conditions, i.e. partial shading. The design procedures, working principles and formulations of the MPPTs are discussed in detail with the help of various simulation models, figures, graphs and tables etc. Numerous simulation studies and experimental tests have been conducted to confirm the efficient operation of proposed MPPTs. Also, based on these tests, comparative analysis has been carried out, which reveals that the proposed MPPTs exhibit superior performance compared to past-proposed MPPTs.

In addition, a new modulation control scheme to vary duty cycle of the DC-DC converter is presented, which will assist the MPPTs in their operations. A load criteria for resistive and battery loads is also defined for the stable operation of PV systems.

Contents

List of Figures

List of Tables

Chapter 1

Introduction

This chapter starts with the discussion that why we need renewables, their possible impact in future and the importance of photovoltaic in the arena of renewables. After that, the chapter proceeds with the concerns of research community regarding the efficiency of PV system, which stresses the researchers of this field to design the robust MPPT techniques for the optimal operation of PV systems, and is also the focus of the thesis.

1.1   Why renewables?

With the World of new era surrounded by uninterrupted evolution of technologies having no boundary limits, the Energy demand around the Globe is rapidly pacing at the rate of knots. Energy demand is expected to be escalated by 56% from 2010 to 2050 [1-2], which may pile up the carbon dioxide emissions from 31.2 to 45.5 billion metric tons in 2040 [1-3]. Along with the increasing burden of toxic climate, the sustainability is another factor to maintain as the reserves of raw material, i.e. fossil fuels of conventional sources are reducing with every passing year [4]. These forewarning circumstances prompt the world community especially the scientists, researchers and industrialists etc. to hunt the energy sources not only beneath the Earth, but also above its surface which are abundant in nature i.e. Renewables.

Renewable energy sources such as hydro, biomass, wind, solar and marine, etc. provide several benefits: clean technology, reliable sources with long-term sustainability, locally available especially in developing countries and increased security with increasing cost-effectiveness [5]. Renewable sources are steadily gaining position in the global energy mix [6], primarily in power sector. According to [3], the

percentage contribution of renewable sources in electricity supply is 21%, which is expected to rise up to 31% by 2035 [6-7].

1.2   Photovoltaics – An integral renewable energy source

Amongst the renewable sources, Photovoltaic (PV) is regarded as the primary source, which comes under the umbrella of solar energy. Compared to other sources, PV systems are easy to install, have almost negligible maintenance costs

Figure 1.1 – Special PV applications: (a)-(b) PV solar car parking system, (c) Solar car, (d)-(e) PV array on the space station, (f) PV pay-station and (e) Building integrated PV (BIPV) systems [8]

and requires less balance of systems, such as: 1) PV system is almost mechanically free unlike wind turbines, 2) Compared to biofuels and wind turbines, PV panels are silent and create almost zero pollution, thus more suitable for house roof tops and urban area applications and 3) Since dams and wind turbines are installed with the proper evaluation of the surrounding area, PV panels just need to be setup where there is sunlight. Apart from these advantages, there are numerous applications where only PV system can be worked out as the renewable energy source as shown in Fig. 1.1 [8]: solar car, solar parking pay station, aerospace applications, shelters for car parking and building integrated PV (BIPV) systems.

PV plants normally setup in two configurations to supply electricity i.e. Grid connected PV and Stand-Alone PV. PV plants are growing rapidly around the globe [9-10]. At the end of 2009, the cumulative capacity of PV installations was more than 23 GW. After one year, it became 40.3 GW in 2010 and registered the record growth in 2011, which brought the total capacity up to 70.5 GW. The global PV market stabilized in 2012 and progress was maintained in the upcoming year [10]. Consequently, in 2013, the PV becomes the third largest renewable source after hydro and wind power with the installed capacity of 138.9 GW – an amount which can
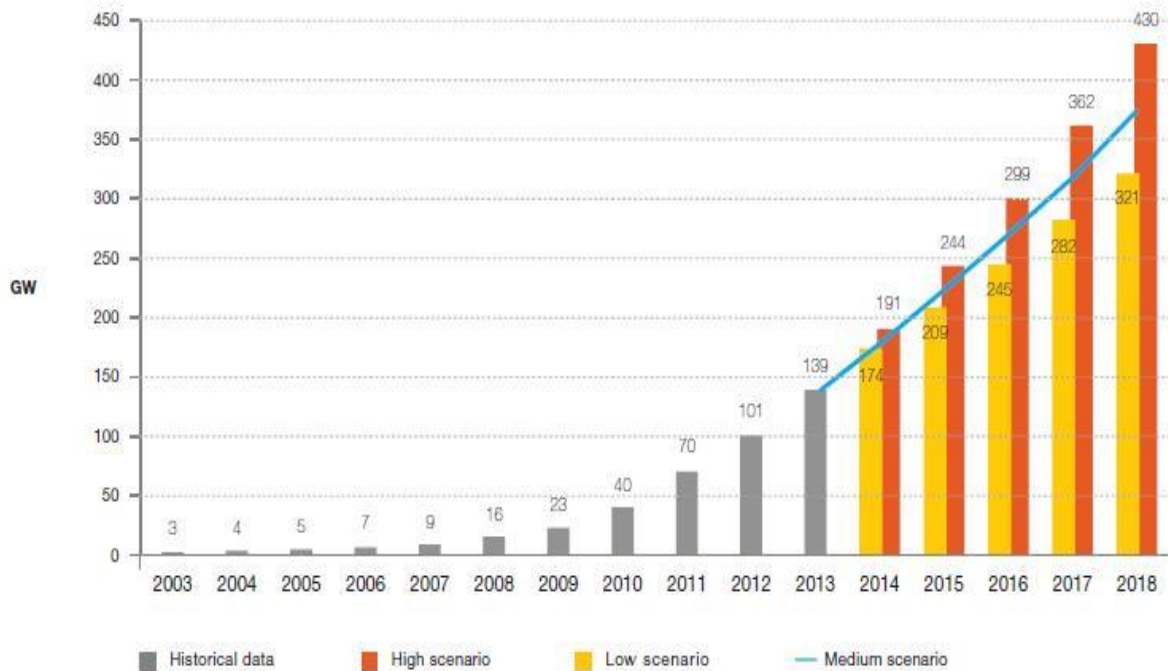
Figure 1.2 – Expected global PV cumulative scenario until 2018

produce at least 160 terawatt hours (TWh) per year [9-10]. Fig. 1.2 shows the graph of global installed capacity of PV where up to 2013, the installed capacity is mentioned. While from 2014 to 2018, the expected install capacity in case of low scenario and high scenario is presented. It can be seen that in 2018, under high scenario, the capacity of PV installed can be more than 3 times to that of installed capacity in 2013. While, it is still showing the considerable rise under low scenario case i.e. more than 2 times to the capacity that the world has in 2013 [9].

An aggressive but reasonable scenario is plotted in Fig. 1.3 in the form of bar charts according to information presented in the report [5], where it is predicted that by 2040, the 50% of the global energy could be supplied by the renewable sources. Furthermore, it is expected that PV installations around the world could become the
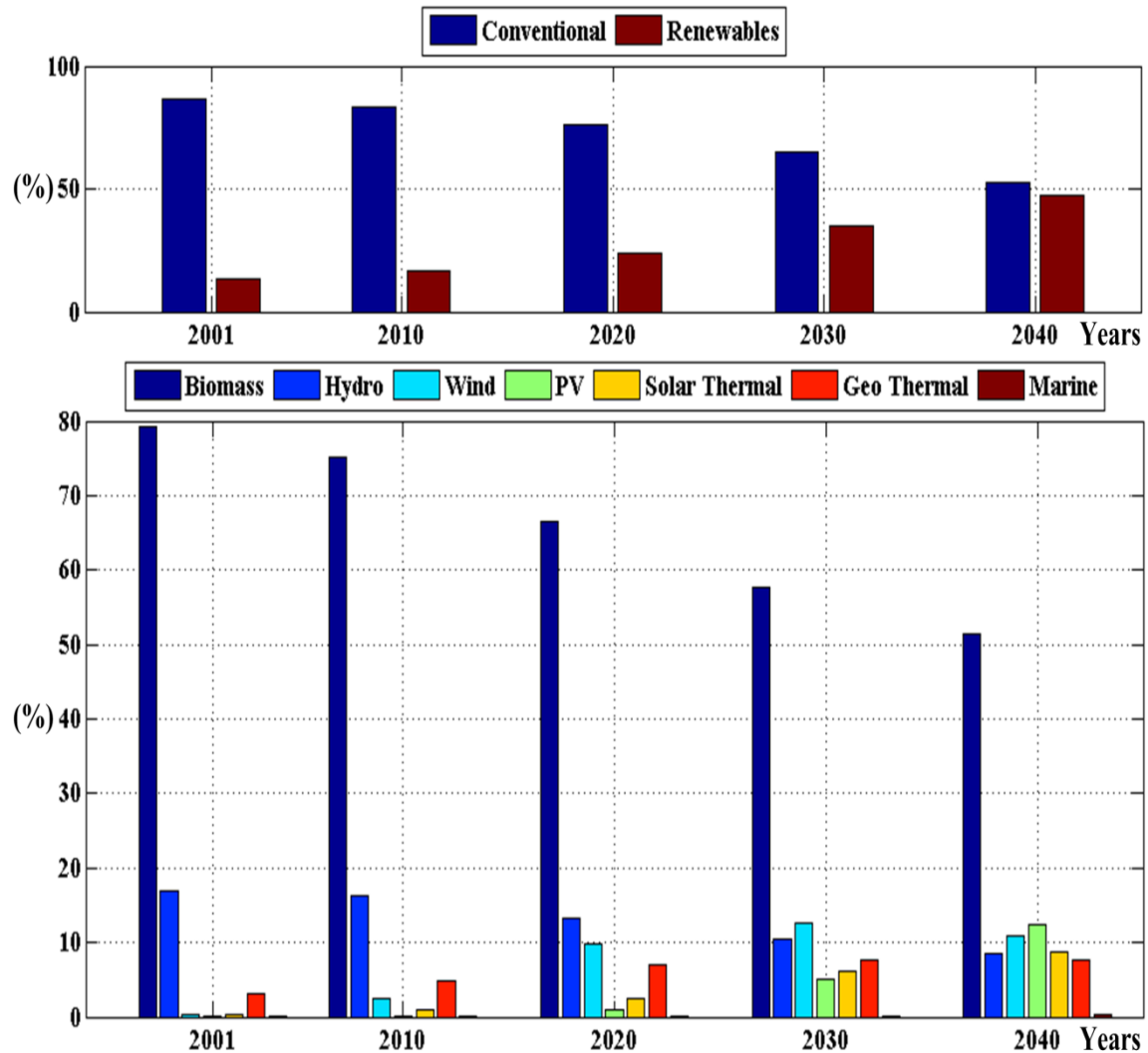
Figure 1.3 – Realistic predictions regarding renewables and PV installations

second largest contributor in electricity generation after biomass. According to data presented in [5], the evolution of energy production from years: 2001 → 2010 → 2020 → 2030 → 2040 is presented in Fig. 1.3. It can be seen that as we move forward from 2010 to 2040, renewable sources are expanding while conventional sources are suppressing. Simultaneously, amongst the renewable sources, the PV capacity is expanding rapidly compared to other renewables.

1.3 Basic units of PV – PV cells

The basic unit of PV array is a PV module/panel while the basic unit of PV
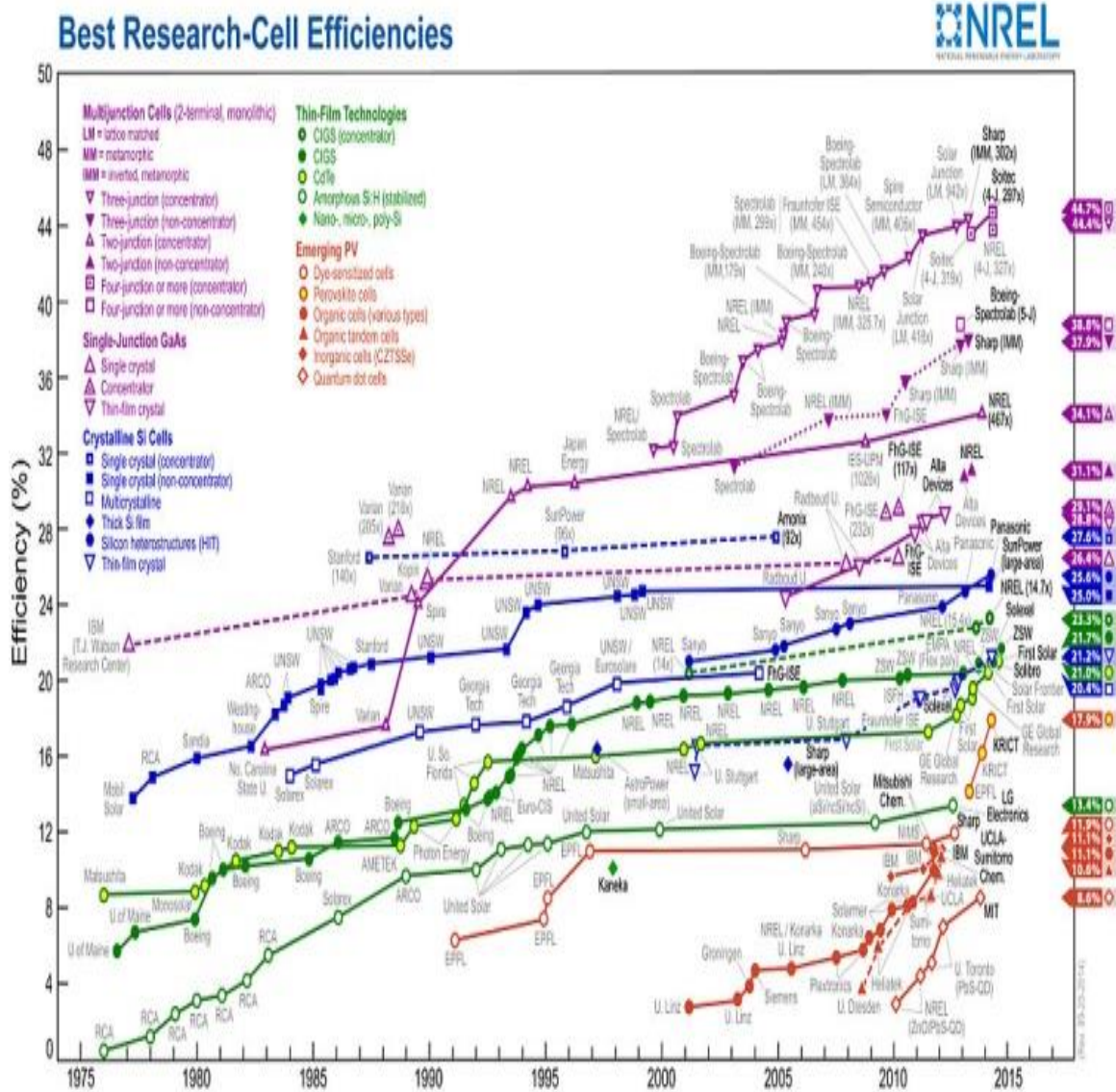
Figure 1.4 − Cell efficiencies manufactured from distinct cell technologies according to NREL

module is PV cells. PV cells are manufactured with a wide range of distinct methods [11]. Each method has its own pros and cons. Fig. 1.4 illustrates the energy conversion efficiency of solar cells measured at National Renewable Research Laboratory (NRRL) for leading and emerging technologies since 1976 [12]. Maximum Solar cell efficiencies attain for Amorphous and Multi-crystalline silicon cells are 13.4% and 20.4% respectively. Besides that, the new technology based multi-junction cells achieve the laboratory efficiency of 44.4%. These high efficient cells may not be the most economical. For instance, a low volume production of 30% efficient multi-junction cell made from expensive materials like gallium arsenide/indium selenide might cost 100 times more than the 8% efficient amorphous silicon cell produced in mass production [12]. This tradeoff between the price and efficiency of cells tilts the balance towards the standard crystalline cells, which cover almost 80% of the PV market as shown in Fig. 1.5 [13]. Energy conversion efficiencies for commercially available multi-crystalline Si solar cells hovers around 14-19% [14].

1.4   Call for efficiency improvement - MPPT techniques

Despite all the advantages of PV as discussed earlier, the paramount drawback with PV is that it will not deliver the maximum power automatically. Furthermore, PV installations are not most economic even with recent cost-effective PV modules and
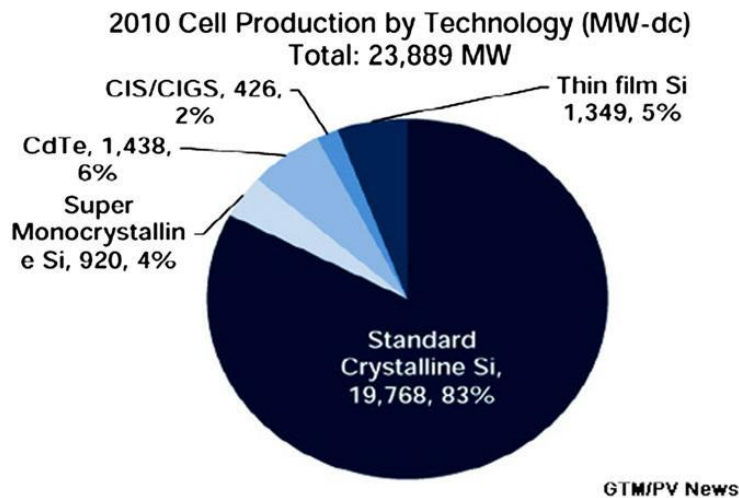
Figure 1.5 – Market of PV according to cell technology [13]

ever-reliable sun source [15]. Considering the initial high capital cost of PV installations and low energy conversion of PV cells [16], it is utmost important that PV array should operate at maximum power under all kinds of climate conditions [15-18].

PV array poses a unique maximum power point (MPP) on its current-voltage (I-V) curve under uniform weather conditions as shown in Fig. 1.6. It is worth noting that operating point of PV array determines the overall efficiency of PV system for both grid-connected PV [18] and stand-alone PV systems [19]. And if PV array is not operating at optimal point, i.e. MPP, it will produce the trickle down effect to the user-end loads. Besides that, the I-V characteristics of PV array varies non-linearly with varying weather conditions, consequently MPP varies. Hence, maximum power point tracking (MPPT) techniques are an integral part and parcel of PV system, which are responsible to drive the PV array at MPP under all kinds of weather condition.

On the other hand, the matter is further complicated as PV array exhibits multiple local maxima (LMs) on its I-V curve during partial shading condition as shown in Fig. 1.6, one of them is a global maximum (GM). Partial shading is a phenomenon when some of the modules within a PV array receive different irradiance levels compared to the other PV modules [20]. Irradiance level means the sunlight level. According to [21-22], the power loss due to the incapability of PV array to operate at GM can go up to 70%. As a result, a much more robust MPPT is required, which will detect the GM amongst all the LMs.
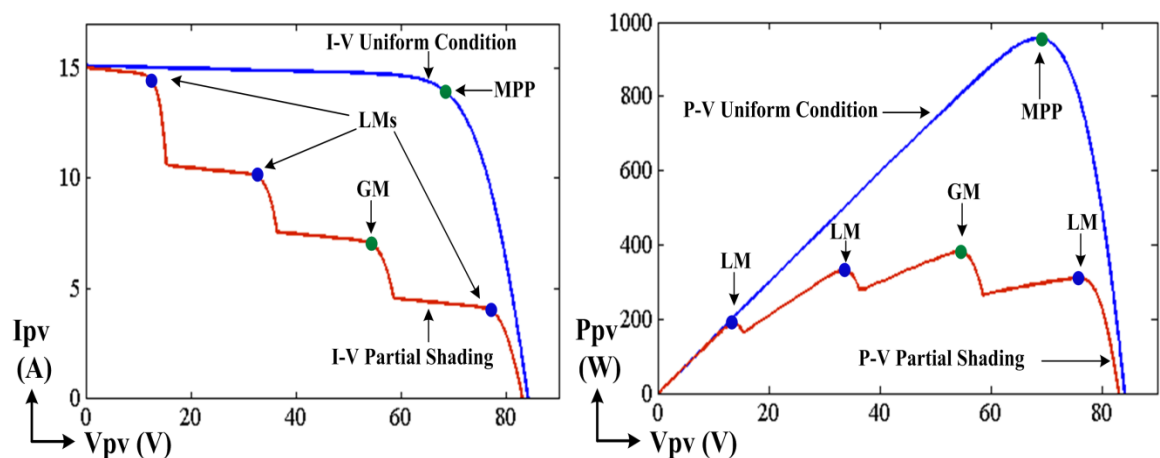
Figure 1.6 – I-V and P-V curves of PV under uniform and partial shading conditions

1.5   Focus of the thesis

Currently, a consensus can be sensed between the researchers and scientists of PV community that it is imperative to boost the power yield of PV array by improving the MPPT capability of PV systems. A proof of this can be found from the increasing number of MPPT techniques from the surveys in the years 2007 [23], 2012 [24], 2013 [25-27] and 2014 [28]. Even there are suggestions that the upcoming PV modules should have in-built MPP tracker.

The focus of this thesis is:

1) To design the innovative MPPT technique for uniform conditions compared to the past-proposed MPPTs.

2) To design the robust MPPT technique for partial shading conditions compared to previous MPPTs.

Both techniques are theoretically analyzed and comprehensive testing is carried out through extensive simulations in Matlab/Simulink. A sophisticated experimental apparatus is setup in order to validate the theoretical formulations and design principles of the proposed MPPTs. The experimental setup contains the special-mobile vehicle in which PV array is installed, which is used to conduct the dynamic tests.

It is worth noting that the design, diagnosis and analysis of the proposed work is not limited to one type of module and not even one type of simulation models of the PV array. Distinct PV modules and PV models (according to their respective expertise) are employed in the proposed work. The summary of these are:

- A comprehensive simulation model [29] designed for uniform conditions is utilized with the cooperation of multi-crystalline [30] and mono-crystalline [31] PV modules. The module [31] is also used for experimental work.

Table 1.1 – PV modules data according to STC condition

Manufacturer	Model	Technology	P_{mpp} (W)	V_{mpp} (V)	I_{mpp} (A)	V_{oc} (V)	I_{sc} (A)
Kyocera	KC200GT [30]	Multi-Crys.	200	26.3	7.61	32.9	8.21
FVG-Energy	36-125 [31]	Single-Crys.	80	18.2	4.4	22.1	4.87
Siemens	SM55 [33]	Single-Crys.	55	17.4	3.15	3.45	21.7

- For partial shading, PV simulation model developed by [32] is used with PV module [33]. While the PV model [34] is also taken into account.

   The datasets of these modules under STC are mentioned in Table 1.1.

1.6   Limitations of the thesis

The main work of this thesis revolves around the designing of new MPPT techniques. Although the techniques are validated using the stand-alone PV system, the basic fundamentals and design parameters of the MPPT techniques will not be changed when shifted to grid-connected PV system. Hence, proposed MPPT techniques can easily be implemented on the grid-connected PV in its true form.

To further discuss the role of MPPTs, consider Fig. 1.7 in which both types of PV systems are shown along with the MPPT control. It can be seen that MPPT is mainly dealing with the input side of PV system, i.e. PV array and DC-DC converter. While, shifting from stand-alone to grid-connected PV system will cost another inverter in order to convert the DC form of electricity into AC.
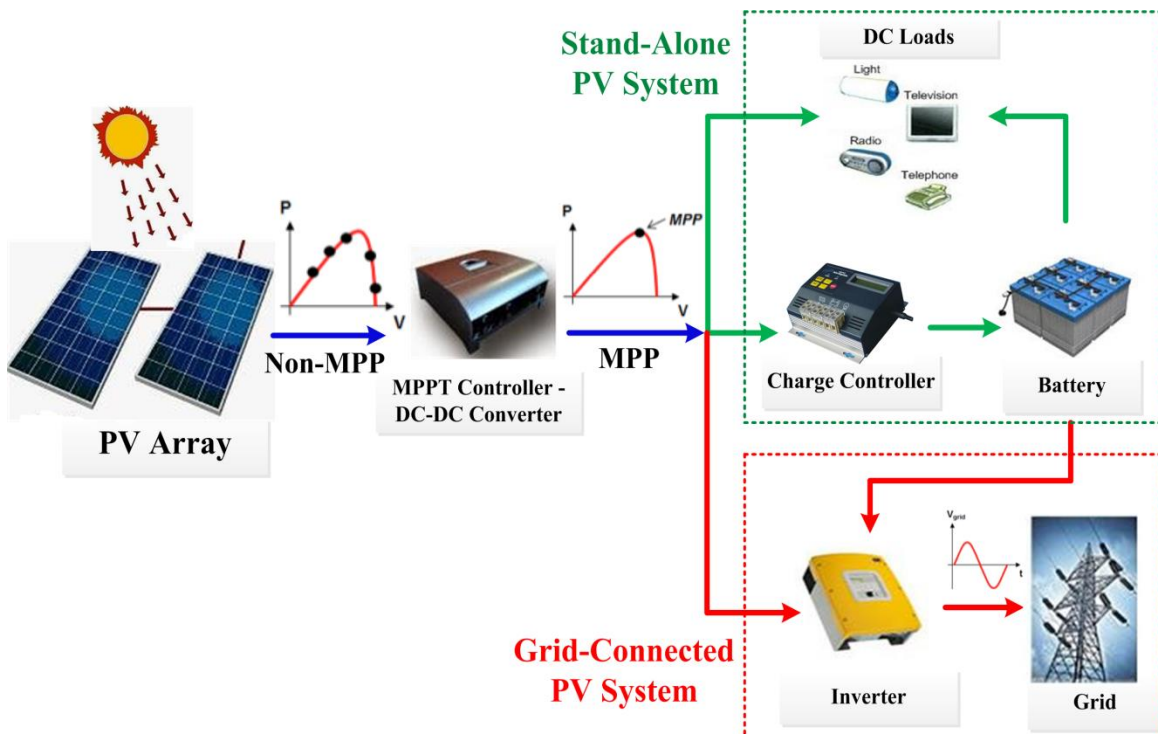
Figure 1.7 – MPPT for stand-alone and grid-connected PV systems

Chapter 2

I-V characteristics of PV array and optimum impedances of MPPs

This chapter explains the non-linear characteristics of I-V curve of PV array with respect to weather conditions and the impact of this on MPP points. The phenomenon of impedance matching is described to attain the MPP. From the observations of this chapter, some concluding remarks are made, which are considered during the designing of MPPTs.

2.1 PV cell and influence of solar radiation

The basic unit of photovoltaic is the solar cell, which is responsible for the generation of photocurrent when exposed to sunlight. Hence, the efficiency of the cell depends upon the spectral distribution of the solar radiation, which consists of the electromagnetic radiations of multiple wavelengths. The spectrum of solar radiation can be considered equivalent to a spectrum of black body with 6000 K [11]. However, the evaluation of the solar spectrum on PV cell is difficult to attain as it is influenced by a number of factors such as temperature variations on solar disc and atmospheric behavior [35]. The irradiated solar energy (irradiation) in the outskirts of Earth is 1.353 kW/m^2. On the Earth's Surface, the irradiation is nearly 1 kW/m^2 [29]. This can be considered as the reference irradiation, however it may vary from land to land with respect to the geographic location.

Although the American Society for Testing and Materials standardized two terrestrial spectral distributions: the direct-normal and global air mass of 1.5 i.e. AM1.5. The latter spectral is used as the standard in the PV industry [29]. Manufacturer's datasheet give the characteristics of the PV device according to the

standard test conditions (STC) which corresponds to the irradiation of 1000 W/m² at temperature of 25°C with an AM1.5 [29].

Solar cell converts the sunlight in the direct current (DC) form of electricity through a single diode junction or multiple junctions [11]. Due to incident sunlight, the radiation (consists of photons) with sufficient energy creates the photo-carriers (electron/hole pairs) within the cell. Consequently, the carrier separation generates the photo-voltage while the charge motion creates a photo-current, which moves against the diode junction [11]. Electrical model of the Ideal PV cell can be considered as the current source with diode in parallel as shown in Fig. 2.1(a) [29].

$$I_{pv,cell} = I_{ph,cell} - I_{d,cell} = I_{ph,cell} - I_{s,cell}\left[exp\left(\frac{V_{d,cell}}{nV_{T,cell}}\right) - 1\right] \qquad (2.1)$$

Where, $I_{pv,cell}$ is the output current of the cell, $I_{ph,cell}$ is the photo-current generated by the cell due to incident sunlight and $I_{d,cell}$ is the diode current which can be obtained from the Shockley diode equation [36]. In diode equation, $V_{d,cell}$ is the voltage across the diode, $I_{s,cell}$ is the saturation current, n is the diode ideality constant, $V_{T,cell}$ the voltage of P-N junction at 25°C and is equal to kT/q where q is the electron charge ($1.60217646 \times 10^{-19}$ C), k is the Boltzmann constant ($1.3806503 \times 10^{-23}$ J/K), T (in Kelvin) is the temperature of the p–n junction,

Since the typical cell produces the voltage in the range of 0.5 – 1.5 V. These cell are connected by means of series-parallel configurations to enhance the overall
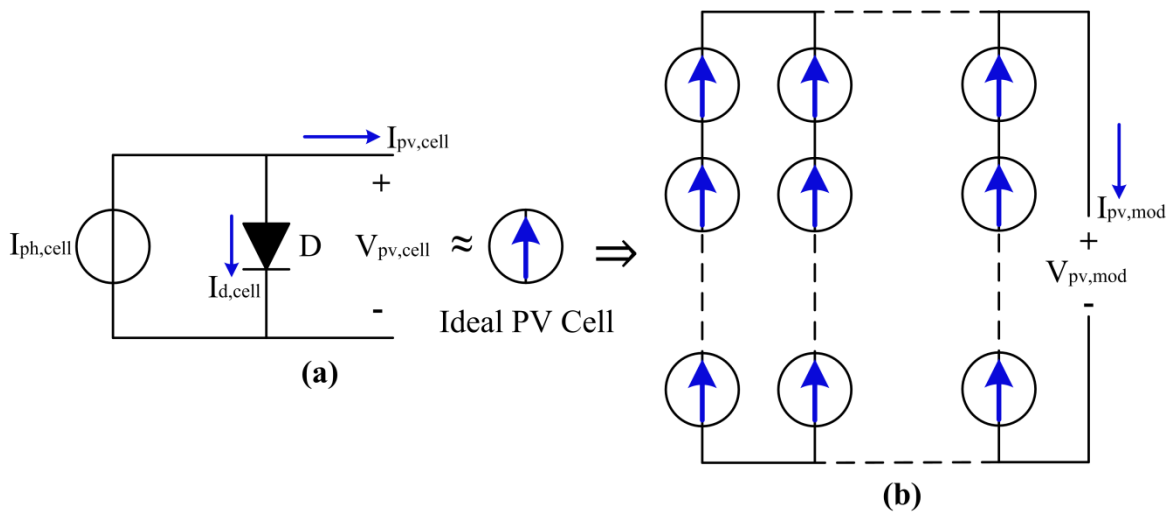
Figure 2.1 – (a) Ideal PV cell model (b) PV module formed from PV cell

voltage and current of the PV device. Such a device is commonly known as PV module. It is worth noting that generally, the data available from the Manufacturer's datasheet belongs to the package i.e. PV module [30-31,33], despite the fact that the power ratings of the PV module depend upon the number of cells present in it. The transformation of PV cells into PV module is shown in Fig 2.1(b), which can also be expressed mathematically as:

$$I_{pv,mod} = I_{ph,mod} - I_{d,mod} \qquad (2.2)$$

2.2 Characteristics of practical PV module/array

The practical PV module is modeled with either single diode model [29] or two diode model [32,37]. Both of these are based on Shockley diode equation [36]. Assuming the good compromise between the simplicity and accuracy, single diode model is presented in this work [29]. The practical single diode model is based on four parameters (Current Source, Diode, R_s & R_p) i.e. it contains two more parameters compared to ideal model as shown in Fig. 2.2 (a). The mathematical presentation of the practical PV module can be expressed as:

$$I_{pv,mod} = I_{ph,mod} - I_{d,mod} - I_{p,mod} \qquad (2.3)$$
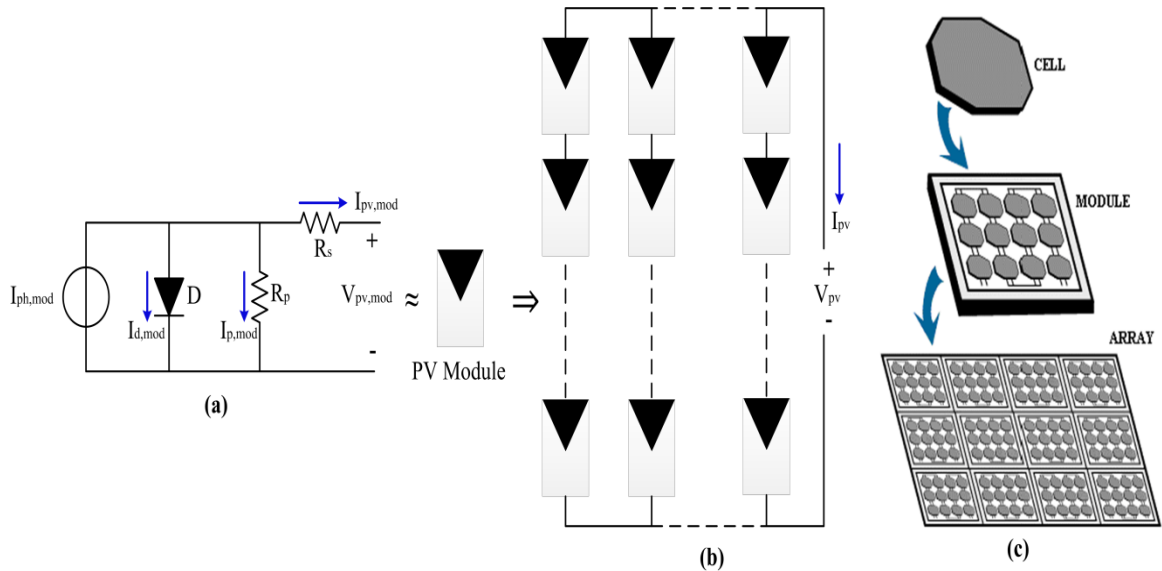
Figure 2.2 – (a) Practical PV module, (b) PV array formed from PV modules and (c) Transformation from cell to array

$$I_{pv,mod} = I_{ph,mod} - I_{s,mod}\left[exp\left(\frac{V_{d,mod}}{nV_{T,mod}}\right) - 1\right] - \frac{V_{d,mod}}{R_p} \qquad (2.4)$$

Where, $V_{d,mod}$ is the voltage of the module across the diode and can be replaced as expressed in Eq. (2.5) as

$$I_{pv,mod} = I_{ph,mod} - I_{s,mod}\left[exp\left(\frac{V_{pv,mod}+I_{pv,mod}R_s}{nV_{T,mod}}\right) - 1\right] - \frac{V_{pv,mod}+I_{pv,mod}R_s}{R_p} \qquad (2.5)$$

Where R_s is the series resistance of the module, which accounts for the losses due to the internal series resistance of the module and interconnection between the cells. While, R_p approximates the losses due to the leakage currents at the borders (junctions) and within the cell due to geometric imperfections of crystal and impurities [38-39]. In order to achieve the desired voltage and power levels, PV modules are connected in series and parallel configurations to form the PV array as illustrated in Fig. 2.2 (b). Therefore, Eq. (2.5) can be translated to mathematically express the I_{pv} of PV array as:

$$I_{pv} = I_{ph} - I_s\left[exp\left(\frac{V_{pv}+I_{pv}R_s}{nV_T}\right) - 1\right] - \frac{V_{pv}+I_{pv}R_s}{R_p} \qquad (2.6)$$

Where, V_{pv} is the cumulative voltage of the array and is equal to voltage of PV module connected in series i.e. $N_s \times V_{pv,mod}$. I_{pv} is the cumulative current and is equal to current of module connected in parallel i.e. $N_p \times I_{pv,mod}$. V_T is the thermal voltage with N_s modules connected in series. I_{ph} is the photocurrent generated by the PV array and is equivalent to $N_p \times I_{pv,mod}$. I_s is the saturation current and is equal to $N_p \times I_s$. R_s and R_p are the equivalent series and parallel resistances of the PV array. The complete transformation of PV cell to PV array is shown in Fig. 2.2 (c).

Fig. 2.3(a) reveals the practical PV array installed worldwide in which two types of diodes are added: 1) By-pass diodes and 2) Blocking diodes [40-41]. Normally PV array is defined in the form of strings connected in parallel, where each string is comprised of equal numbers of series connected modules. Modern PV modules have in-built bypass diodes as shown in Fig. 2.3(b). It can be seen that there are 60 PV cells present in the module. And for each group of 20 cells, a bypass diode is connected. However, the designer installs the blocking diodes as they are not
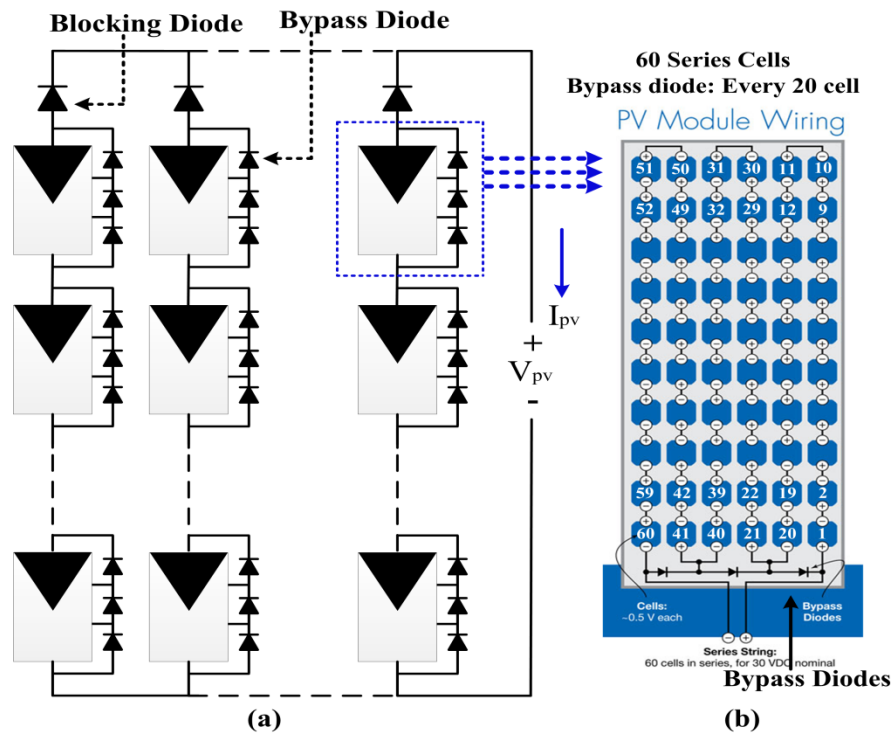
Figure 2.3 – (a) Practical PV array with bypass and blocking diodes (b) Modern PV module with in-built bypass diodes

commonly available inside the PV modules. The reason to install blocking diodes is to guard the array from being affected by the current unevenness between the strings [41]. However, the bypass diodes are used to protect the modules/group of cells, when some of the cell groups or modules behave as loads rather than generators [42-43]. This phenomenon is occurred due to the non-uniform distribution of irradiance on the PV array commonly known as partial shading. Those less irradiated modules or group cells, which behave like a load, if not sheltered through the additional path of current through bypass diodes may cause the hot spot effects or even severely damage them [44-46]. These effects are discussed in detail in the later sections of this thesis.

2.3 I-V and P-V characteristics of PV array

Eq. (2.6) clearly indicates that I_{pv} depends upon the photocurrent (I_{ph}) and the operating voltage (V_{pv}) of the PV array. The amount of I_{ph} depends upon the weather conditions i.e. irradiance and temperature. In order to evaluate the I-V characteristics,
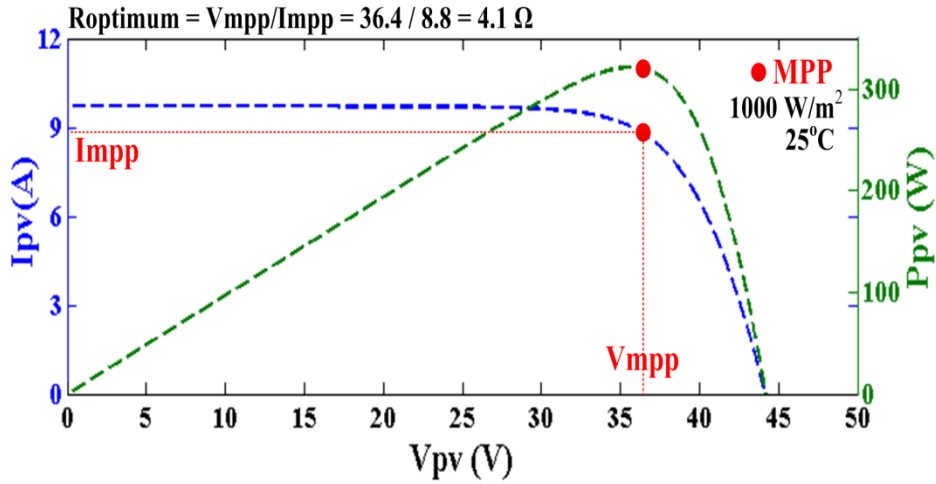
Figure 2.4 – MPP of PV array under STC conditions

the comprehensive PV model [29], which is based on Eq. (2.6), is modeled in Matlab/Simulink. With the help of this model, I-V curve of PV array at STC (1000 W/m^2 - 25°C) is shown in Fig. 2.4, where the PV array consists of FVG 36-125 [31] modules connected in 2x2 series-parallel configuration. The STC data of FVG 36-125 module is given in Table 1.1 of Ch. 1. Fig. 2.4 reveals that the I-V curve contains a unique MPP which can be attained when the PV array starts operating at V_{mpp} = 36.4 V and I_{mpp} = 8.8 A. Therefore, PV array always exhibits some specific internal impedance and the optimum impedance ($R_{optimum}$) corresponds to the MPP point, which can be expressed as:

$$R_{optimum} = \frac{V_{mpp}}{I_{mppp}} = \frac{36.4}{8.8} = 4.14 \; \Omega \qquad (2.7)$$

It can be evaluated that operating point of the PV array depends upon the load. Hence, maximum electrical power can be harnessed by combining the array with a suitably matched resistive load (R_L) [11]. For instance, to set the PV array at MPP under STC condition, R_L can be set equivalent to $R_{optimum}$ of 4.14 Ω. This mechanism is precisely known as impedance matching as shown in Fig. 2.5(a) [45,47].

2.3.1 I-V curve variations with weather conditions

The PV array with a fixed resistance mechanism will not survive for a long period and most probably, may not work at all. It is because of the non-linear behavior
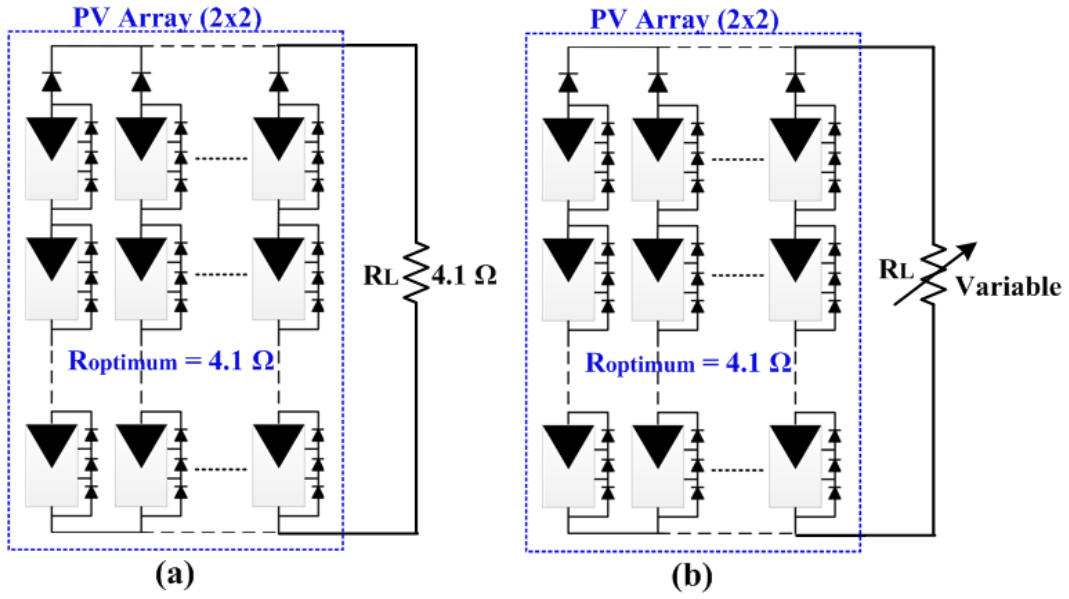
Figure 2.5 – Impedance matching mechanism: (a) Fixed load and (b) Variable load

of I-V curve with respect to varying weather conditions. Since, weather conditions cannot be constant for a fairly long period, as a result, I-V curve of PV varies non-linearly with weather conditions, which leads to the variation in MPP values. The following relations depict the relation of MPP parameters of PV array with respect to weather conditions, i.e. irradiance and temperature [45,48]:

$$I_{mpp} = K_v I_{sc} \tag{2.8}$$

$$V_{mpp} = K_i V_{oc} \tag{2.9}$$

$$I_{sc} = (I_{sc,n} + K_I \Delta T) \frac{G}{G_n} \tag{2.10}$$

$$V_{oc} = V_{oc,n} + K_V \Delta T \tag{2.11}$$

Eqs. (2.8) and (2.9) express that voltage and current which corresponds to MPP (V_{mpp} and I_{mpp}) are the fractions of open-circuit voltage (V_{oc}) and short-circuit current (I_{sc}) of the PV array respectively. Where, K_i is the proportionality factor for I_{mpp}, which normally varies from 0.85 to 0.95 and K_v is the proportionality factor for $V_{mpp,}$ which varies from 0.75 to 0.85. On the other hand, Eq. (2.10) reveals that the value of

I_{sc}, which determines the I_{mpp}, is majorly influenced by G/G_n i.e. ratio of present irradiance level ($G - W/m^2$) to irradiance of STC i.e. G_n ($1000\ W/m^2$). While, it is less influenced by change in temperature as the magnitude of product ($K_I\ \Delta T$) is not significant because the value of temperature coefficient (K_I) of I_{sc} is in fractions. While, Eq. (2.11) indicate that V_{oc}, which determines the V_{mpp}, depends majorly on temperature, i.e. change in temperature and temperature coefficient (K_V) of V_{oc}. In Eqs. (2.10) and (2.11), $I_{sc,n}$ and $V_{oc,n}$ are the short-circuit current and open-circuit voltage of the PV array at STC, respectively. The values of these parameters can be obtained from Manufacturer's datasheet.
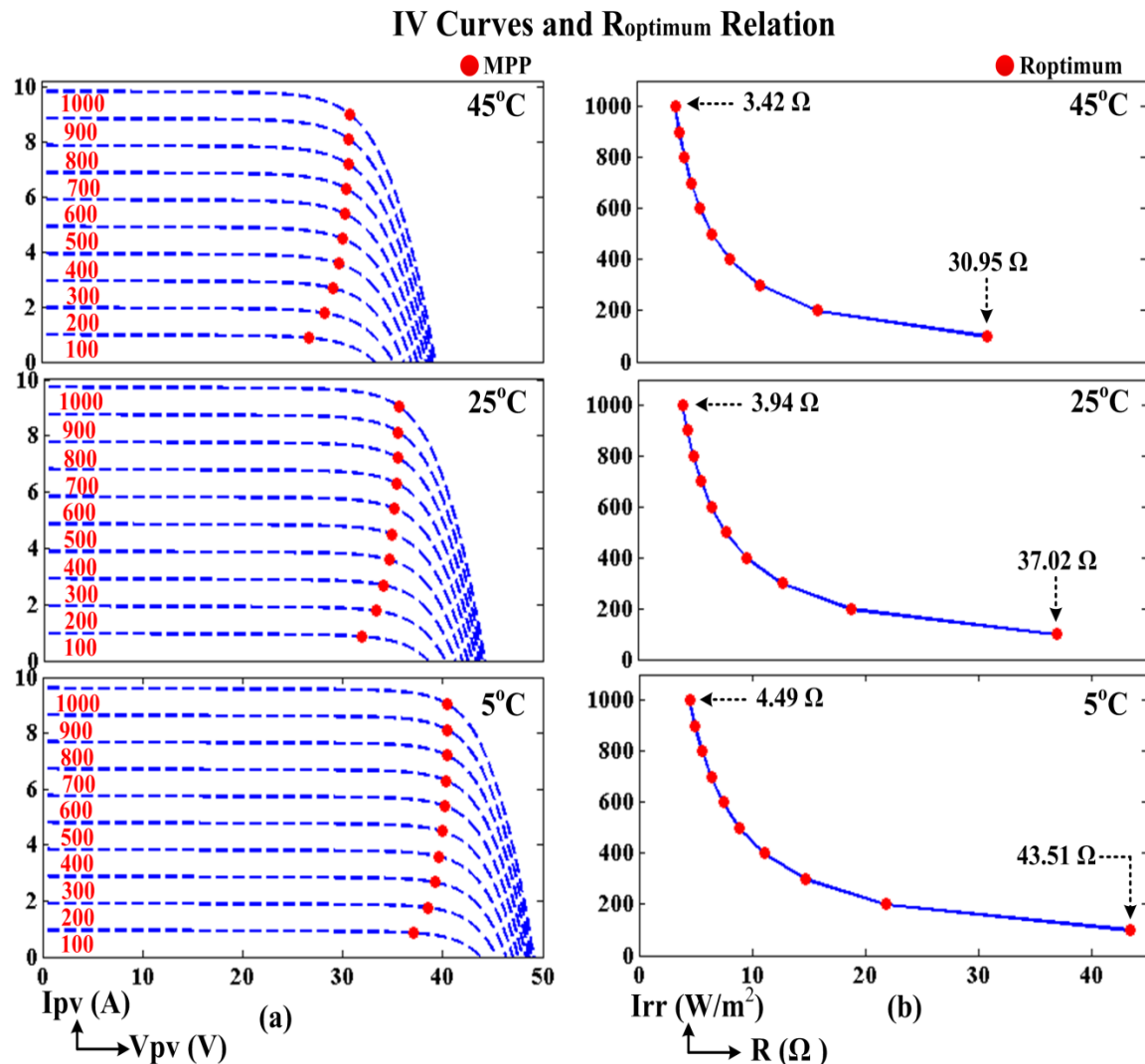
Figure 2.6 – (a) I-V Curves of PV array under varying irradiance from 1000 W/m² to 100 W/m² and temperature conditions: (a) 45°C - top, (b) 25°C - middle and (c) 5°C - bottom. (b) R$_{optimum}$ values correspond to MPPs of respective weather conditions

2.3.2 I-V variations and optimum impedances of MPPs

The above discussion clearly concludes that the MPP parameters of PV array varies with weather conditions. Fig. 2.6 illustrates the effects of irradiance and temperature variations on I-V curves of PV array and values of $R_{optimum}$ required to attain MPP, which is attained using the same simulation model and PV array as described in Sec. 2.3. It can be seen from Fig. 2.6(a) that the variations in irradiance is changed from 1000 W/m^2 to 100 W/m^2 for each of three vastly different temperature conditions, i.e. 45°C (top), 25°C (middle) and 5°C (bottom). Consider the temperature condition of 45°C and its corresponding $R_{optimum}$ graph, i.e. top graph of Fig. 2.6(b). At 1000 W/m^2, MPP corresponds to $R_{optimum}$ = 3.42 Ω, while it goes up to 30.95 Ω when irradiance falls down to 100 W/m^2, which clearly indicates the increase of 10 times in $R_{optimum}$ value while going from higher irradiance to low irradiance. It can be evaluated that PV array can't survive with fixed value of R_L even if the temperature level is constant.

On the other hand, while going from high temperature levels to low temperature levels i.e. 45°C to 25°C and 25°C to 5°C, the voltage values of MPPs (V_{mpp} values) are shifted towards right thus depicting the increase in V_{mpp} values as temperature falls. This is because of the reason that V_{oc} of array increases as temperature falls. However, as far as the $R_{optimum}$ values are concerned, the situation is further complicated. It can be seen that when temperature is at 45°C, the $R_{optimum}$ moves from 3.42 Ω to 30.95 Ω i.e. difference of 27.53 Ω. While, this difference increases to 33.08 Ω at 25°C. At 5°C, the $R_{optimum}$ goes from 4.49 Ω to 43.51 Ω i.e. difference of more than 39 Ω. This relation of $R_{optimum}$ with varying weather conditions indicate not only the necessity of varying load as shown in Fig. 2.5(b) but also the calibration of R_L value is critical.

2.4 Concluding remarks

The discussion in the previous section can be concluded as:

- The change in irradiance produces the major effect in I_{sc} while it creates a minor effect in V_{pv}. And, the change in temperature mainly influences the V_{oc}

of the array. Hence, the variations in I-V curves of PV array can be traced with the help of V_{oc} or I_{sc} values of the array.

- For optimal operation of PV array, the impedance matching phenomena is followed, which dictates that the fixed load mechanism is not sustainable.

- The value of load is critical to cover up the wide range of MPPs.

Chapter 3

System architecture and load criteria for MPPTs

This chapter explains the system architecture required to implement the maximum power point technique. Impedance matching has been specifically discussed with respect to boost converter. Behavior of resistive and battery loads is analyzed and its effects on the coverage of MPP are discussed. A criterion is defined and two new formulae are developed to adjust the values of resistive and battery loads.

3.1   System architecture

It is cleared from the previous discussion that impedance matching is essential in order to drive the PV array at MPP on consistent basis. Consequently, MPPT designers always plug the DC-DC converter between the PV array and the load. DC-DC converters are mainly based on three topologies: 1) Buck, 2) Boost and 3) Buck-Boost. Although each topology has its pros and cons, but Boost converter topology is popularly used in the domain of PV array because of its stable operation. The work presented in this thesis also utilizes the same topology. However, the proposed work can be easily modified to other converters using same procedures.

An architecture of stand-alone PV system is displayed in Fig. 3.1, which shows that in order to develop an MPPT technique, the designer has to deal with two major challenges: 1) Soft computing – To design an algorithm which measures the values from the sensors and estimates the maximum power point voltage/current (V_{mpp}/I_{mpp}) or both as its MPPT output variable, 2) Hard computing – To design the converter control   technique which adjusts the duty cycle (D_{mpp}) of the converter in order to set the operating voltage/current (V_{pv}/I_{pv}) of PV array at MPPT output variable (V_{mpp}/I_{mpp})

such that the PV array starts operating at MPP.

In Fig. 3.1, a DC-DC converter (boost topology) is present between the PV array and the load. The main purpose of DC-DC converter is to vary the load resistance (R_L) through Pulse width modulation (PWM) of D such that the R_L matches the internal impedance ($R_{pv\_internal}$) of the PV array [47,49]. The operation of boost converter can be mathematically expressed as:

$$V_o = \frac{1}{1-D} V_{in} \tag{3.1}$$

Assuming the ideal efficiency of the converter i.e. $P_{in} = P_{out}$,

$$V_o I_o = V_{in} I_{in} \tag{3.2}$$

We know that $I_o = V_o/R_o$ and $I_{in} = V_{in}/R_{in}$, Eq. (3.2) can be modified as:

$$\frac{(V_o)^2}{R_o} = \frac{(V_{in})^2}{R_{in}} \tag{3.3}$$

Taking V_{in} from Eq. (3.1) and putting it in Eq. (3.3), we get

$$R_o = \frac{1}{(1-D)^2} R_{in} \tag{3.4}$$

Adjusting the Eq. (3.4) according to variables mentioned in Fig. 3.1, we get

$$R_L = \frac{1}{(1-D)^2} R_{pv\_seen} \tag{3.5}$$
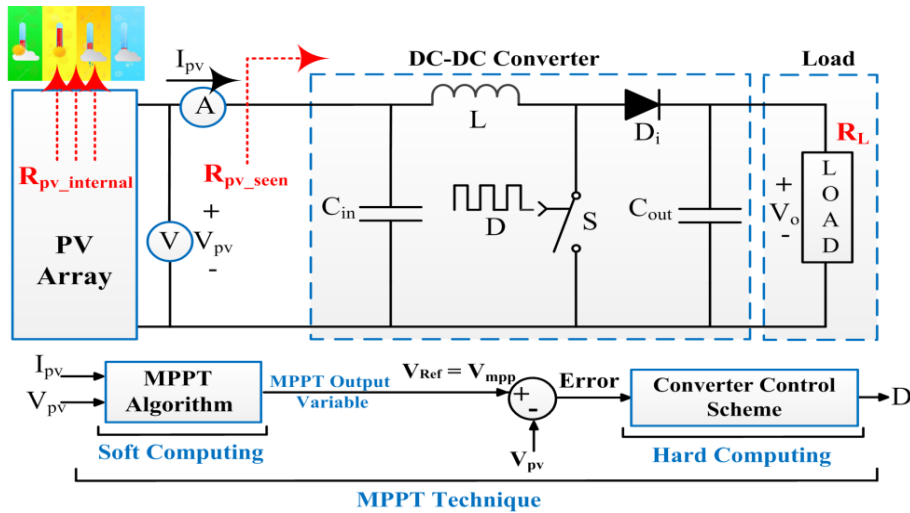
Figure 3.1 – Architecture of PV system in the presence of MPPT technique

$$R_{pv\_seen} = (1 - D)^2 R_L \tag{3.6}$$

It can be seen from Fig. 3.1 that R_{pv_seen} is not a hardware component. It is actually the impedance seen by the PV module, in which R_L is reflected. Hence, Eq. (3.6) expresses that MPPT designer can vary the R_{pv_seen} by varying the D even if R_L is fixed. Whenever, D is properly optimized i.e. D_{mpp}, the R_{pv_seen} becomes equal to the internal impedance ($R_{pv\_internal}$) of the array. At this stage, PV array starts operating at MPP. It is pertinent to note that $R_{pv\_internal}$ depends upon weather condition. Consequently, with varying weather conditions, $R_{pv\_internal}$ varies. Therefore, the responsibility of MPPT technique is to make the R_{pv_seen} close to $R_{pv\_internal}$ as fast as possible. A non-MPP and MPP operations of PV array in terms of relations are expressed in Eq. (3.7) & Eq. (3.8) respectively,

$$R_{pv\_seen} = (1 - D)^2 R_L \Rightarrow \frac{V_{pv}}{I_{pv}} = \frac{1}{(1 - D)^2} R_L \Rightarrow R_{pv\_seen} \neq R_{pv_{seen}} \tag{3.7}$$

$$R_{pv\_seen} = (1 - D_{mpp})^2 R_L \Rightarrow \frac{V_{mpp}}{I_{mpp}} = \frac{1}{(1 - D_{mpp})^2} R_L \Rightarrow R_{pv\_seen} = R_{pv_{seen}} \tag{3.8}$$

The above discussion clearly mentioned that R_L has significant relation with D and $R_{pv\_internal}$ [49]. Hence, it is quite possible that with specific R_L, the MPPT designer may not cover all the MPPs of all the weather conditions even the designer has the accurate value of V_{mpp}/I_{mpp}.

Eq. (3.9) expresses the D of the converter employed in PV system, where T_t is the total cycle time and T_{on} represents the time during which the signal is high. The converter is always operated at some frequency determined by the T_t, while the magnitude of D is varied with the pulse width modulation (PWM) of T_{on}. It can be confirmed from Eq. (3.9) that regardless of any frequency, the maximum value of D (D_{max}) is 1 when $T_{on} = T_t$ and the minimum value of D (D_{min}) is 0 when $T_{on} = 0$. Hence, the limits of D can be set as from $0 \rightarrow 1$.

$$D = \frac{T_{on}}{T_t} \tag{3.9}$$

In general, the PV operating voltage (V_{pv}) is the variable, which is regulated through the PWM of D in order to set the operating point of the PV array [50]. The
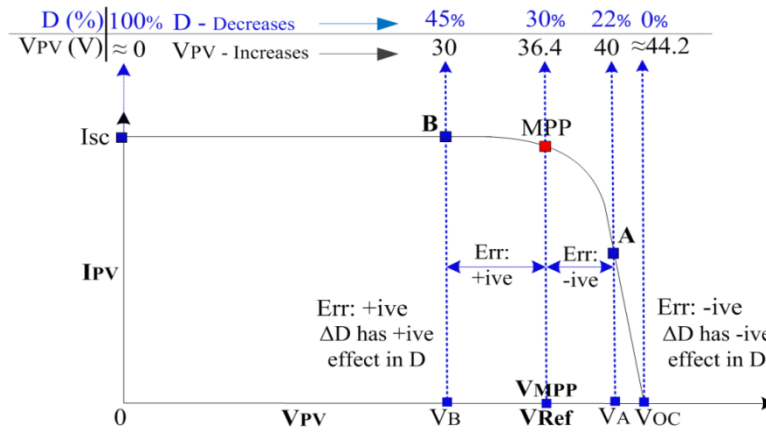
Figure 3.2 – Duty cycle and V_{pv} relation of PV array

techniques developed in this thesis, which are explained later, also sets the V_{Ref} of PV array by regulating the V_{pv} courtesy D.

Consider the typical I-V curve of the PV array under standard testing condition (STC) i.e. 1000 W/m²-25°C shown in Fig. 3.2. PV array contains two stings and each string contains two modules of type FVG 36-125 [31], the voltage range of PV array is 0 to 44.2 V under STC. Ideally, it can be evaluated from Fig. 3.1 that when D of the converter is set at 1 (100%), the switch is completely closed and it behaves like a short circuit. As a result, PV array operates at $V_{pv} = 0$ and $I_{pv} = I_{sc}$ ($I_{sc} = 9.74$ A at STC). This connection between D and V_{pv} is indicated in Fig. 3.2. On the other hand, when D is set at 0 (0%), PV array operates approximately at the open-circuit voltage of the PV array. It can be seen from Fig. 3.2 that the operational range of D is between 0 and 1, where D = 0 corresponds to $V_{max} = V_{oc}$ and D = 0 corresponds to $V_{min} = 0$. Hence, D_{max} is set at 0 while D_{min} is set at 1 and D should be operated with in these boundary limits i.e. $0 < D < 1$.

3.2 Effects of load, D_{max} and coverage of MPPs ($V_{mpp}s$)

It can be confirmed from the previous section that D of the converter determines the operating point of PV array, therefore following points are worth noting:

1) All the effects are discussed with respect to Boost converter.

2) Since D = 0 corresponds to maximum voltage i.e. $V_{pv} = V_{oc}$, which can be

23

confirmed from Fig. 3.2, the coverage of MPP (V_{mpp} which lies between 0 and V_{oc}), is determined with respect to D_{max} = 0.05 as 0.05 (5%) caution is set [51].

3) Ideally, D should cover the V_{pv} values of PV from 0 to V_{oc} in which V_{mpp} lies under all kinds of weather conditions. Hence, the real objective is to understand the effect on the coverage of V_{mpp} values with respect to D under: 1) different kinds of loads and 2) variable weather conditions i.e. irradiance and temperature variations.

3.2.1 Resistive load effects

The above discussion clearly reveals the value of D_{max}, which corresponds to V_{pv_max} is 0.05. Therefore, to find out the V_{pv_max} for resistive loads, Eq. (3.6) can be transformed as:

$$R_{pv\_seen\_max} = (1 - D_{max})^2 R_L \Rightarrow R_{pv\_seen\_max} = (1 - 0.05)^2 R_L \qquad (3.10)$$

We know that $R_{pv\_seen\_max}$ = V_{pv_max} / I_{pv}, the above equation can be modified as:

$$V_{pv\_max} = 0.903 \times I_{pv} \times R_L \qquad (3.11)$$

The above equation clearly reveals that if I_{pv} falls significantly due to low irradiance, this will also reduce the V_{pv_max} significantly. Thus, reducing the ability of PV system to cover each and every MPP. This is where the role of R_L is crucial. To evaluate this, PV array of 2x2 SP configuration is used and simulations are carried out. Each PV module is of type FVG 36-125 [31]. Fig. 3.3 illustrates the I-V curves of PV array where irradiance is varied from 1000 to 100 W/m^2. While 20°C of temperature is varied on either side from STC of 25°C i.e. 5°C, 25°C and 45°C. $R_{pv\_seen\_max}$ at D_{max} = 0.05 is evaluated under two randomly selected values of loads: 1) 9.4 ohm (shown in Fig. 3.3(a)) and 2) 23.5 ohm (shown in Fig. 3.3(b)). The black line represents the $R_{pv\_seen\_max}$, which also gives an indication about the maximum V_{pv} value (V_{pv_max}) under different conditions.

Figure 3.3 illustrates that any MPP point above $R_{pv\_seen\_max}$ (D_{max} = 0.05) can be reached while MPP points occurring below this line cannot be reached. For instance, with 9.4 ohm resistance and at 45°C, the MPPT achieves V_{pv_max} of 36.58 V when irradiance is at 1000 W/m^2 covering the V_{mpp} while it drops to 7.75 V when irradiance

is at 100 W/m^2 missing the MPP point by a huge margin. Thus justifying the Eq. (3.11) that when resistance is low (9.4 ohm) and I$_{pv}$ is low (low irradiance), V$_{pv\_max}$ is low. Furthermore, the MPP points cannot be achieved when irradiance is at or below 400 W/m^2 and temperature is at 45°C. It can be noticed from Fig. 3.3(a) that R$_{pv\_seen\_max}$ line is virtually the same for three vastly different temperature conditions i.e. 5°C, 25°C, 45°C. For instance, at 100 W/m^2 the V$_{pv\_max}$ for all three temperature conditions hover around at similar V$_{pv\_max}$ values i.e. 7.75 V, 7.65 V and 7.53 V. However, during higher irradiance of 1000 W/m^2, the R$_{pv\_seen\_max}$ line exhibits different V$_{pv\_max}$ values i.e. 36.58 V, 41.14 V and 45.7 V. This difference in V$_{pv\_max}$ is due to increase in V$_{oc}$ values as temperature falls significantly from 5°C to 25°C and 25°C to 45°C, which shifts MPP points further away. As a result, the MPP points cannot be covered even at or below 500 W/m^2 when temperature is at 5°C, which it can cover when temperature is at 45°C.

To confirm the simulation, experimental test has been conducted using the 9.4 ohm resistance as shown in Fig. 3.4. Where the upper graph shows the real-time
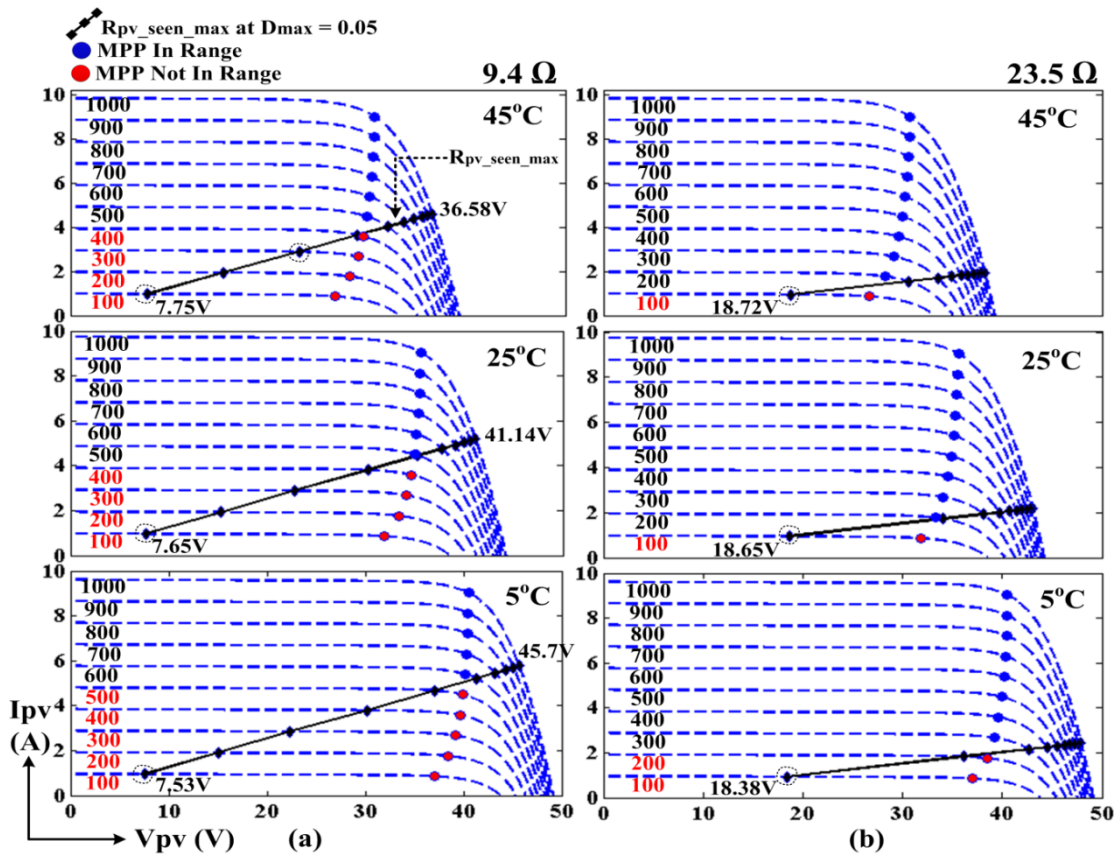
Figure 3.3 – Coverage of MPP values at D$_{max}$ = 0.05 under resistive load

sketches taken from the oscilloscope while they are translated into the lower graph for better understanding. Details of the experimental setup are described in Ch. 4. Upper graph indicates that three tests are conducted under three distinct weather conditions: a) High (I_{sc} = 9.76 A), b) Medium-high (I_{sc} = 4.91 A) and Low-medium (I_{sc} = 2.67 A), where weather conditions are differentiated based on I_{sc} values compared to I_{sc} (STC) = 8.8 A. The format of the testing is: 1) Scan the I-V curve for 10 ms using 1 mF capacitor, 2) Set the D_{min} equals to 0.95 and 3) Set D_{max} equals to 0.05. Lower graph of Fig. 3.4 contains two experimental R_{pv_seen} lines: 1) $R_{pv\_seen\_min}$ at D_{min} = 0.95 and 2) $R_{pv\_seen\_max}$ at D_{max} = 0.05, while only simulation $R_{pv\_seen\_max}$ line at D_{max} = 0.05 is mentioned. It can be seen that simulation and experimental $R_{pv\_seen\_max}$ lines at D_{max} = 0.05 virtually match each other. Furthermore, when conditions are
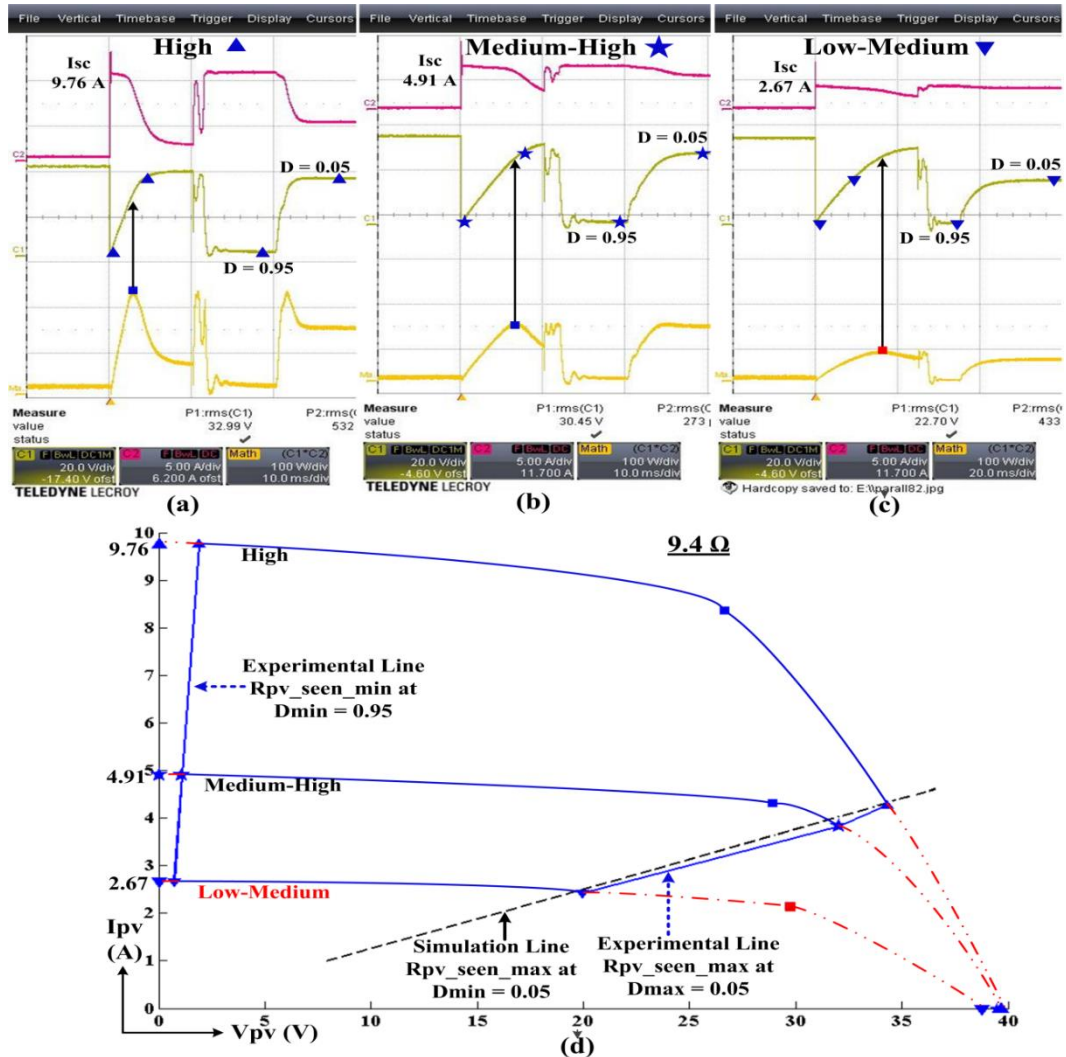
Figure 3.4 – Correlation between experimental and simulation results of PV array

26

at low-medium, the MPP cannot be captured with 9.4 ohm as confirmed by Fig. 3.4(c) and lower graph of Fig. 3.4 Thus justifying the simulation results and theoretical formulations.

On the other hand, moving towards higher resistance of 23.5 ohm as shown in Fig. 3.3(b), the situation becomes better as more MPP points are in the range of PV system, but still designer can't capture the MPP points of conditions 100 W/m^2 during 45°C, 25°C and 200 W/m^2 during 5°C. Since no significant study is present in literature, this leads towards the need of some criteria, which gives the optimal resistance such that PV system can attain MPP values under all conditions.

To obtain the optimal R$_L$ value, one thing which can be noticed from Fig. 3.3 that 23.5 ohm covers more MPP values as its V$_{pv\_max}$ value is at 18.65 V under 100 W/m^2 - 25°C compared to V$_{pv\_max}$ = 7.65 V of 9.4 ohm. The criterion is set as shown in Fig. 3.5 that R$_L$ should be configured such that V$_{mpp}$ of 1000 W/m^2 - 25°C can be attained even with the I$_{pv}$ of 100 W/m^2 - 25°C when PV is operating at D$_{max}$ = 0.05. Since the data of standard testing conditions (STC) i.e. 1000 W/m^2-25°C, is available from the Manufacturer's datasheet, the optimal R$_L$ value can be formulated as:

$$R_L = \frac{1}{(1 - D_{max})^2} \times \frac{V_{mpp}(STC)}{10\% \times I_{mpp}(STC)} \tag{3.12}$$

The above equation is the re-arrangement of Eq. (3.10). It should be noted that the value of I$_{pv}$ at 100 W/m^2 is not available in the datasheet, so 10% of I$_{mpp}$ (STC) is
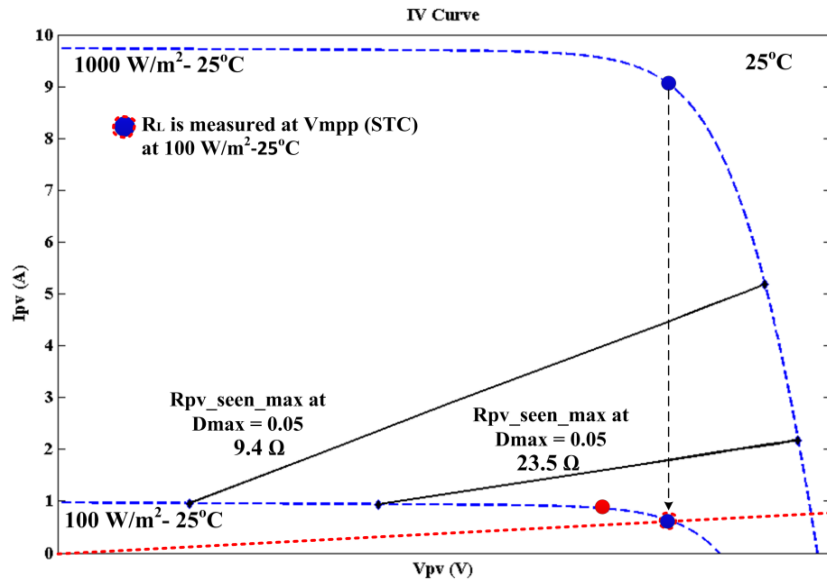
Figure 3.5 – Mechanism of optimal resistive evaluation

set for the current value. The PV array utilized in this section contains 2x2 SP configuration, which means V_{mpp} (STC) = 36.4 V and I_{mpp} (STC) = 8.8 A, the R_L can be calculated using the above equation as:

$$R_L = \frac{1}{(1-0.05)^2} \times \frac{36.4}{0.1 \times 8.8} = 46\Omega \tag{3.13}$$

Fig. 3.6 shows the experimental test (same format as of Fig. 3.4) with 47 ohm, as it is the standard value close to 46 ohm. It can be seen that each and every MPP values are in the range of the technique. To summarize the discussion, the experimental results of 9.4 ohm (Fig. 3.4) and 47 ohm (Fig. 3.6) are presented in Fig. 3.7. Which indicates that the coverage area of MPP points for 47 ohm is wider
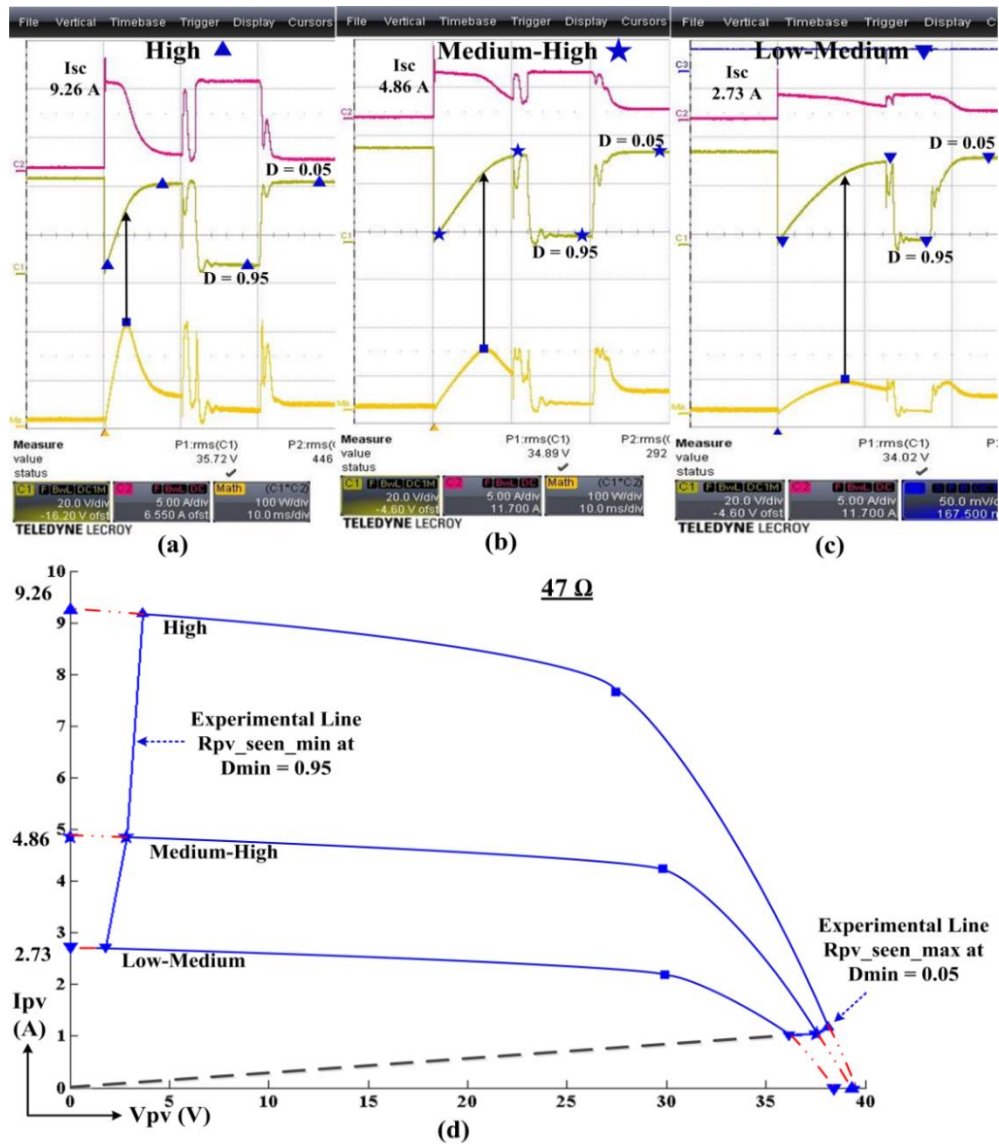
Figure 3.6 – MPP coverage of PV array using 47 ohm
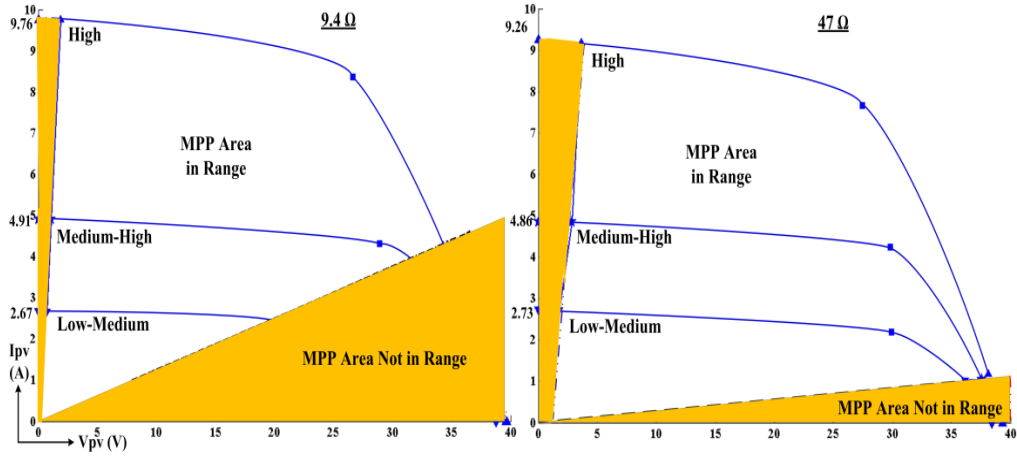
Figure 3.7 – MPP and Non-MPP areas against: a) 9.4 ohm and b) 47 ohm

compared to 9.4 ohm. It can be noticed further that when PV array is operating at D_{min} = 0.95, the non-MPP area of 47 ohm is bigger compared to 9.4 ohm. Since MPP never falls in this region, therefore it is of no interest.

3.2.2 Battery load effects

Figure 3.8 shows the simulation and experimental results under the battery load (V_B = 24 V), according to the same format as discussed in the resistive section. Since the battery provides a low impedance and absorbs all the available current, $R_{pv\_see\_max}$ line at D_{max} can be determined as:

$$V_B = \frac{1}{1-D} V_{pv} \tag{3.14}$$

$$R_{pv\_seen\_max} \Rightarrow V_{pv\_max} = (1 - D_{max})V_B \tag{3.15}$$

$$R_{pv\_seen\_max} \Rightarrow V_{pv\_max} = (1 - 0.05)V_B = 0.95 \times V_B \tag{3.16}$$

The above equation expresses that under battery load, $R_{pv\_seen\_max}$ line is determined by the battery voltage (V_B). Since V_B is almost constant, the $R_{pv\_seen\_max}$ line is almost straight when PV array is operating at D_{max} = 0.05. Which can be confirmed from Fig. 3.8(a) as $R_{pv\_seen\_max}$ line is straight under all kinds of conditions. Furthermore, it can be evaluated that $R_{pv\_seen\_max}$ line always sticks to the V_{pv} nearly equals to 24 V as battery of V_B = 24 V is utilized, which means that we cannot go beyond this voltage thus missing all the MPPs. Fig. 3.8(e) shows that the simulation line and experimental line matches each other when PV array is operating at D_{max} =

0.05 and further reveals that all MPP are missed as well. Which can be confirmed from experimental results shown in Fig. 3.8(c),(d),(e) that the MPPs of distinct weather are not in the range. Since, I_{pv} is not producing any major influence during battery loads, hence criterion is easy to set:

$$V_B = \frac{1}{1-D_{max}} V_{mpp}(STC) \Leftrightarrow T \geq 25^oC \qquad (3.17)$$

$$V_B = \frac{1}{1-D_{max}} V_{mpp}(T) \Leftrightarrow T < 25^oC \qquad (3.18)$$

It should be noted that unlike $R_{pv\_seen\_max}$ line of resistive load, the nature of $R_{pv\_seen\_max}$ line of battery load is straight as it only depends upon the battery voltage i.e. V_B. Therefore, when temperature becomes higher than 25°C, it will reduce the V_{oc} values. Consequently, MPP values occur at V_{pv} values less than $V_{mpp}(STC)$. On
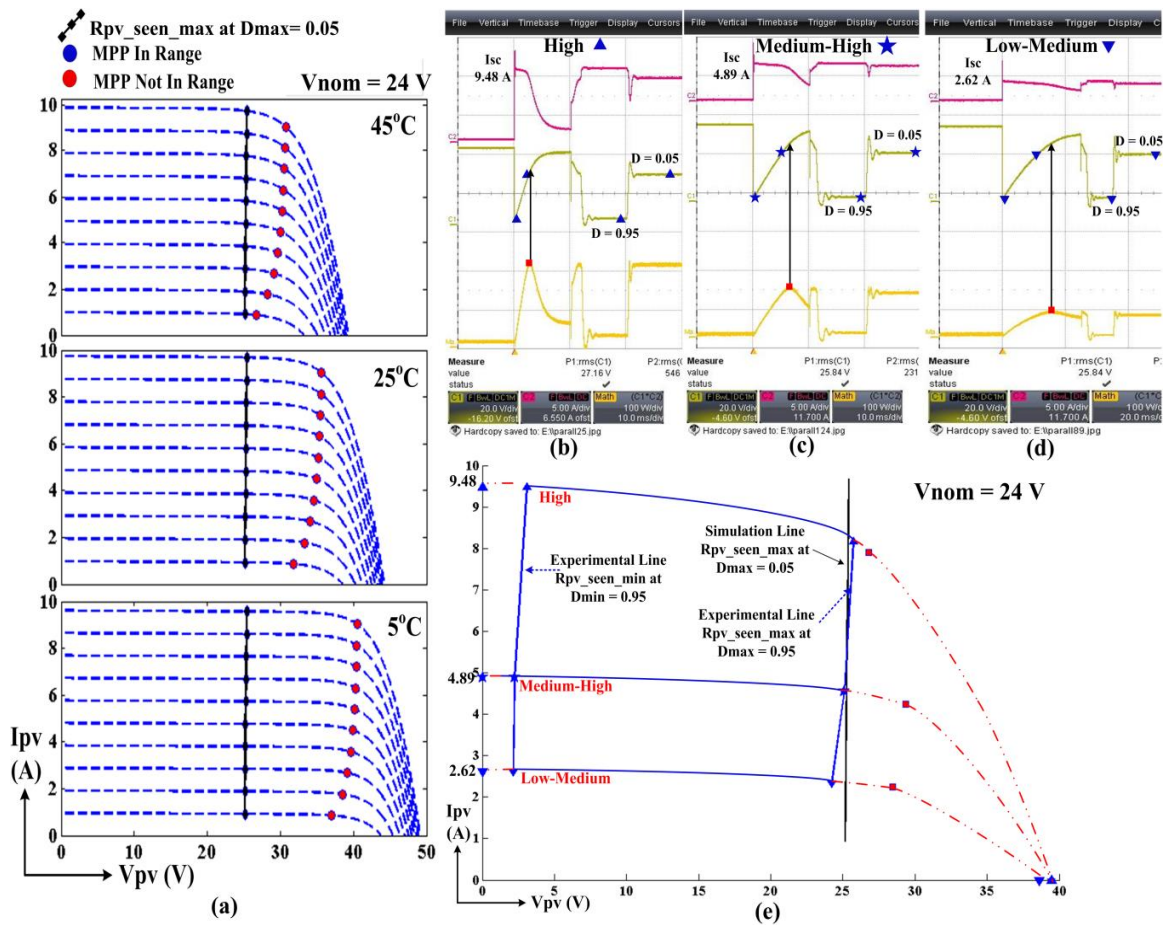
Figure 3.8 – Simulation and experimental results of MPP coverage using battery of $V_B = 24$ V

the other hand, when T < 25°C, the V_{oc} values become high which means that MPP points occur at V_{pv} values greater than $V_{mpp}(STC)$. To address this issue, $V_{mpp}(T)$ is introduced in Eq. (3.18) when T < 25°C, which can be found out as [52]:

$$V_{mpp}(T) = V_{mpp}(STC) + K_{Voc}\Delta T \qquad (3.19)$$

Where, K_{Voc} is the temperature coefficient of open-circuit voltage that can be obtained from Manufacturer's datasheet. Furthermore, to guess the change in temperature ΔT, the metro-graphical data of the location may be needed. However, for locations where temperature normally hovers around 25°C, the criterion can be set with $D_{max} = 0.25$ instead of $D_{max} = 0.05$ to be on the safer side. PV array used in this
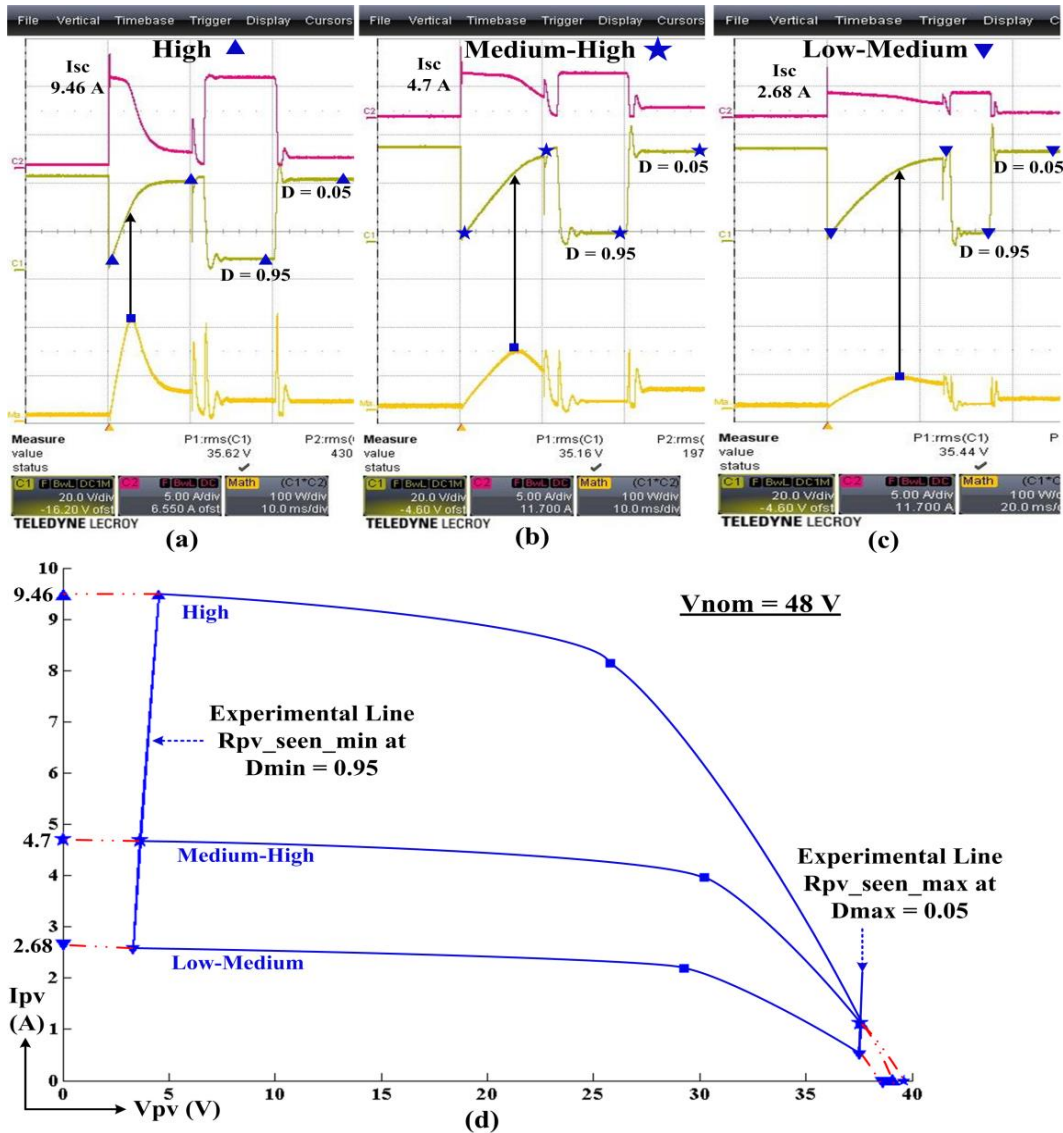
Figure 3.9 – Experimental validation of MPP coverage using battery of $V_B = 48$ V

section contains V_{mpp} (STC) = 36.4 V, therefore V_B is calculated as:

$$V_B = \frac{1}{1 - D_{max}} V_{mpp}(STC) = \frac{1}{1 - 0.25} \times 36.4 = 48.5\ V \qquad (3.20)$$

Battery with nominal voltage V_B = 48 is utilized with the PV array. Fig. 3.9 shows the experimental results at three different irradiance levels, which can be confirmed from real-time sketches shown in Fig. 3.9 (a),(b) and (c). Lower graph illustrates the R_{pv_seen} lines at D_{min} = 0.95 and D_{max} = 0.25. It can be seen that all the MPP points are captured. Fig. 3.10 illustrates the MPP area while working with two battery loads: 1) V_B = 24 V and 2) V_B = 48 V.
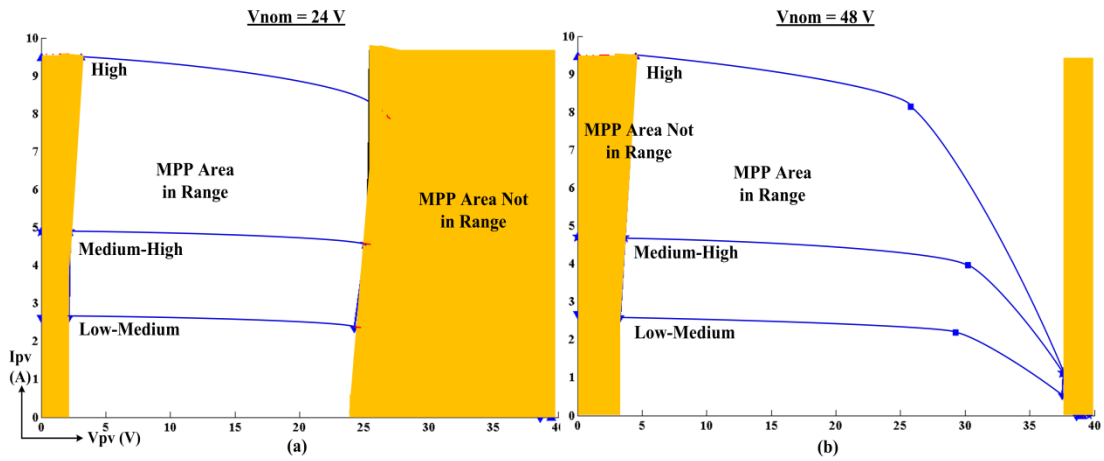
Figure 3.10 – MPP and Non-MPP areas against: a) V_B = 24 V and b) V_B = 48 V

Chapter 4

Design, diagnosis and validation of MPPT for uniform weather conditions

This chapter initially gives the critical overview about the state of the art MPPTs present in literature for uniform conditions and highlights the drawbacks present in these MPPTs. In view of these drawbacks, a novel technique is designed which is explained in this chapter. Furthermore, the technique has been modeled in MATLAB/Simulink to conduct the simulation studies and comparative analysis has been conducted. Finally, the effectiveness of the proposed technique is proved experimentally. Both simulation and experimental results confirm that the proposed MPPT outperforms the past-proposed MPPTs.

4.1 MPPTs for uniform conditions – A literature survey

PV array executes the unique maximum power point (MPP) on its current-voltage (I-V) curve [47]. Since the I-V characteristic of PV array changes non-linearly with weather conditions, i.e. irradiance and temperature, consequently the MPP varies. Considering the high initial capital cost of a PV system along with its low conversion efficiency [16], it is essential to operate the PV array at MPP on consistent basis [47]. In order to tackle this challenge, the maximum power point tracking (MPPT) technique is employed in PV system, which works in combination with DC-DC converter as already described in Ch. 2.

Till date, numerous MPPT techniques have been designed and some of them are surveyed by [17,23]. Many MPPT designers took the assistance from advanced control schemes like Takagi–Sugeno model based fuzzy control is used in [53] and fuzzy cognitive networks are employed with fuzzy logic control in [54]. While

particle swarm optimization based MPPT is adopted in [52]. The major drawbacks of these techniques are that they require complex optimization schemes and may require prior training procedures. However, it can be concluded from the surveys conducted by [17,23], that perturb and observe (P&O) is the most widely used technique because of its simplicity, ease of implementation and yet exhibits satisfactory performance [55]. However, it is widely reported that P&O may struggle with varying weather conditions and always produces power loss oscillations around MPP in steady weather conditions [45,56]. As a result, P&O needs to be optimized in order to remove deficiencies inherited by P&O [55].

Several techniques have been developed in the past to optimize the P&O. In [57], the algorithm is improved with the current-based sliding control. However, to tackle with fast varying irradiance, this technique utilizes another appropriate voltage compensation loop, which makes the algorithm complex. Similarly, a complex procedure of fuzzy logic control is adopted to optimize P&O in [58]. In another work [59], the adaptive perturb is calculated for the P&O using the two successive power signals. This technique achieves better performance compared to P&O but requires two PI controllers. One for the soft computing to calculate the adaptive perturb and the other one for the hard computing i.e. duty cycle of the converter. Optimization process of two PI controllers at the same time increases the implementation cost of this MPPT technique.

On the other hand, several MPPT techniques took the hybrid approach to enhance the performance of P&O [45,60-63]. In [60], the technique samples the open-circuit voltage (V_{oc}) and short circuit current (I_{sc}) to decide the MPP. However, the information regarding the procedure to measure V_{oc} and I_{sc} is missing. Techniques [45,61-63] have been based on the combination of P&O and V_{oc} techniques. Techniques [61-62] measure V_{oc} to estimate the V_{mpp} but did not adopt any strong strategy for the D of the converter i.e. hard computing. In another work [63], a new relation is developed to estimate V_{oc} using temperature sensing and adopts a PI controller for hard computing. Although this technique does not require the shedding of PV array from the load but cost of temperature sensors along with the sensitivity of temperature is a major issue for this technique. Nevertheless, according to

comparative study presented in [27], this technique has been declared as the most efficient one. During the work of this thesis, a new technique has been developed [45], which contains two new relations for the D of the converter, and achieves better performance compared to MPPT [63]. This technique measures the V_{oc} to calculate V_{mpp} and formulates I_{mpp} through I_{sc} estimation. Since the estimation of I_{sc} is achieved with moderate accuracy, this technique takes help from PI controller to adjust D.

4.2 Salient features of the proposed MPPT and test setups

Considering these drawbacks, this chapter presents a new hybrid MPPT technique, which is a combination of P&O and V_{oc} techniques. The main aim is to improve the energy harvesting of PV array by enhancing the dynamic (varying weather) and steady (static weather) performances of the technique compared to past proposed MPPTs and simultaneously, avoid the complex control schemes. The salient features of the proposed MPPT, which gives it an edge over previous techniques, are as follows:

- V_{mpp} is calculated by measuring V_{oc} of the PV array with a proper clue of duration of V_{oc} measurement.
- New relation is developed to estimate I_{mpp} without measuring the I_{sc} of PV array.
- With the assistance of V_{mpp} and $I_{mpp,}$ a duty cycle (D_{mpp}) relation is developed for the converter. This will eliminate the need to use any control schemes (PI/PID etc.)
- Frequency of V_{oc} measurement ($V_{oc,freq}$) is identified. Based on $V_{oc,freq}$, the criterion is defined with respect to sampling rate (Sa_{rate}) of the PV system which will decide when to measure V_{oc} under varying weather conditions.
- Effects of weather conditions on PV array are evaluated under resistive and battery loads, and limits criteria are computed to judge the steady weather conditions.
- The control algorithm is designed in such a manner that the technique should not produce any power loss oscillations around MPP during steady weather

conditions. At the same time, the MPP tracking of the technique will be fast under varying weather conditions.

For comparative analysis, the proposed technique and other MPPTs are modeled in MATLAB/Simulink using the PV array model [29]. Since the PV array model is developed with Kyocera KC200GT module [30], same module is utilized for simulations and the array of 2x6 is used in the form of serial-parallel (S-P) configuration. Finally, the experimental tests are conducted comprehensively for the proposed technique and P&O under two kinds of loads, i.e. resistive and battery, and their respective performances are analyzed. In the experimental setup, the PV module FVG 36-125 is used [31] with an array of 2x2 S-P configuration. It should be noted that a new hybrid MPPT technique presented in this chapter is the improved version of technique [45]. However, all the designing aspects of technique have been described in detail in this chapter.

4.3 Fundamental relations of the proposed MPPT technique

There are five main fundamental relations of the proposed technique: 1) V_{mpp}, 2) I_{mpp}, 3) D_{mpp}, 4) criteria for varying weather conditions and 5) limits criteria for steady weather conditions. The last two criteria are formulated in the next section. A typical I-V curve is shown in Fig. 4.1, which shows that the V_{mpp} and I_{mpp} can be calculated from the following two relations:

$$V_{mpp} = K_v V_{oc} \qquad\qquad (4.1)$$

$$I_{mpp} = K_i I_{sc} \qquad\qquad (4.2)$$

Where, K_v and K_i are the proportionality constants of voltage and current respectively. It is worth noting that proposed MPPT always contains the updated information of K_v and K_i, which is explained later in detail the Sec. 4.5.

4.3.1 V_{mpp} calculation

For the accurate calculation of V_{mpp} through Eq. (4.1), the proposed technique measures open-circuit voltage of the PV array. Since V_{oc} measurement requires the
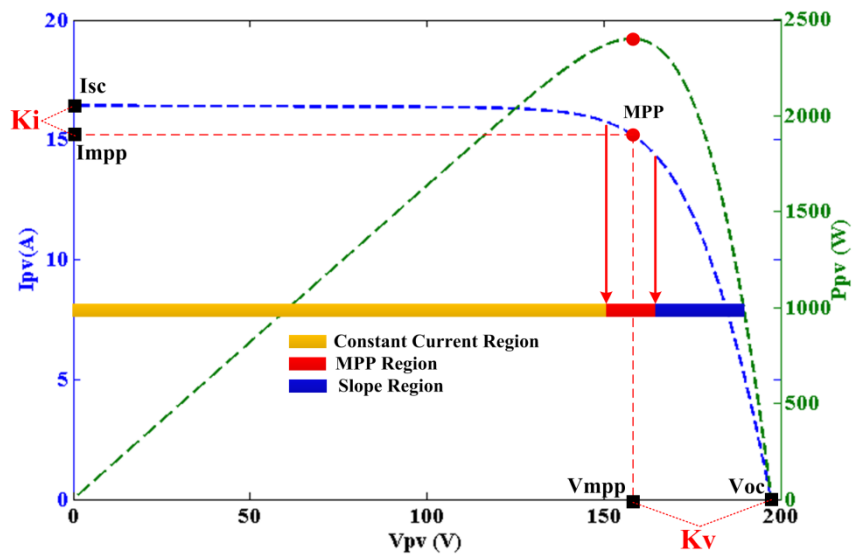
Figure 4.1 – MPP of PV array with respect to V_{oc} and I_{sc}

PV array to be separated from the load, which offers loss of power, duration of V_{oc} measurement is critical. For this, the PV system setup shown in Fig. 4.2 is implemented in the experimental setup, details of which are explained in Sec. 4.4.7. It can be seen from Fig. 4.2 that that the PV array can be disconnected from the load using a fast switching device (S2). Although numerous papers, for instance [45,60-62], have been utilized the V_{oc} of the array in their respective algorithms. However, the experimental evaluation of the behavior of PV array when it is separated from the load, using a fast switch, is limited.

Fig. 4.3 shows the experimental curves of the PV array, where it is operating at D = 90% until it is disconnected from the load at 'Arrow-1' position using a switch (n-Mosfet). Consequently, it can be seen that the I_{pv} to the load immediately becomes
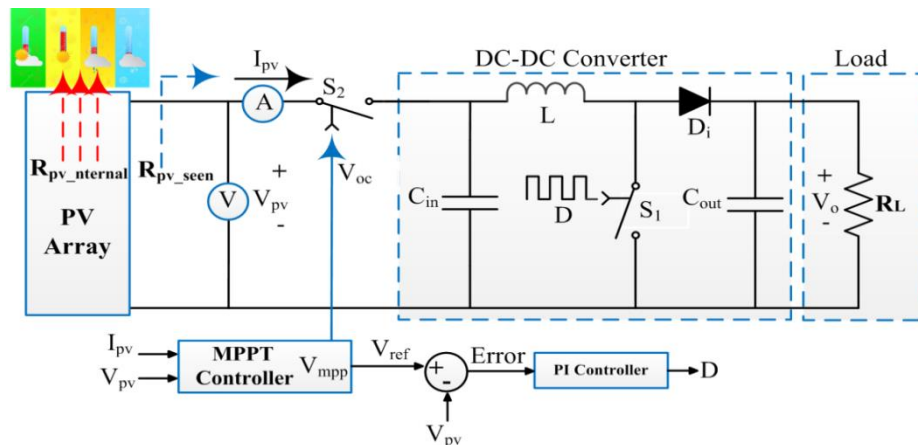
Figure 4.2 – Modified PV system architecture to measure V_{oc}
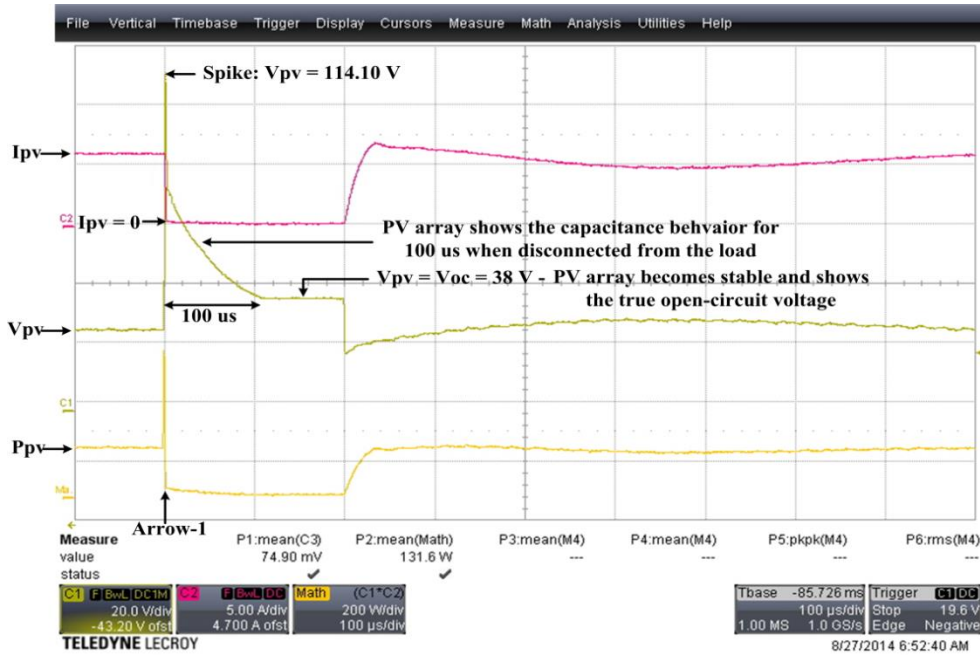
Figure 4.3 – Experimental test of duration of V_{oc} measurement

equal to zero while V_{pv} shoots up and executes a spike of 114.4 V. Nearly after 100 μs, V_{pv} settles down to the true V_{oc} of 38 V. Since the outgoing I_{pv} is immediately terminated with the switch, the PV array depicts the capacitive behavior due to its internal physics. It can be concluded that the designer cannot measure the V_{oc} immediately and has to wait for atleast 100 us after disconnecting the PV array. To be on the safe side, the proposed technique measures V_{oc} after 200 us, whenever needed.

4.3.2 I_{mpp} estimation

It is cleared from the previous section that the proposed technique already offers the loss of power during V_{oc} measurements. Hence, the main aim is to estimate the I_{mpp} with reasonable accuracy without short-circuiting the PV array as short-circuit also offers power loss. Consider the practical PV model shown in Fig. 4.4, which can be expressed in mathematical form as [29]:

$$I_{pv} = I_{ph} - I_s(\exp(\frac{V_{pv} + I_{pv}R_s}{V_T}) - 1) - \frac{V_{pv} + I_{pv}R_s}{R_p} \tag{4.3}$$

Where, I_{ph} is the photocurrent produced by the PV array due to incident sunlight, I_s is the reverse saturation current, V_T is the thermal voltage, R_s and R_p are the equivalent series and parallel resistances of the array respectively.
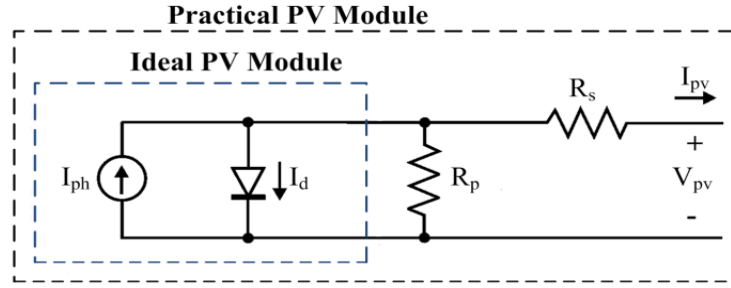
Figure 4.4 – Equivalent circuit: Ideal and practical PV module

In order to consider the above equation, information of R_s and R_p is required, which is difficult to attain [29]. Therefore, to estimate the I_{mpp}, the proposed work considers the ideal single diode model as shown in Fig. 4.4, which neglects the influence of R_s and R_p [61,63]:

$$I_{pv} = I_{ph} - I_s(\exp(\frac{V_{pv}}{V_T}) - 1) \tag{4.4}$$

Assuming the I_{ph} equals to the I_{sc} and since the exponential factor is very large even with small forward voltage, factor '-1' can be neglected. Hence, Eq. (4.4) can be simplified as:

$$I_{pv} = I_{sc} - I_s(\exp(\frac{V_{pv}}{V_T})) \tag{4.5}$$

In the above equation, the major challenge is to deal with I_{sc}, I_s and V_T. To tackle the I_s, we know that at open-circuit voltage, i.e. $V_{pv} = V_{oc}$, I_{pv} is equal to zero which can be seen from Fig. 4.1, therefore Eq. (4.5) can be written as:

$$I_{sc} = I_s(\exp(\frac{V_{oc}}{V_T})) \tag{4.6}$$

Re-arranging the Eq. (4.6), we can get I_s:

$$I_s = I_{sc}(\exp(-\frac{V_{oc}}{V_T})) \tag{4.7}$$

Putting I_s from the above equation in Eq. (4.5), we get:

$$I_{pv} = I_{sc}(1 - \exp(\frac{V_{pv} - V_{oc}}{V_T})) \tag{4.8}$$

In Eq. (4.8), I_s is eliminated. To deal with V_T, consider that the PV array is

operating at MPP i.e. $I_{pv} = I_{mpp}$ and $V_{pv} = V_{mpp}$, therefore the above equation can be re-iterated as:

$$I_{mpp} = I_{sc}(1 - \exp(\frac{V_{mpp} - V_{oc}}{V_T})) \tag{4.9}$$

Re-arranging the Eq. (4.9), V_T can be found out as:

$$V_T = \frac{V_{mpp} - V_{oc}}{\ln(1 - \frac{I_{mpp}}{I_{sc}})} \tag{4.10}$$

Putting the value of V_T from the above equation in Eq. (4.8), we get

$$I_{pv} = I_{sc}(1 - \exp(\frac{(V_{pv} - V_{oc})\ln(1 - \frac{I_{mpp}}{I_{sc}})}{V_{mpp} - V_{oc}})) \tag{4.11}$$

We know that $V_{mpp} = K_v V_{oc}$, $I_{mpp} = K_i I_{sc}$ and $I_{sc} = I_{mpp}/K_i$, therefore putting these relations in Eq. (4.11), we get

$$I_{pv} = \frac{I_{mpp}}{K_i}(1 - \exp(\frac{(V_{pv} - V_{oc})\ln(1 - K_i)}{V_{oc}(K_v - 1)})) \tag{4.12}$$

Re-arranging the above equation for I_{mpp}, we get

$$I_{mpp} = \frac{K_i\, I_{pv}}{1 - \exp(\frac{(V_{pv} - V_{oc})\ln(1 - K_i)}{V_{oc}(K_v - 1)})} \tag{4.13}$$

It should be noted that the technique always contains the updated information of K_i and K_v, V_{oc} (by disconnecting the array) and V_{pv}, I_{pv} (through sensors). Hence, Eq. (4.13) can be viewed as the benchmark equation to estimate the I_{mpp} for any given operating point (V_{pv}, I_{pv}) of the PV array.

Eq. (4.13) reveals that the role of K_i and K_v is important for the accurate estimation of I_{mpp}. Therefore, consider the Table 4.1 in which K_i and K_v values of the PV array are evaluated in MATLAB/Simulink using the comprehensive PV model [29] against various weather conditions. As already described in the Sec. 4.2 that for simulations, the PV array contains 2x6 S-P arrangement and Kyocera KC200GT module is used.

It can be seen that the variation in the values of K_i for different conditions is almost negligible while the variation in K_v values is comparatively large. This is also

Table 4.1 – K_i and K_v variations with weather conditions

Weather Conditions		K_i Variations			K_v Variations		
Irradiance (W/m²)	Temperature (°C)	I_{sc}	I_{mpp}	K_i	V_{oc}	V_{mpp}	K_v
500	20	8.196	7.593	0.926	193.58	159.03	0.822
600	21	9.838	9.114	0.926	194.786	159.374	0.818
700	22	11.483	10.65	0.928	195.697	159.138	0.813
800	23	13.128	12.176	0.928	196.394	158.833	0.808
900	24	14.775	13.701	0.927	196.928	157.5	0.799
1000	25	16.423	15.227	0.927	197.334	157.5	0.799

one of the facts, which prompts this work to measure V_{oc} from the PV array, rather than estimate it, as K_v is evaluated from the ratio of V_{mpp} and V_{oc}, once MPP is reached. Table 4.1 further helps in the designing of algorithm that K_v values should be updated more frequently compared to K_i, the details of this mechanism are discussed during the designing of algorithm later in Sec. 4.4.5.

Work done in [45] also presented the method to estimate I_{mpp}, which is compared with the proposed I_{mpp} estimation. Both estimations of I_{mpp} are evaluated under various weather conditions using the same simulation setup [29]. Error is calculated using the standard relation, i.e. V_{mpp} - V_{pv}. Depending upon the nature (+/-) of Error, Table 4.2 is divided into two sections as shown in Fig. 4.5: 1) Error is positive, which means that the PV array is operating at V_{pv} less than V_{mpp} i.e. constant current region and 2) Error is negative, which means that the PV array is operating at
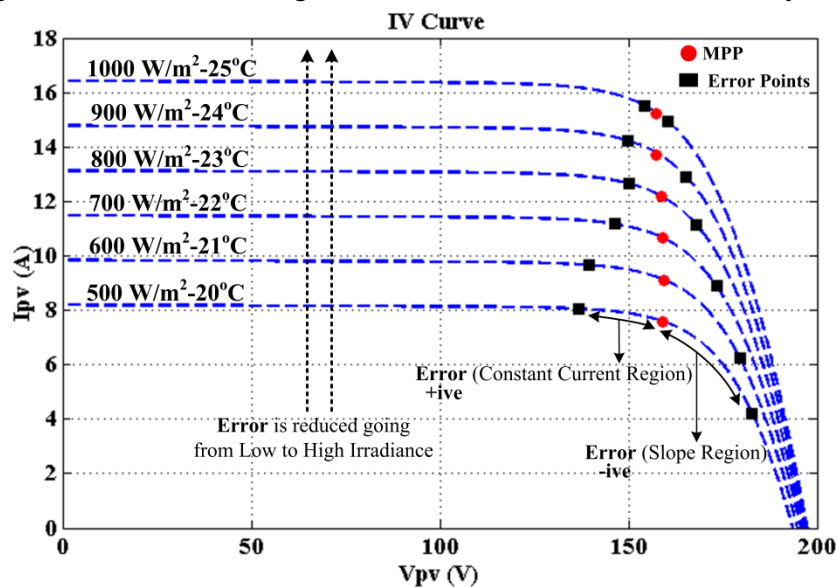
Figure 4.5 – Effect of error variations in weather conditions to evaluate I_{mpp} values

V_{pv} greater than V_{mpp} i.e. slope region. To have a broader overview, the values of I_{mpp} for both techniques are estimated at wider range of operating voltage (V_{pv}) values. It can be seen from Table 4.2 that at weather condition 500 W/m^2 - 20°C, the V_{pv} is deliberately set at point (away from MPP) which gives the error of +22.1 V for constant current region and -23.82 V for a slope region. As we move towards higher irradiance levels, the V_{pv} has brought closer to V_{mpp} like for weather conditions 1000 W/m^2 - 25°C, the error hovers around 3 V for both regions, which can be confirmed from Fig. 4.5. Finally, the difference between the ideal I_{mpp} (Id. I_{mpp}) and estimated I_{mpp} (Est. I_{mpp}) of both techniques are displayed against each operating voltage for both regions in Table 4.2.

Table 4.2 confirms the trends that work presented in [45] offers more error in I_{mpp} estimation than the proposed I_{mpp} estimation. For constant current region, the operating voltages are not making a major difference as both techniques exhibit similar trends in error in their respective I_{mpp} estimations. Like I_{mpp} of the proposed technique moves between 0.003 A (min) to 0.04 A (max). However, method [45] gives relatively higher error in I_{mpp} estimation compared to proposed technique, i.e. 0.266 A (min) and 0.456 A (max). On the other hand, the operating voltages make the considerable impact as far as the slope region is concerned. It can be seen that as the error reduces from conditions 500 W/m^2 - 20°C to 1000 W/m^2 - 25°C i.e. V_{pv} becomes close to V_{mpp}, the error in I_{mpp} estimation for both techniques is also reduced. However, in this region, the method presented in [45] generates the significant error in

Table 4.2 – I_{mpp} estimations of the proposed technique and technique [45]

Weather Conditions		Ideal MPP Parameters		Error: V_{mpp}-V_{pv} = +ive (Contant Current Region)			Error: V_{mpp}-V_{pv} = -ive (Slope Region)		
Irr. W/m^2	T. ^{o}C	V_{mpp} V	I_{mpp} A	Error wrt V_{mpp}	Proposed | Id. I_{mpp}-Est. I_{mpp}|	Work [45] |I_{mpp}-Est. I_{mpp}|	Error wrt V_{mpp}	Proposed |I_{mpp}-Est. I_{mpp}|	Work [45] |I_{mpp}-Est. I_{mpp}|
500	20	159.03	8.196	+22.1	0.013	0.456	-23.82	0.678	5.962
600	21	159.374	9.838	+19.81	0.003	0.534	-20.24	0.792	5.335
700	22	159.138	11.483	+12.73	0.036	0.521	-14.22	0.336	3.898
800	23	158.833	13.128	+8.63	0.05	0.470	-9.097	0.211	2.538
900	24	157.5	14.775	+7.6	0.11	0.5245	-7.7	0.092	2.328
1000	25	157.5	16.423	+3.1	0.04	0.266	-3.087	0.114	0.889

I_{mpp} estimation. For instance, at conditions 500 W/m^2-20°C (Error from V_{mpp} is -23.82 V), the method [45] estimates the I_{mpp} which is almost 6 A at drift of ideal I_{mpp}. While, the proposed technique executes the marginal errors in I_{mpp} estimation in slope region.

4.3.3 D_{mpp} estimation

To formulate the D_{mpp} of the proposed technique, the relation is developed for the boost converter. However, the same approach can be followed to find out the D relations for other types of DC-DC converters (buck, buck-boost etc). As already discussed in Chapter 3, PV array delivers the maximum power when the load resistance (R_L) matches the internal impedance ($R_{pv\_internal}$) of the array. Since $R_{pv\_internal}$ varies with weather conditions and R_L will not change accordingly, MPPT designers plug the DC-DC converter between the PV array and the load (R_L) as shown in Fig. 4.2. Through this mechanism, R_L can be varied by changing the D which is reflected at the input side of the converter, i.e. impedance seen by the PV module (R_{pv_seen}). If D is not optimized, R_{pv_seen} will not match the $R_{pv\_internal}$ due to which the PV array will not operate at MPP as indicated in Eq. (4.14):

$$R_{pv\_seen} = (1 - D)^2 R_L \Rightarrow R_{pv\_seen} \neq R_{pv_{internal}} (Non - MPP) \qquad (4.14)$$

At optimum duty cycle (D_{mpp}), R_{pv_seen} (in which R_L is reflected) becomes equal to the $R_{pv\_internal}$ of the PV array. Consequently, PV array starts operating at the voltage (V_{mpp}) which delivers the maximum power. This phenomenon is indicated in Eq. (4.15):

$$R_{pv\_seen} = (1 - D_{mpp})^2 R_L \Rightarrow R_{pv\_seen} = R_{pv\_internal} (MPP) \qquad (4.15)$$

Re-arranging the Eqs. (4.14) and (4.15) according to R_L and simultaneously, translating them into voltage/current form as:

$$R_L = \frac{1}{(1 - D)^2} \frac{V_{pv}}{I_{pv}} \Leftrightarrow Non - MPP \qquad (4.16)$$

$$R_L = \frac{1}{(1 - D_{mpp})^2} \frac{V_{mpp}}{I_{mpp}} \Leftrightarrow MPP \qquad (4.17)$$

Since Eq. (4.17) is an MPP equation, so R_{pv_seen} is translated into MPP

variables (V_{mpp}/I_{mpp}) while Eq. (4.16) contains the non-MPP variables (V_{pv}/I_{pv}). Assuming the R_L to be constant [45], Eqs. (4.16) and (4.17) can be combined to find D_{mpp} as:

$$D_{mpp} = 1 - ((1-D)\sqrt{\frac{V_{mpp} \, I_{pv}}{V_{pv} \, I_{mpp}}})$$ (4.18)

Eq. (4.18) can be understood as for present weather condition, the technique estimates the V_{mpp} and I_{mpp} and stores them in memory. While D is the present duty cycle which determines the present operating point (V_{pv},I_{pv}) of the array. MPPT designer can get the D, V_{mpp} and I_{mpp} from memory and V_{pv}, I_{pv} from sensors and therefore able to set the PV operating point of the next iteration from Eq. (4.18). It can be noticed that when PV array starts operating at MPP i.e. $V_{mpp} \approx V_{pv}$ and $I_{mpp} \approx I_{pv}$, the Eq. (4.18) is transformed into the form D_{mpp} = D.

We have already derived the relations for I_{mpp} as expressed by Eq. (4.13) and V_{mpp} can be calculated with the help of Eq. (4.1). Putting them into Eq. (4.18), we get

$$D_{mpp} = 1 - (\,(1-D)\sqrt{\frac{K_v V_{oc}(1 - \exp(\frac{(V_{pv} - V_{oc})\ln(1 - K_i)}{V_{oc}(K_v - 1)}))}{K_i V_{pv}}})$$ (4.19)

Eq. (4.19) defines the optimum duty cycle relation of the proposed technique. Since this relation is obtained by inducting the I_{mpp} and V_{mpp}, proposed technique will only formulate this relation in its operation. Furthermore, Eq. (4.19) requires the values of K_v, K_i,V_{oc} and V_{pv}. The proposed MPPT always contains the values of these parameters, which is explained later in Sec. 4.5.

It should be noted that both proposed technique and technique [45] utilize the V_{mpp} and I_{mpp} in calculating the D_{mpp} of the converter. It can be realized from the discussion in Sec. 4.3.2 (Table 4.2) that since the I_{mpp} estimation of technique [45] is not very precise, especially when the errors are on the higher side, this technique also takes the services of PI controller to adjust the D_{mpp} in order to make V_{pv} close to V_{mpp}. However, the proposed technique estimates the I_{mpp} with negligible errors in constant current region and marginal errors in slope region as indicated in Table 4.2, as a result it will not take the assistance from PI controller. This, in turn, benefits the

algorithm not to use the complex control schemes to tune the PI controller. Thus making the complexity of the algorithm low.

4.4   Basic algorithm, weather conditions and sampling rate

4.4.1   Basic algorithm

Figure 4.6 shows the basic outline of the control algorithm, which contains three loops: 1) E-MPP loop, 2) R-MPP loop and 3) S-loop. E-MPP loop contains the D_{mpp} relation expressed in Eq. (4.19) in order to set the V_{pv} of PV array near MPP vicinity i.e. MPP region. Since D_{mpp} relation is developed from I_{mpp} and V_{mpp} estimations, it may not set the PV array at MPP precisely. Therefore, E-MPP loop is known as the estimated MPP loop. After that, the algorithm enters into R-MPP, which is the real MPP loop. It contains the modified P&O algorithm, which will tune the D_{mpp} further to set the PV array at MPP accurately. Then the algorithm proceeds into S-loop known as the stable loop. Since the algorithm enters in this loop when PV array is operating at MPP, the algorithm holds the operating point of PV array at MPP until the weather condition changes. Whenever condition changes, the algorithm returns back to E-MPP loop and the whole process is re-initiated to search the new MPP according to new conditions. Hence, the dynamic and steady response of the technique can be figured out as:

- Dynamic response: E-MPP and R-MPP loops define the dynamic response
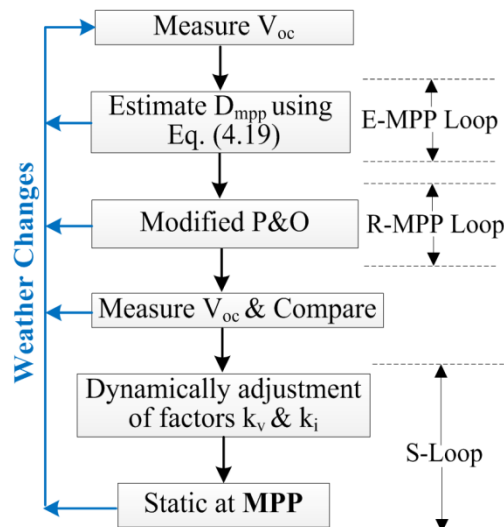
Figure 4.6 – Basic outline of the proposed MPPT

of the proposed MPPT as these two loops are responsible: 1) to focus the MPP according to present weather condition as quickly as possible and 2) hover around the MPP points during continuous varying weather conditions.

- Steady response: S-loop defines the steady response of the proposed MPPT i.e. to stick to the MPP until weather condition changes.

4.4.2   Evaluation of weather conditions

The proposed MPPT will evaluate the weather condition in two different ways. One is during dynamic operation (E-MPP/R-MPP loops) and other one is during steady operation (S-loop).

4.4.2.1 Weather evaluation - E-MPP/R-MPP loops

Since the weather condition (irradiance and temperature) reflected in V_{oc} of the PV array, the technique takes the idea of environment from V_{oc} value. Fig 4.6 shows that the technique always measures the V_{oc} at two instants: 1) before entering into the E-MPP loop such that the relations of proposed MPPT are adjusted according to present weather conditions using V_{oc} and 2) after leaving the R-MPP loop, the V_{oc} is measured again and compare it with the previous sampled V_{oc} to access that weather condition changes or not.

However, it is quite possible that the technique still working in its E-MPP/R-MPP loops and weather condition changes i.e. fast varying weather conditions. Since V_{oc} measurement takes 200 us which offers the loss of power, the real challenge is to identify the frequency of V_{oc} measurement ($V_{oc,freq}$). Hence, the hint regarding the time constant ($T_{Weather}$) during which weather remains the same becomes critical. It has been reported by [64] that the rate of change of weather conditions cannot be faster than 100 ms (0.1 s). Therefore, the $V_{oc,freq}$ is set at 100 ms. After every 100 ms during E-MPP/R-MPP loops, the technique measures V_{oc} regardless of weather conditions. Furthermore, considering the 0.2 ms ($V_{oc,meas}$ = 200 us) loss of power per 100 ms ($V_{oc,freq}$ = 100 ms) during fast varying conditions, the advantage expected to be gained by closing the gap to the MPP not only covers the loss power of 0.2 ms but also gives the improved efficiency.

4.4.2.2   Weather evaluation – S-loop

In S-loop, the proposed technique holds the MPP courtesy D_{mpp} settled by R-MPP/E-MPP loops. The real aim in this loop is to evaluate the weather conditions (static or changed) without measuring the V_{oc} value as it offers the loss of power. Hence, the technique will set the limit criteria for I_{pv} and V_{pv} such that if PV array crosses these limits, the technique understands that the conditions are changed and restart the process. In order to set the limits, the behavior of PV array is carried out by performing the experiments using two loads: 1) Resistive Load of 47 Ω and 2) Battery with nominal voltage of 48 V. Details of experimental setup are mentioned in Sec. 4.7.

Resistive load (47 Ω): Upper graphs of Fig. 4.7 show the real time sketches of experiments using sophisticated oscilloscope. While they are translated into lower graphs for the better understanding of MPPT designers. Initially, D_{mpp} is set at 0.741 (74.1%) to attain the $V_{mpp} = 26.97$ V at high irradiance as shown in the lower graph of Fig. 4.7(a). While Fig. 4.7(b) shows that in order to operate the PV array at $V_{mpp} = 28.90$ V when irradiance is low, D_{mpp} becomes equal to 0.629 (62.9%). It can be noticed that the difference between two V_{mpp} values is just 1.93 V but the difference in D_{mpp} values of two cases is significant i.e. 11.2%. This behavior of PV array under resistive load can be understood from the Eq. (4.20), which is the re-arranged form of Eq. (4.17):

$$D_{mpp} = 1 - \sqrt{\frac{1}{R_L} \times \frac{V_{mpp}}{I_{mpp}}} \Rightarrow R_{pv\_seen} = (1 - D_{mpp})^2 R_L \qquad (4.20)$$

Eq. (4.20) expresses that if R_L and V_{mpp} remain at similar values but I_{mpp} changes significantly i.e. $I_{mpp} = 7.647$ A (high irradiance shown in Fig. 4.7(a)) and $I_{mpp} = 4.475$ A (low irradiance shown in Fig. 4.7(b)), this will change the D_{mpp} significantly. Which in turn brings the notable change in the load line seen by the PV array (R_{pv_seen}). That's why, R_{pv_seen} lines are entirely different for two cases even the V_{mpp} values of two cases are close as shown in Fig. 4.7.

Fig. 4.7(a) further reveals that after attaining the MPP at high irradiance level, the conditions fall to low irradiance ($I_{sc} \approx 4.728$ A) while the PV array is operating at
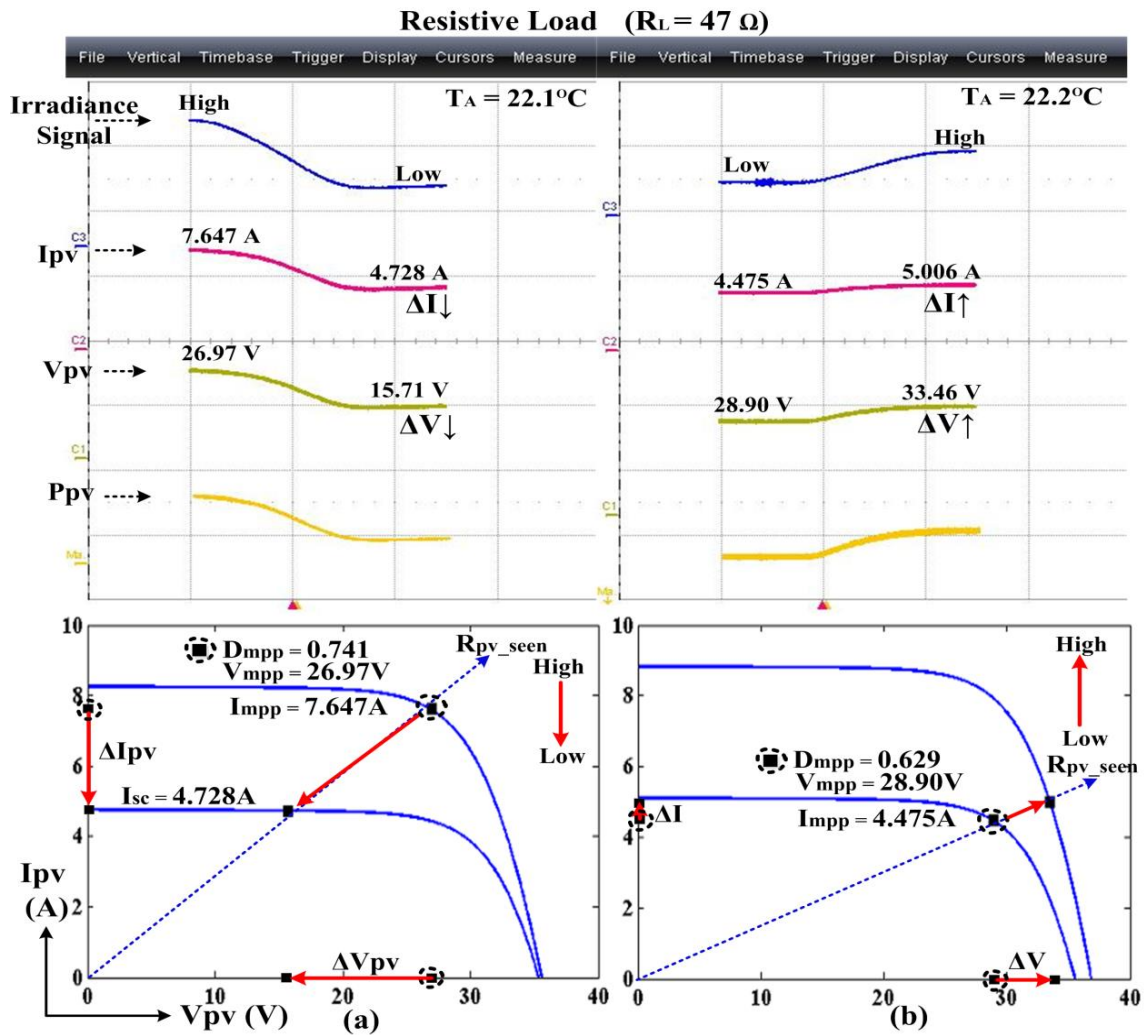
Figure 4.7 – Experimental tests to evaluate varying weather condition - resistive load

the same D_{mpp}. As a result, PV array follows the R_{pv_seen} load line and settles down at constant current region. Thus exhibiting a significant change in I_{pv} (ΔI_{pv}) and V_{pv} (ΔV_{pv}). On the other hand, moving from low to high irradiance as shown in Fig. 4.7(b), PV array again follows the R_{pv_seen} but it settles down in slope region. Due to which the PV array exhibits marginal change in I_{pv} while V_{pv} change is more pronounced.

Battery load (V_{Nom} = 48 V): Fig. 4.8 shows the response of the PV array while moving from high to low irradiance levels and vice-versa under the battery load. In first case (Fig. 4.8(a)), to attain the V_{mpp} = 27.21 V at high irradiance (I_{mpp} = 7.872 A), D_{mpp} is set at 0.494 (49.4%). However, in order to reach the V_{mpp} = 28.38 V at low irradiance (I_{mpp} = 4.841 A) as shown in Fig. 4.8(b), the D_{mpp} is configured at 0.477
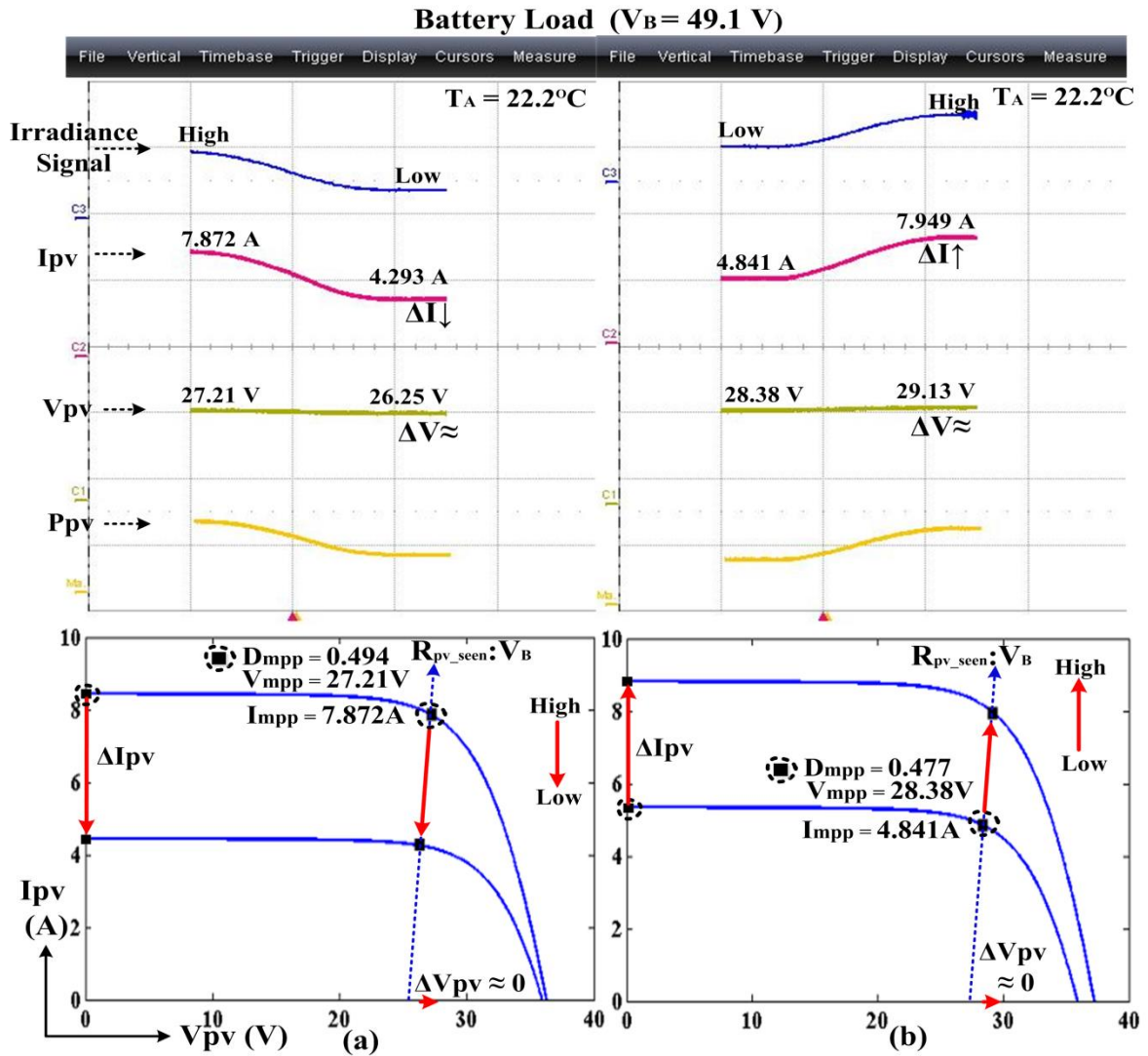
Figure 4.8 – Experimental tests to evaluate varying weather condition - battery load

(47.7%) which is close to the D_{mpp} value of first case as V_{mpp} values of two cases are close. Since the battery load provides low impedance and absorbs all the available current, I_{mpp} is not producing a significant effect unlike resistive load. Hence, the load line ($R_{pv,seen}$) seen by the PV array is determined by the battery voltage (V_B) from the relation:

$$V_B = \frac{1}{1 - D_{mpp}} V_{mpp} \Rightarrow R_{pv\_seen}: V_{mpp} = (1 - D_{mpp})V_B \qquad (4.21)$$

It can be noticed that going from high to low irradiance levels (Fig. 4.8(a)) or low to high irradiance levels (Fig. 4.8(b)) while holding their respective D_{mpp} values, PV array once again follows the load line determined by V_B as expressed in Eq.

(4.21). Hence, PV array falls in the same region as the load line is virtually straight for both cases. Which means that the PV array exhibits significant change in I_{pv} but ΔV_{pv} is almost negligible [65]. All these conditions can be summarized as:

- Resistive Load (High to Low): $\Delta V_{pv}\downarrow$ (significant) and $\Delta I_{pv}\downarrow$ (significant).
- Resistive Load (Low to High): $\Delta V_{pv}\uparrow$ (significant) and $\Delta I_{pv}\uparrow$ (marginal).
- Battery Load (High to Low): $\Delta V_{pv}\approx$ (same) and $\Delta I_{pv}\downarrow$ (significant).
- Battery Load (Low to High): $\Delta V_{pv}\approx$ (same) and $\Delta I_{pv}\uparrow$ (significant).

It can be confirmed that while using the battery load, there is no need to check the ΔV_{pv} and only ΔI_{pv} will do the job. However, ΔV_{pv} gains importance while addressing the resistive load. For instance, Fig 4.7(b) shows there might be a possibility that ΔI_{pv} change is not strong enough that it passes the threshold limit (ΔI_{lim}) set by the MPPT.

ΔI_{lim} Criteria: For the proposed technique, in order to remain in the S-loop i.e. to hold the MPP point, the following condition should be satisfied:

$$\left| I_{mpp} - I_{pv} \right| \leq \Delta I_{lim} \tag{4.22}$$

Where, I_{pv} is value of current at the present instant and ΔI_{lim} is the threshold limit of I_{pv}. Normally the threshold limit for I_{pv} (ΔI_{lim}) is selected with respect to the I_{pv} (STC) of PV array. Technique [60] set the ΔI_{lim} as 1% of I_{pv} (STC). However, considering the measuring tolerance of the sensor and noise disturbances present in the system [66], the magnitude of ΔI_{lim} should not be too small. Otherwise, the PV array cannot differentiate between the two scenarios: 1) ΔI_{lim} is violated because of the noise/sensing error of the PV system or 2) due to the change in weather conditions. Consequently, the steady efficiency of the technique is compromised as the technique will not stay in S-loop. For instance, PV array has I_{pv} (STC) = 10A then with 1% of limit [58], ΔI_{lim} will be 0.1A which is too low.

On the other hand, if the ΔI_{lim} is set too high, the PV array stays in S-loop for longer period and even may not break the ΔI_{lim} for notable change in irradiance. Due to which the dynamic efficiency of the technique suffers. Considering these facts, the proposed technique set the ΔI_{lim} when there is a change in irradiance of atleast 20 W/m^2 which can be calculated as:

$$\Delta I_{\text{lim}} = I_{pv,stc} - (I_{pv,stc} \times (\frac{980\text{W/m}^2}{1000\text{W/m}^2})) \tag{4.23}$$

ΔV_{lim} Criteria: The proposed technique utilizes the voltage steps (ΔV) in its P&O. Hence, threshold limit of V_{pv} (ΔV_{lim}) of the technique is fairly easy to set i.e.

$$\Delta V_{lim} = \Delta V \tag{4.24}$$

$$\left| V_{mpp} - V_{pv} \right| \le \Delta V_{lim} \tag{4.25}$$

It means that when PV array is operating at V_{mpp} in S-loop, then algorithm always samples the present value of V_{pv}. If the difference between the two is less than the ΔV_{lim}, the algorithm will stay in the S-loop.

4.5   Control algorithm of the proposed MPPT technique

Figure 4.9 shows the detail-working flowchart of each and every stage. The algorithm starts the process by initializing the values of D_{in}, K_i, K_v. Where, initial values of K_i and K_v can be calculated from the manufacturer's datasheet using the STC data:

$$k_i = \frac{I_{mpp}(STC)}{I_{sc}(STC)} \tag{4.26}$$

$$k_v = \frac{V_{mpp}(STC)}{V_{oc}(STC)} \tag{4.27}$$

It can be seen from the flowchart that in each stage, the D blocks are displayed with dotted outer lines followed by a special '$' block. The working of this block is shown on right side of flowchart. Whenever algorithm enters in this '$' block after computing D, the designer has to wait for some duration famously known as sampling rate (Sa_{rate}) before sensing the $V_{\text{pv}}/I_{\text{pv}}$ values which are used in future decisions. The sampling rate, normally varies from 5 ms to 50 ms depending upon the PV system [56], is essential to ensure that the PV array reaches the steady state [45,56,67] after every change in D due to the dynamics of the PV system. Any control decision taken during the transient period may mislead the MPPT algorithm.

Considering the high-speed digital devices of current era, the soft computing
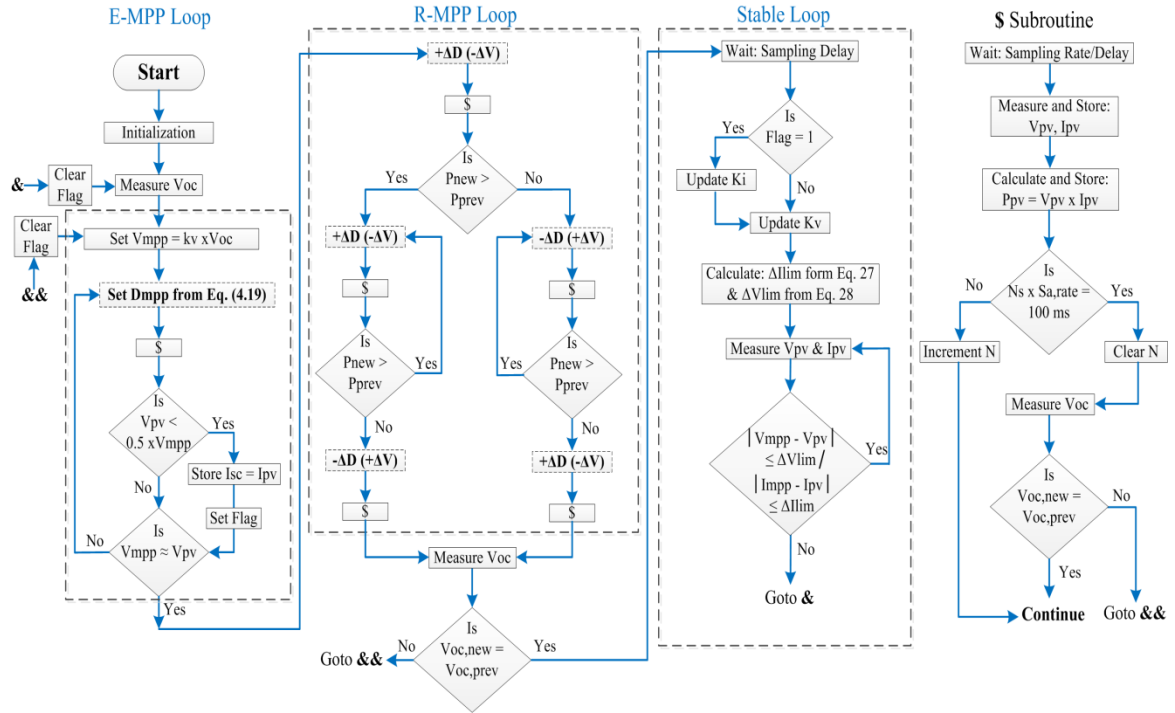
Figure 4.9 – Operational flowchart of the proposed technique

calculations like duty cycle relation from Eq. (4.19) can be executed merely in micro-seconds. Since the MPPT designer has to wait for the Sa_{rate} (milli-seconds) after every change in D, the real time consuming factor can be linked with the fact that for how many times the MPPT technique has to tune the D. Neglecting the processing time of the digital device and considering the sampling rate (Sa_{rate}), the time response (T_r) of the technique can be formulated with respect to the number of samples (N_s) required to tune D in order to reach MPP as expressed in Eq. (4.28):

$$T_r = N_s \times Sa_{rate} \tag{4.28}$$

Another thing which can be noticed in '$\$$' block is when to measure the V_{oc} i.e. to judge the varying weather conditions. Since the $V_{oc,freq}$ is set at 100 ms (already discussed in the previous section), the above equation is also used to determine the sample at which V_{oc} will be measured i.e.

$$N_{voc}: N_s \times Sa_{rate} = 100 \text{ ms} \tag{4.29}$$

Consider that Sa_{rate} of PV system is 10 ms, the algorithm measures V_{oc} at every tenth sample.

4.5.1 E-MPP loop

Figure 4.9 shows that before entering into the E-MPP loop, the algorithm measures V_{oc}, which is required to calculate the D_{mpp} value from Eq. (4.19) and V_{mpp} from Eq. (4.1). To use the D_{mpp} in control algorithm, the Eq. (4.19) can be re-written as:

$$D_{new} = 1 - ((1 - D) \sqrt{\frac{K_v V_{oc} (1 - \exp(\frac{(V_{pv} - V_{oc}) \ln(1 - K_i)}{V_{oc}(K_v - 1)}))}{K_i V_{pv}}}) \qquad (4.30)$$

It can be seen from Fig. 4.9 that after every D_{new} computation, the algorithm first checks the condition that V_{pv} is less than $0.5 \text{x} V_{mpp}$ i.e. 50% of V_{mpp}. If it is true, it means that the PV array is operating in constant current region where I_{pv} is approximately equal to I_{sc}. Hence, the value of I_{sc} is stored and flag is set such that the value of K_i (which requires I_{mpp} and I_{sc}) can be updated later when MPP is reached. After that, algorithm checks the condition that V_{pv} is equal to V_{mpp}. Whenever this condition becomes true, the algorithm proceeds to R-MPP loop.

4.5.2 R-MPP loop

It is expected that the technique brings V_{pv} of the array near MPP region when it leaves the E-MPP loop as shown in Fig. 4.10. R-MPP loop is a modified P&O loop, which sets the V_{pv} of PV array from estimated MPP to real MPP by fine-tuning the D_{mpp}. The working principle of this loop is shown in Fig. 4.9 while its operation is shown in Fig. 4.10. It can be seen that the first step of $-\Delta V$ of this loop will decide the direction in which the real MPP is present. If P_{new} is greater, it means that MPP is present in the same direction as shown in Fig. 4.10 and algorithm proceeds with $-\Delta V$ steps. Flowchart of Fig. 4.9 further shows that the last step of R-MPP loop is the opposite step to the direction in which it is proceeding. This mechanism can be judged from Fig. 4.10 that after reaching the MPP by taking $-\Delta V$ steps, the algorithm crosses the MPP with another $-\Delta V$ i.e. second-last step. Consequently, P_{new} is less than P_{prev} therefore the algorithm returns back to MPP with $+\Delta V$ (opposite to the direction), which is the last step of R-MPP loop and proceeds to the S-loop. It should be noted that during R-MPP loop, the algorithm always contains the information of V_{oc} via '$'
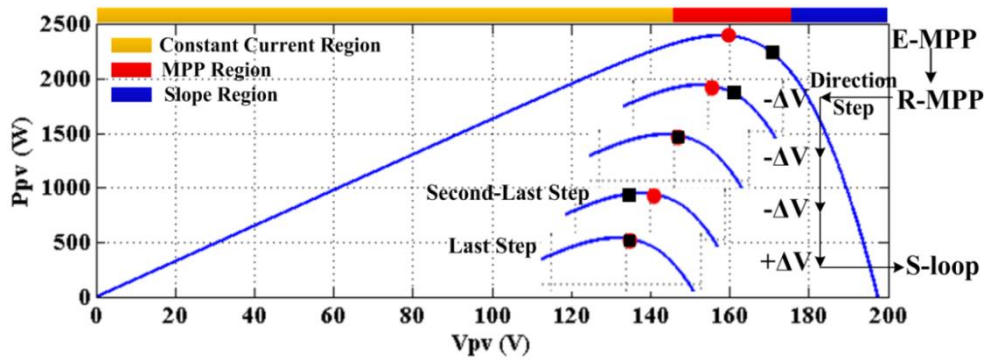
Figure 4.10 – Detection of MPP precisely

blocks. Whenever, it finds out that V_{oc} is changed, it will return to E-MPP loop with the help of '$' block instead of going into S-loop.
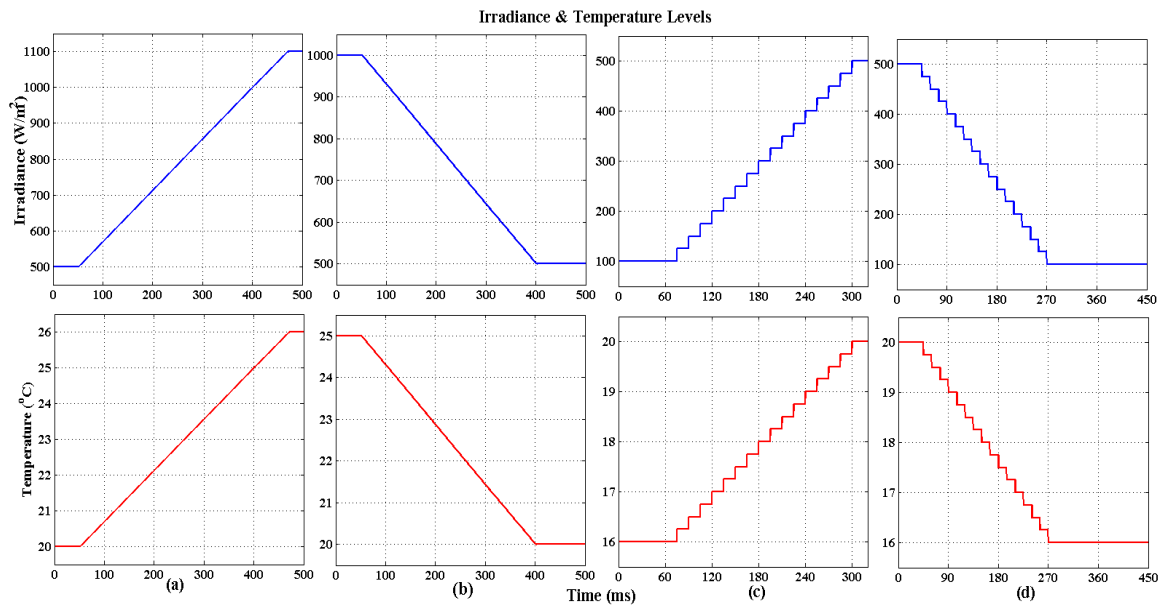
4.5.3 S-loop

Figure 4.9 shows that the algorithm measures the V_{oc} again before moving to S-loop to assess the weather conditions. Since the algorithm enters in S-loop while operating at MPP accurately, the algorithm has the accurate data of V_{mpp} and I_{mpp} along with V_{oc} and I_{sc} (if flag is set in E-MPP loop). Hence, the algorithm always updates the K_v value (ratio of V_{mpp}/V_{oc}) while K_i value (ratio of I_{mpp}/I_{sc}) is updated based on the flag status. The flag is set only when PV array somehow moves in constant current region as already explained in E-MPP loop. Since K_i value is not changed significantly with variable weather conditions unlike K_v as shown in Table 4.1, the algorithm can afford not to update K_i every time. After that, the algorithm calculates the ΔV_{lim} and ΔI_{lim} from Eqs. (4.24) and (4.23), respectively. Finally, the technique continuously monitors the two conditions. Whenever, either of the limits is crossed, the technique will return back to E-MPP loop to re-initiate the process.

4.6 Comparative study and analysis

4.6.1 Simulation setup

PV system shown in Fig. 4.2 is modeled in Matlab/Simulink using the same setup as described in Sec. 4.2 (last paragraph). Boost converter is used between the resistive load and the array, the switching frequency of which is set at 20 kHz while

Figure 4.11 – Wide spectrum of weather conditions

the C_{in} and C_{out} are configured at 300 μF and 10 μF respectively, and the inductor L is set at 200 μH. Sampling rate of the PV system is set at 5 ms. For comparative analysis, three techniques: 1) Proposed MPPT, 2) MPPT [45] and P&O are implemented in the simulation setup and their performances are carried out under four tests of weather conditions as shown in Fig. 4.11. To cover the wide spectrum of weather conditions, the tests (a) and (b) contain the ramp rising and ramp falling conditions between medium and high irradiance levels. While tests (c) and (d) contain the step rising and step falling conditions between low and medium irradiance levels. In all test cases, initially the weather conditions are made fixed such that each algorithm reaches the MPP and then conditions are changed. Since technique [45] measures the V_{oc} at every sample (irrespective of 100 ms weather conditions, i.e. $V_{oc,freq}$ = 100 ms), the proposed technique is also configured to measure V_{oc} at every sample to have a fair comparison between the two.

4.6.2   Test-1

This test case contains the ramp rise scenario between medium and high irradiance-temperature levels, i.e. 500 W/m^2 - 20°C to 1100 W/m^2 - 26°C as shown in Fig. 4.11(a). As already said that initially the conditions are fixed at 500 W/m^2 - 25°C

upto 50 ms such that the algorithms are allowed to settle at their respective MPPs. After that the irradiance is linearly increased at a rate of 1.5 W/m^2 per ms and temperature is increased at a rate of 0.015^{o}C per ms until the conditions reach the 1100 W/m^2 - 26°C.

   Upper graph of Fig. 4.12 shows the response of three algorithms under the present case, while the lower graph presents the D-pattern of three techniques. It can be seen that the P$_{pv}$ curves of the proposed and MPPT [45] touch the horizontal axis
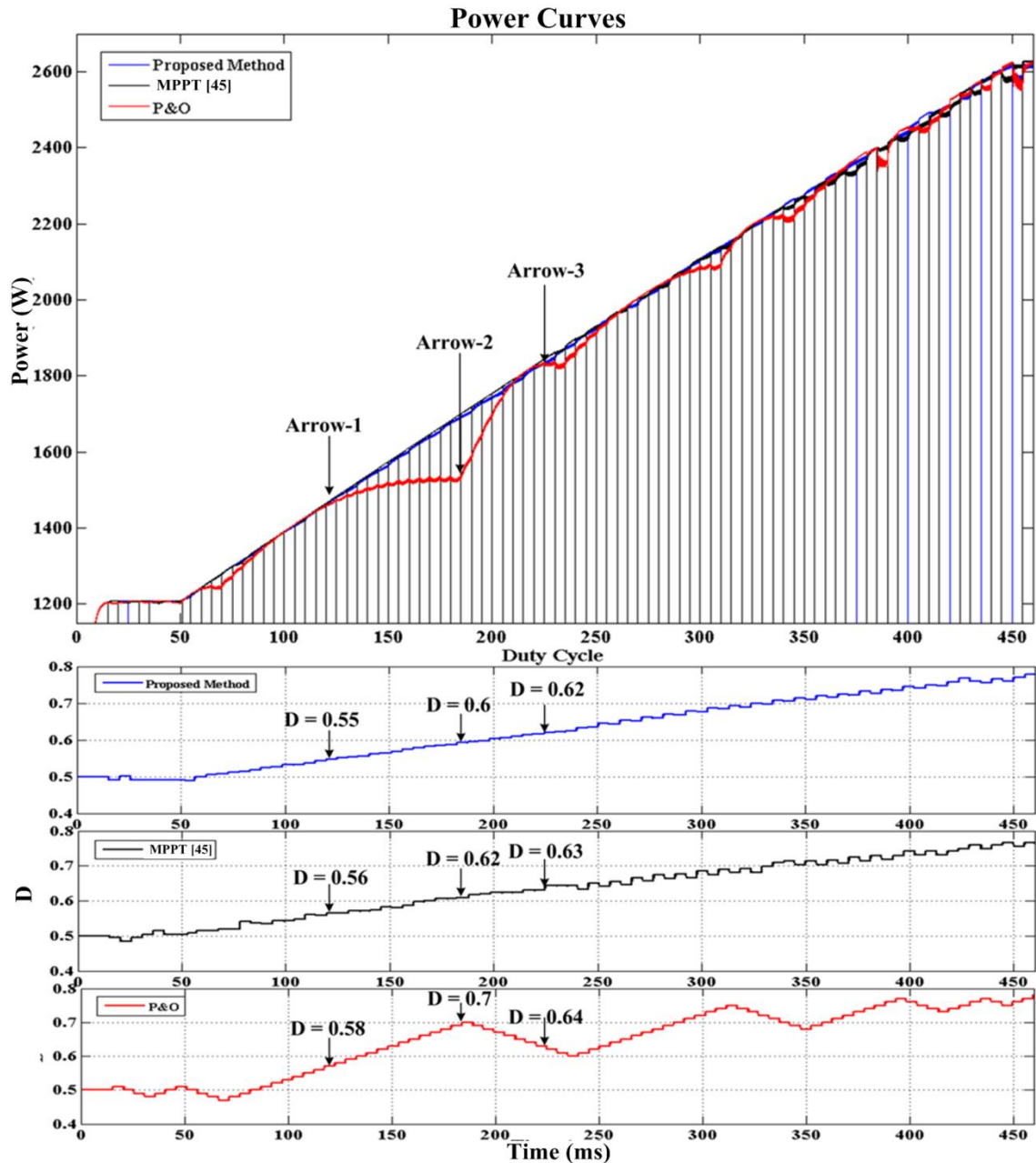

Figure 4.12 – Response of techniques under Test-1

periodically i.e. zero power, which indicate that both techniques measure V_{oc} during this. It should be noted that each technique formulation is finally reflected in D of the converter, as it is the parameter which determines the operating point (V_{pv},I_{pv}) of PV array. Since the D-pattern of proposed MPPT and MPPT [45] is similar as shown in lower graph, both techniques achieve the same level of performance. However, the proposed technique does not utilize the services of PI controller unlike MPPT [45]. On the other hand, P&O exhibits less efficient performance. For instance, P&O struggle to match the other techniques starts at 'Arrow-1' position where all three techniques have similar D values. The inefficiency of P&O becomes evident at 'Arrow-2' position where P&O exhibits the D of 0.7 (70%) which is almost 10% more than the D = 0.6 (60%) of the proposed MPPT. It is because of the reason that moving from 'Arrow-1' to 'Arrow-2' position, P&O finds more power on every new sample. This increase in power is not occurred as a result of closing the gap to MPP but due to the rising weather conditions, which P&O miscalculates due to its one-dimensional approach.

On the other hand, both proposed technique and method [45] measures V_{oc} to assess the weather situation and then estimates V_{mpp} and I_{mpp} to adjust the D. Thus providing better performance compared to P&O under varying weather conditions. Furthermore, it can be seen that when the techniques exhibit the similar values of D, the P_{pv} curves of three techniques once again unite at similar power levels like at 'Arrow-3' position.

4.6.3 Test-2

In this test, the techniques are evaluated under the decaying weather conditions. The conditions are first settled at 1000 W/m^2 - 25°C such that each algorithm reaches the MPP. Afterwards the conditions are allowed to fall up to 500 W/m^2 - 20°C at the same ramp rate to that of Test # 1 as shown in Fig. 4.11(b).

Upper graph of Fig. 4.13 indicates that the proposed technique outperforms other two techniques. It should be noted that under falling conditions on every new sample, new power is less than the previous one. Consequently, if P&O gives +ΔD (-ΔV) in current sample then in next sample it will allocate the opposite step of –ΔD

(+ΔV) since it always receives less power on every new sample. Therefore, P&O moves to and fro between +ΔD and −ΔD because of its limited control architecture. This will hold the D almost at the same level. For instance at 'Arrow-1' position shown in Fig. 4.13, the D values of three techniques are similar. However, moving towards Arrow-2 position, the D of P&O is same i.e. 0.74, while D of the proposed MPPT changes from 0.71 to 0.53.

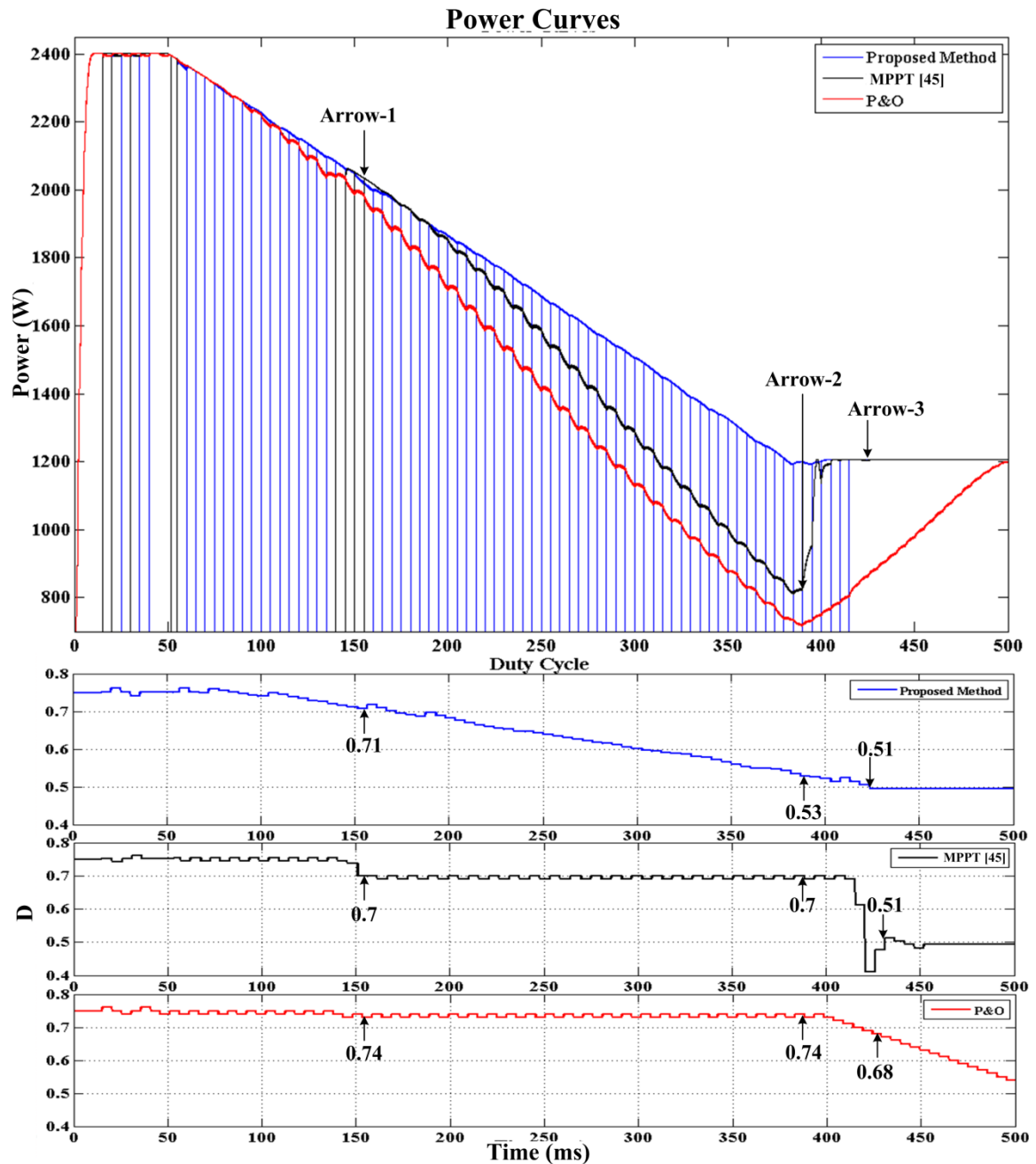Unlike Test-1, the proposed technique outperforms the MPPT [45] by a

Figure 4.13 – Performance of techniques under Test-2

significant margin. This is due to the flow in control architecture of hybrid technique [45] as it gives more emphasis on P&O during falling conditions. Therefore, the similarity between the D-patterns of technique [45] and P&O can be seen in Fig. 4.13. However, once the conditions are settled down, method [45] quickly regains the MPP in few samples with the help of V_{oc} and its control architecture, while P&O takes more samples to reach MPP. This effect can be seen between 'Arrow-2' and 'Arrow-3' position in Fig. 4.13.

4.6.4 Test-3

In this case, the weather conditions are maintained at low to medium irradiance levels. It can be seen from Fig. 4.11(c) that weather conditions are increased from 100 W/m^2-16°C to 500 W/m^2 - 20°C at a step rise of 25 W/m^2- 0.25^{o}C after every 15 ms. Fig. 4.14 shows that the proposed technique exhibits better response compared to other two techniques. It should be noted that once the conditions are given the step rise, the conditions remain the same for 15 ms. Therefore, the estimation of I_{mpp} becomes much more critical as conditions are stable for a short period of time unlike
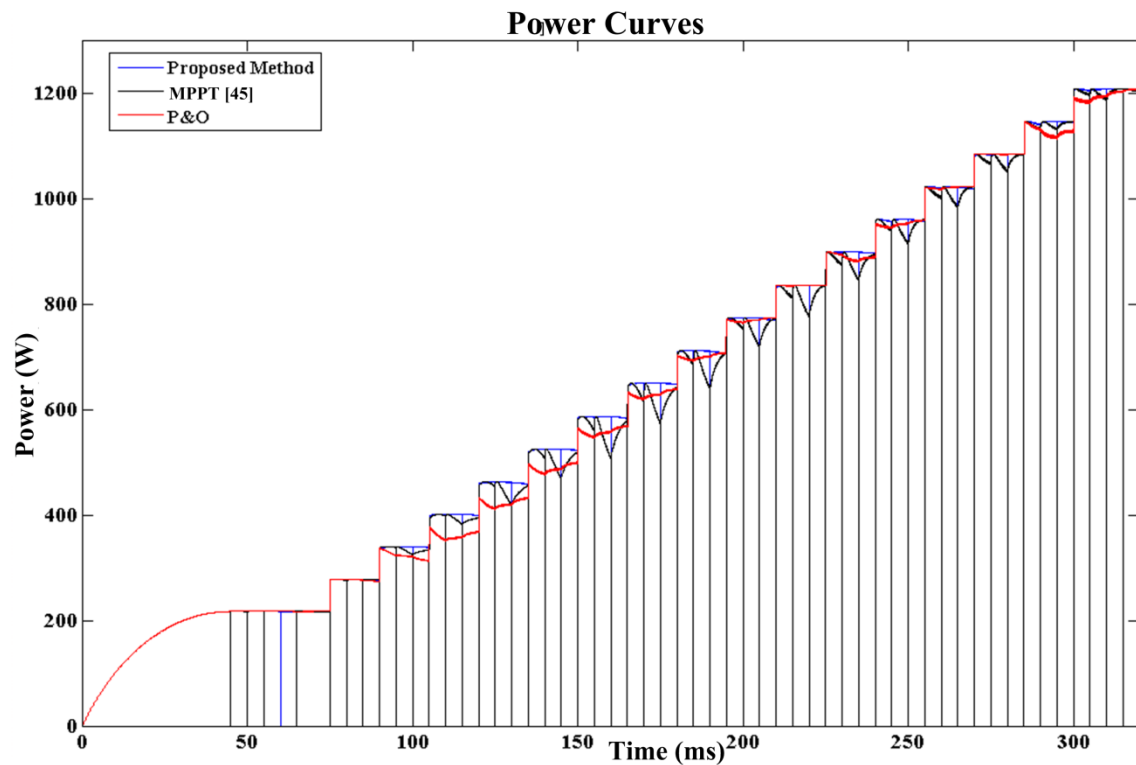

Figure 4.14 – Performance of techniques under Test-3

ramp conditions. Since the estimation of I_{mpp} of the proposed technique is more accurate compared to MPPT [45], therefore method [45] even with the help of PI controller could not achieve the same performance as that of the proposed technique. P&O shows the satisfactory performance but is not performing up to the levels of the other two techniques.

4.6.5 Test-4

In this case, the weather conditions are step decayed from 500 W/m^2-20°C to 100 W/m^2-16°C at the same rate to that of Test # 3 i.e. after every 15 ms as shown in Fig. 4.11(d). It can be confirmed from Fig. 4.15 that the proposed technique has the best performance compared to other two techniques. Since the weather conditions are settled for 15 ms after every change, the performances of MPPT [45] and P&O are enhanced here compared to falling ramp conditions of Test-2.
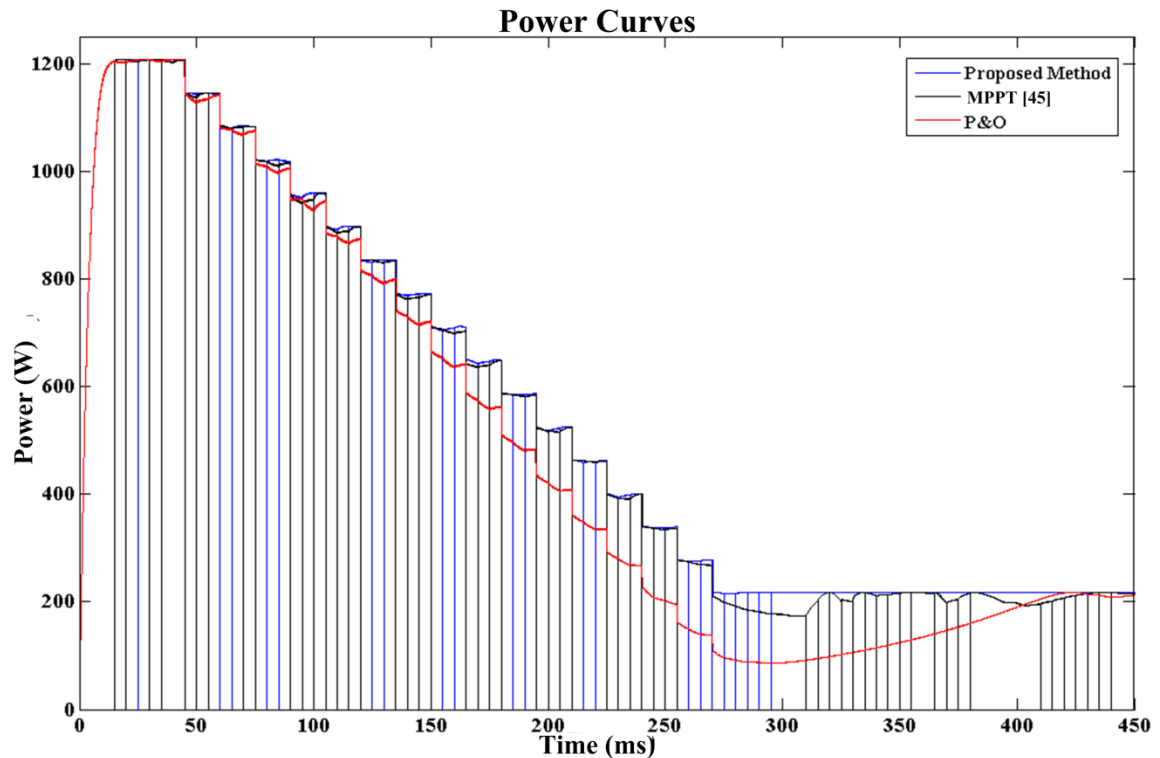

Figure 4.15 – Response of techniques under Test-4

4.6.6 Summary

In order to summarize the performance of MPPTs under four tests, the energy harvesting by the techniques is indicated in Table 4.3. Eq. (4.31) is utilized to give the

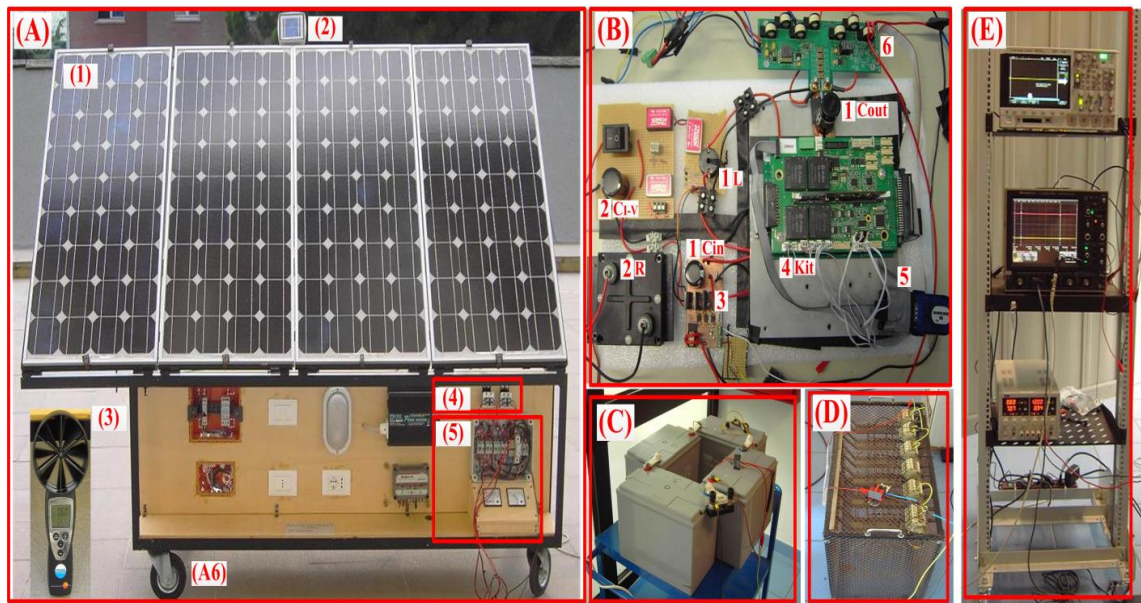**Table 4.3** – Energy harvesting comparison between the techniques

Tests	Energy (Joules)			Energy Comparison	
	Proposed	MPPT[45]	P&O	With MPPT [45]	With P&O
1	863.62	863.50	855.22	0.01%	0.98%
2	855.59	813.19	758.38	5.21%	12.82%
3	197.25	194.23	193.69	1.56%	1.84%
4	248.93	245.80	221.06	1.27%	12.61%

energy efficiency comparison between the proposed and reference techniques, i.e. MPPT [45] and P&O. These comparisons are shown in the second last and last columns respectively. The data of Table 4.3 depicts that the proposed technique outperforms the technique [45] and P&O on each and every test.

$$\eta_{Energy} = \left(\frac{E_{prop} - E_{Ref}}{E_{Ref}}\right) \times 100 \tag{4.31}$$

4.7 Experimental validation

Figure 4.16 shows the complete experimental apparatus with labels on which the MPPT techniques are implemented. The details of labels are shown in Table 4.4. It can be seen that a special mobile vehicle is designed in which the PV array is installed in order to conduct the dynamic tests. The schematic of experimental circuit is shown in Fig. 4.17, which contains three N-type Mosfet switches, i.e. M_{VPV}, M_{IV} and M_{R}.

Figure 4.16 – Complete experimental test-bed with mobile PV array

Table 4.4 – Description of components of experimental setup

Labels	1	2	3	4	5	6
A	PV Array (2x2): Module FVG 36 – 125 [21]	Irradiance Meter	Temperature and Wind Sensor	Blocking Diodes	Power Connection Box	Mobile Wheels
B	Boost Converter: Cin = 150 µF L = 200 µH Cout = 250 µF	I-V Curve Scan: C(I-V) = 1 mF R(I-V) = 33 Ω	Three Mosfets: 1. M_VPV 2. M_IV 3. M_R	Kit: Delfino F28335 DSP Card to embed MPPT algorithms plus Switches, Diodes and protection components of Boost converter	Power Conditioning and Sensors board	Data Acquisition to PC through USB
C	Battery Bank: 49.1 V, Type: Lead-Acid, Battery Nominal Voltage: 12V and Rating: 90Ah					
D	Resistor Bank: 47 Ω with Power Dissipation of 1.1 kW					
E	Advanced Oscilloscopes (to record sketches) and Power Supply					

Operation of the circuit can be realized with the help of table shown in Fig. 4.17. Although the experimental setup has the facility of irradiance meter but is utilized mainly to realize the state of weather conditions. However, for accurate analysis, the PV curve is initially scanned for 10 ms with the help of 1mF capacitor to detect the ideal MPP by setting the position of switches as: $M_{VPV} = 0$, $M_{IV} = 1$ and $M_R = 0$. During normal operation, $M_{VPV} = 1$ (to connect the PV array to load), $M_{IV} = 0$ and $M_R = 1$ (to discharge the C_{I_V} capacitor through R) and for V_{oc} measurement, all three switches are set at 0. Boost converter is used, the components of which are shown in Fig. 4.16 and the respective values are written in Table 4.4. Switching frequency of boost converter is set at 40 kHz. Proposed MPPT and P&O techniques are implemented in the experimental setup. Responses of each technique are collected under various weather conditions against two types of loads, i.e. Resistive (47 Ω) and Battery (48 V) shown in Fig. 4.16. Both techniques are assigned with a $\Delta D = 0.03$ to execute the voltage steps. Sampling rate (Sa_{rate}) of each technique is set at 10 ms. Since the proposed technique requires V_{oc} in its operation, it measures the V_{oc} after every 100 ms ($V_{oc,freq} = 100$ ms) i.e. every tenth sample as $Sa_{rate} = 10$ ms, and 200 us are consumed to attain the V_{oc} value.
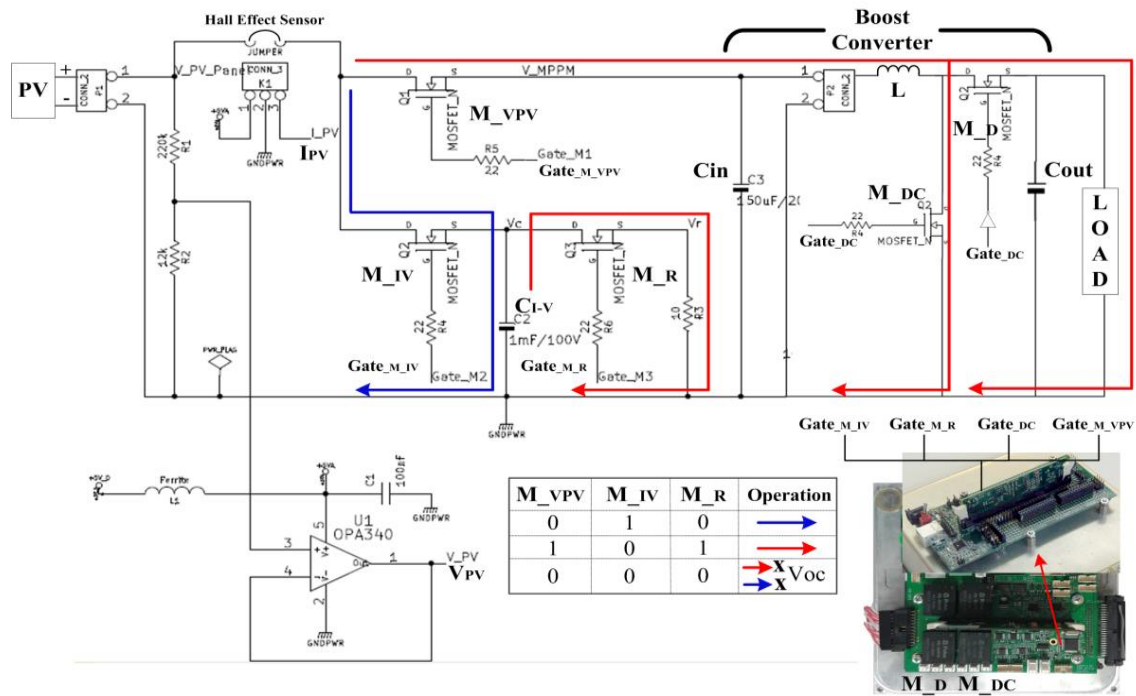
Figure 4.17 – Schematic and operation of experimental circuit

4.7.1 Time response analyses of techniques

4.7.1.1 Resistive load (47 Ω)

The experimental configuration of all the tests conducted in this section contains the same format as shown in Fig. 4.18, which is:

1) I-V curve is scanned for 10 ms to attain the ideal MPP .

2) Initial duty cycle (D_{in}) is set at 0.9 (90%).

3) Operation of the technique is started.

For fair comparison, the tests are conducted under similar weather conditions. In order to differentiate between the distinct irradiance levels, the I_{sc} is measured and compared with I_{sc} (STC) = 8.8 A. Fig. 4.18(a) and Fig. 4.18(b) show the performances of proposed MPPT and P&O. Since the weather conditions exhibit the I_{sc} of 9.93 A (for proposed MPPT) and 9.81 A (for P&O), which are greater than I_{sc} (STC) = 8.8 A, conditions are declared as high irradiance. It can be seen from Fig 4.18(a) that after D_{in} = 0.9, the technique measures V_{oc} before entering into E-MPP loop where it takes 2 samples. After that, technique enters into R-MPP loop where it utilizes 3 samples to reach MPP. In total, the proposed technique utilizes 5 samples to attain the optimal
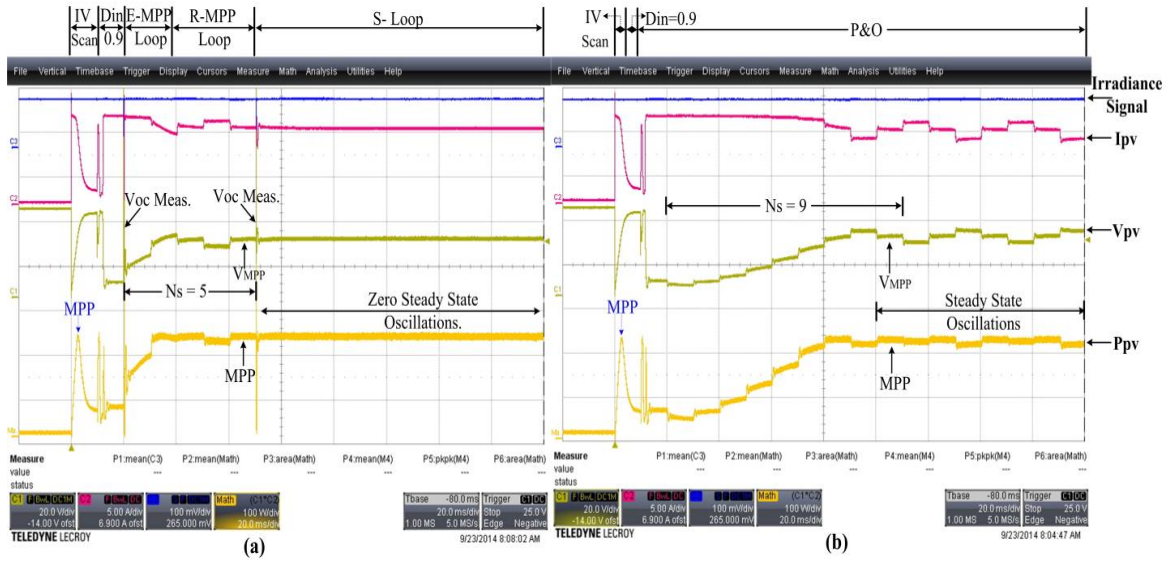
Figure 4.18 – Response of techniques at high irradiance against resistive load

point. Finally, it measures the V_{oc} again to assess the weather conditions. Since weather is not changed as confirmed by the irradiance signal, the proposed technique enters into S-loop where it is stable and executes negligible power loss oscillations. On the other hand, P&O takes 9 samples to reach MPP and after that, it starts producing power loss oscillations around MPP.

Figure 4.19 shows the response of two techniques when the weather is at medium irradiance level. Under present weather condition, the proposed MPPT
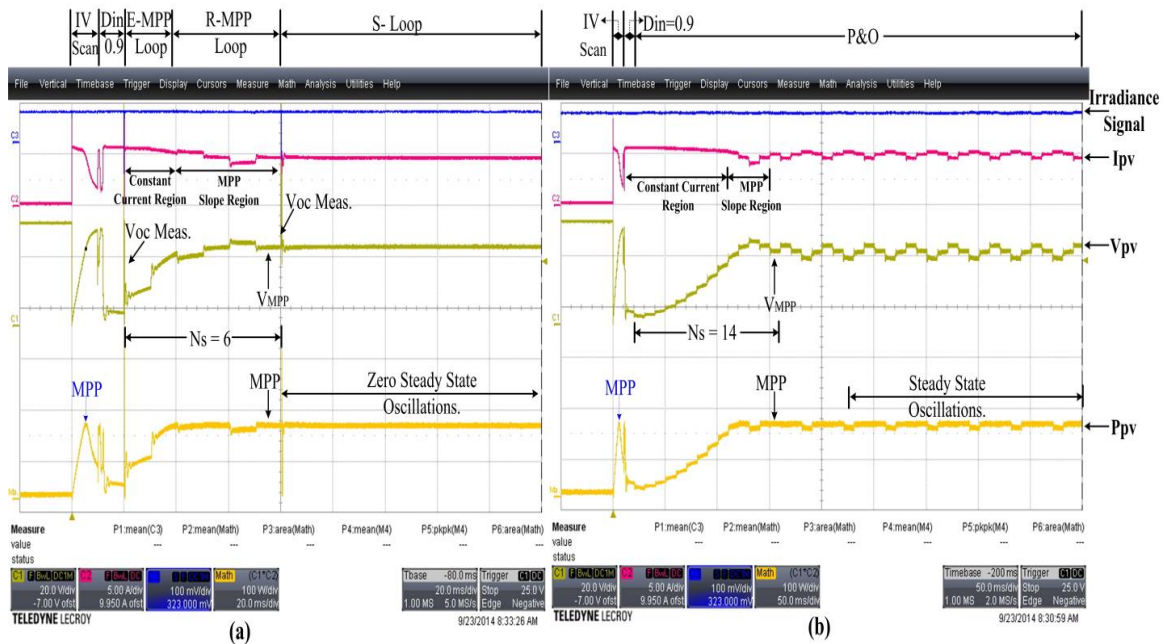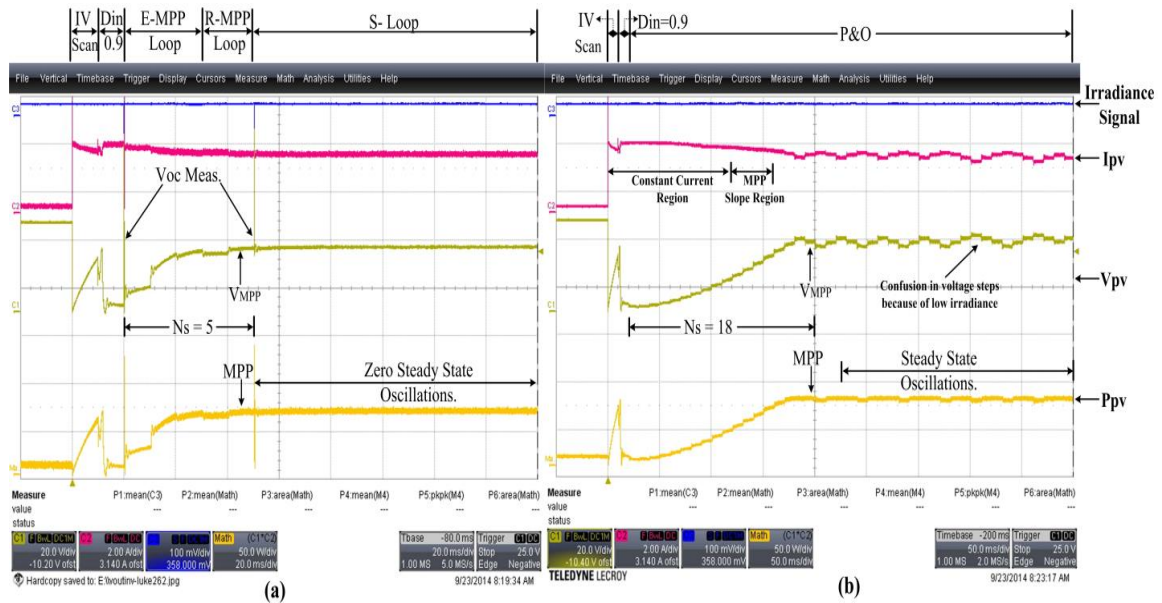

Figure 4.19 – Performance of techniques at medium irradiance against resistive load

Figure 4.20 – Response of techniques at low irradiance against resistive load

consumes 6 samples to attain the MPP. However, P&O needs 14 samples to reach MPP, which are 5 samples more compared to its performance at high irradiance level. On the other hand, Fig. 4.20 gives an idea about the performances of the techniques at low irradiance. Once again, P&O performance degrades further and executes 18 samples to reach MPP while the performance of proposed MPPT remains intact and takes 5 samples to attain the MPP point.

The reason behind the degradation of P&O performance can be evaluated with the help of Table 4.5 in which all these tests are summarized. It can be noticed that in case of P&O, although the V_{mpp} values of different conditions are close, but D_{mpp} values to operate the PV array at these V_{mpp} values are vastly different. For instance, the difference in D_{mpp} values between high and low irradiance is 30% (High: 0.78 (78%) – Low: 0.48 (48%)) while the difference in V_{mpp} values between the two is merely 0.79 V (High: 26.79 V – Low: 27.58 V). This phenomenon can be understood from the Eq. (4.20) that under the resistive load, the heavy fall in I_{mpp} will produce the significant difference in D_{mpp} as already discussed in Sec. 4.4.2.2. It should be noted that since, initial D_{in} is set at 0.9 (90%), both techniques have to cross the constant current region in order to reach the MPP region. Since D_{mpp} values continue to move away from $D_{in} = 0.9$ as the conditions falls which can be seen from Table 4.5, P&O spends more time in the constant current region before reaching the MPP region

because of its one-dimensional approach to locate the MPP i.e. only executing ΔD steps. This deficiency of P&O can be realized from the sequence of figures: Medium: Fig. 4.19(b) → Low: Fig. 4.20(b). On the other hand, the proposed technique estimates the V_{mpp} and skips the constant current region courtesy E-MPP loop and executes almost similar samples in each and every condition. Another fact can be noticed in Fig. 4.20 (b) that since the I_{pv} is low during low irradiance, P&O may confuse in executing its natural voltage steps.

4.7.1.2 Battery load (48 V)

Figures 4.21 and 4.22 show the response of two techniques at high and low irradiance levels respectively against the battery load. On both occasions, the proposed technique exhibits better performance as it takes half samples to search the MPP compared to P&O. It should be noted that the difference in performance of P&O from high to low irradiance is not significant as it executes 2 more samples at low irradiance compared to high irradiance. It is because of the reason that under battery load, the D_{mpp} is not significantly changed with the change in I_{mpp} as indicated in Table. 4.5.
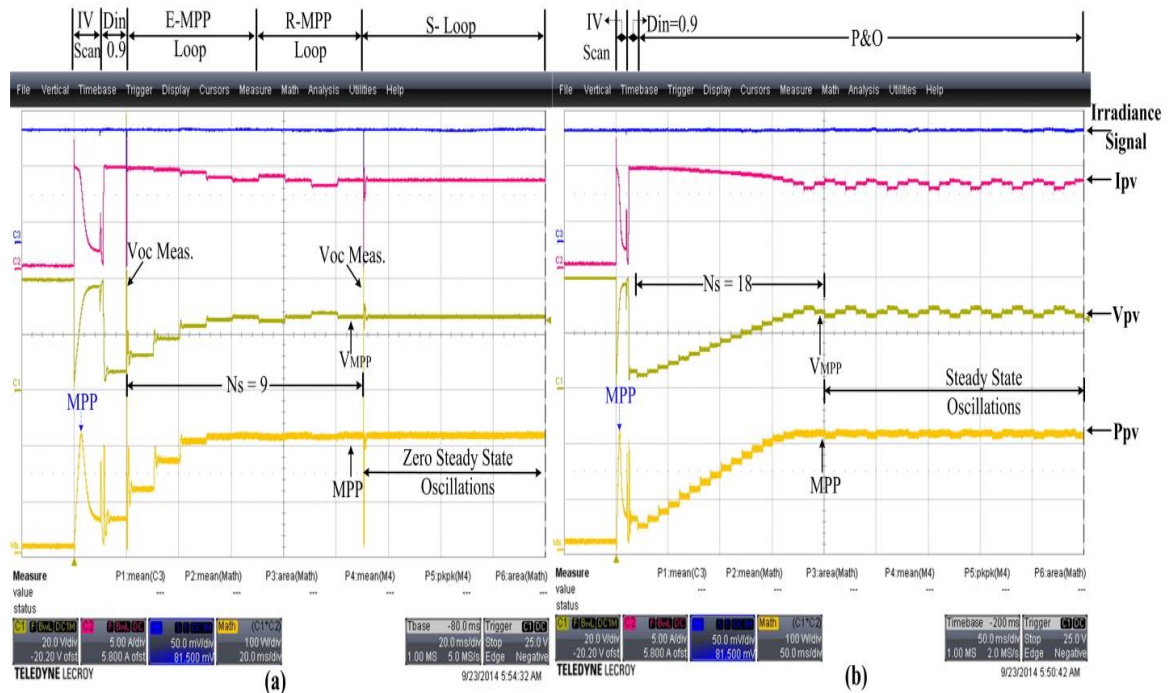

Figure 4.21 – Operation of techniques at high irradiance against battery load
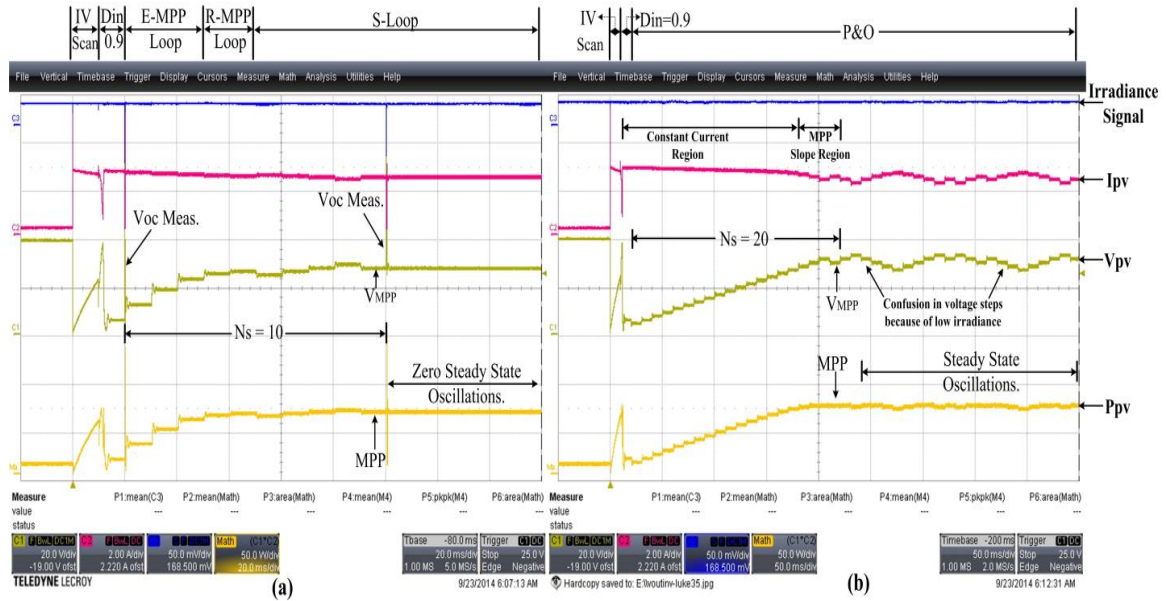
Figure 4.22 – Operation of techniques at low irradiance against battery load

4.7.1.3 Summary

Table 4.5 clarifies that since the Sa_{rate} of both technique is set at 10 ms, the worst response time T_r (calculated from Eq. (4.28)) for the proposed technique to reach MPP from far initial point ($D_{in} = 0.9$) is 100 ms. While the worst T_r for the P&O is double i.e. 200 ms. From these results, it can be evaluated that the response time of proposed technique could be better under varying weather conditions compared to P&O.

Table 4.5 – Time response of techniques under distinct weather conditions

Ld	Weather Conditions		V_{mpp} (V)	D_{mpp}	N_s	T_r (ms)	Weather Conditions		V_{mpp} (V)	D_{mpp}	N_s	T_r (ms)
	I_{sc} (A)	Irr.					I_{sc} (A)	Irr.				
Res. 47 Ω	9.93	High	25.78	0.76	5	50	9.81	High	26.79	0.78	9	90
	5.74	Med	29.08	0.64	6	60	5.60	Med	29.46	0.66	14	140
	2.89	Low	27.6	0.50	5	50	2.87	Low	27.58	0.48	18	180
Bat. 48V	9.13	High	26.39	0.51	9	90	9.01	High	27.91	0.48	18	180
	2.65	Low	27.82	0.46	10	100	2.76	Low	29.6	0.42	20	200

4.7.2 Dynamic and steady state response of techniques

Figures (4.23) and (4.24) show the dynamic response of the two techniques under the resistive load. To conduct this test, the time resolution of scope is set at

5 s/div such that 50 s of real time data can be recorded and then following steps are executed:

- PV array is placed facing the sun and the techniques are allowed to settle at MPP under the present weather conditions.

- PV array is moved clockwise (away from the sun) with the help of mobile vehicle (shown in Fig. 4.16) which is indicated by the "Irradiance variation starts" in the Figs. 4.23 and 4.24.

- PV array is moved anti-clockwise (towards the sun) and stopped at the point indicated by "Irradiance variation ends".

- Dynamic efficiency of the technique is measured with the help of Eq. (4.32) [68], from the time (t1) when the irradiance starts to change up to the time (t2) when irradiance variation ends. Both t1 and t2 are indicated in Fig. 4.23 and 4.24. In Eq. (4.32), P_{MPPT} is the cumulative power of the technique while P_{Ideal} is
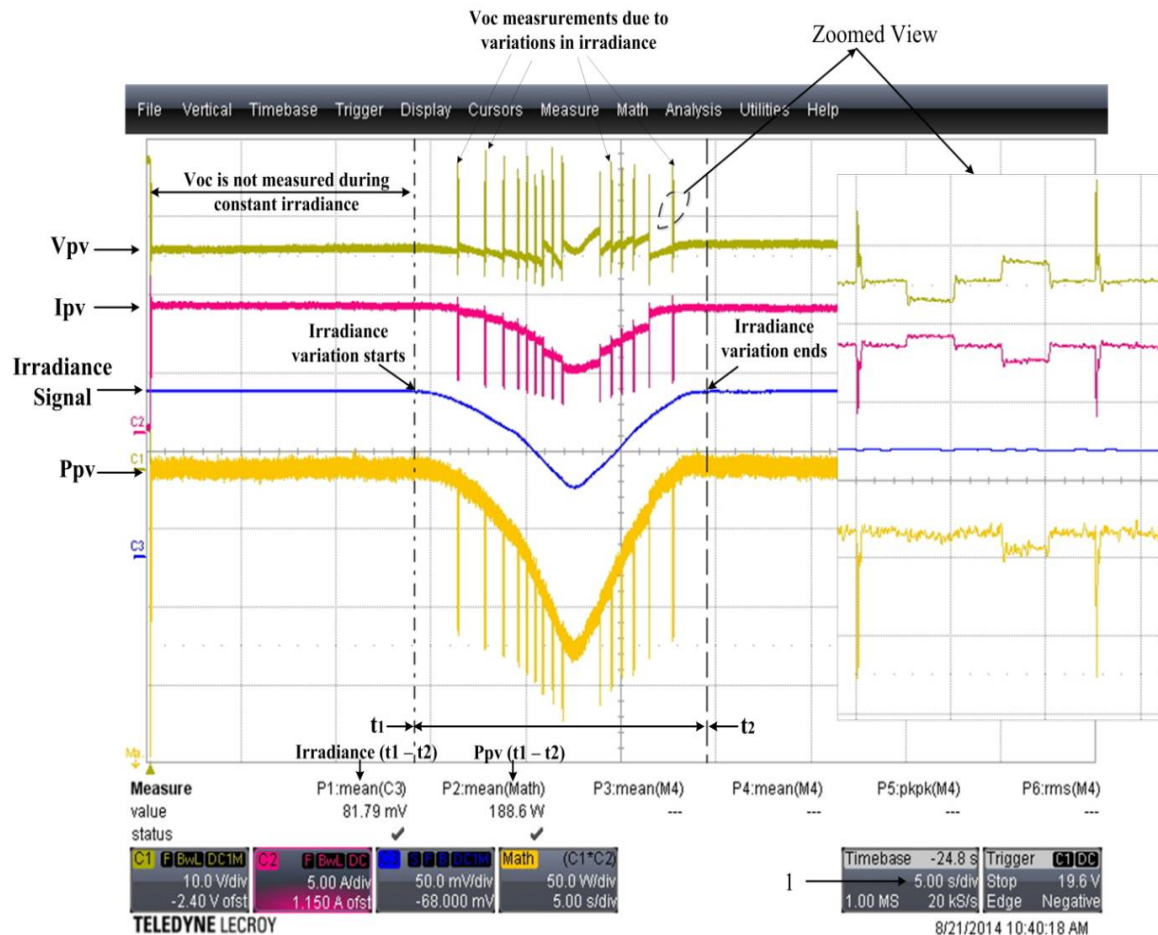

Figure 4.23 – Dynamic response of proposed MPPT under varying weather

the ideal power, which is calculated with the help of irradiance signal.

$$\eta_{Energy} = \left(\frac{E_{prop} - E_{Ref}}{E_{Ref}}\right) \times 100 \tag{4.32}$$

Figure 4.23 shows that the P_{pv} of the array follows the irradiation signal with the aid of the proposed technique, which indicates that PV array is following the MPP line effectively. P_{pv} of array shows the spikes at different instants indicating the V_{oc} measurements. A zoomed view of one of the V_{oc} measurement instant along with the operation of the proposed technique is also shown on the right side. Fig. 4.24 depicts the dynamic response of P&O. Although P&O follows the irradiance line, but the width of the P_{pv} is thick compared to the P_{pv} of the proposed MPPT. This shows that P&O is struggling to focus the MPP line with the same efficiency as that of the proposed MPPT. One of the iteration of P&O is shown in zoomed view on the right side of Fig. 4.24.

On the other hand, Fig. 4.25 and Fig. 4.26 demonstrate the steady response of both techniques under resistive and battery loads respectively. It can be seen that P&O exhibits power loss oscillations around MPP while the proposed technique is stable at MPP in its S-loop. Steady state efficiency of the techniques is calculated with the help
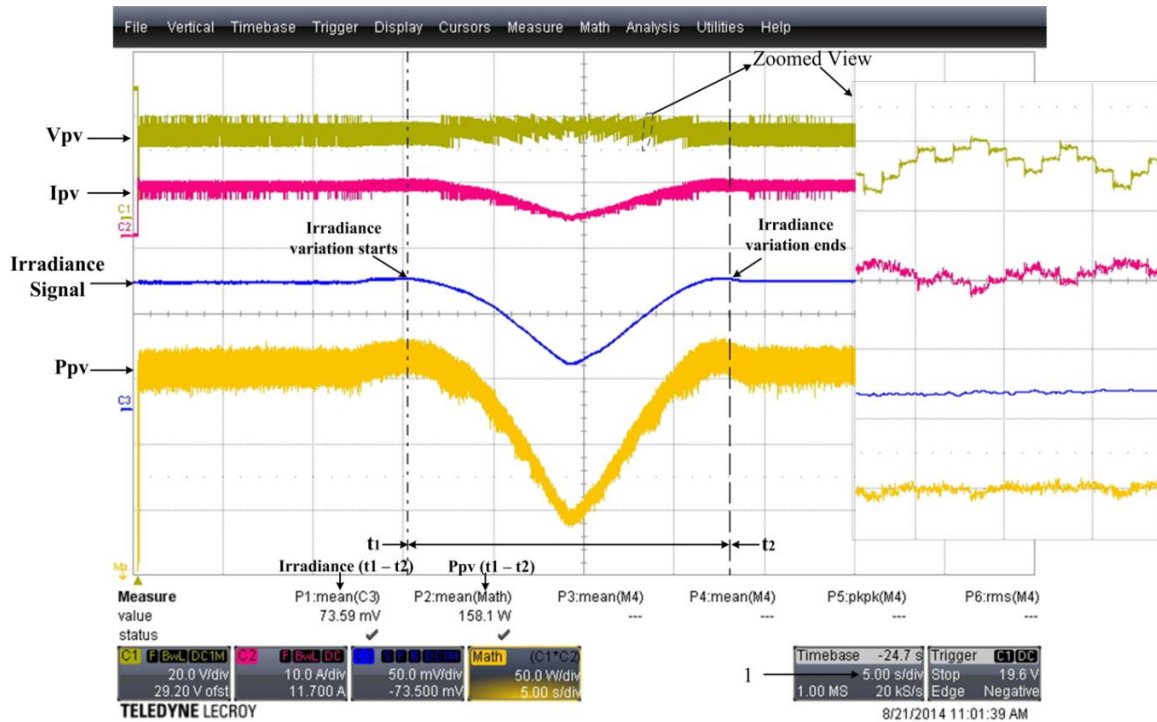

Figure 4.24 – Dynamic response of P&O under varying weather conditions

of Eq. (4.32), and is summarized in Table 4.6. Since the weather conditions are expected to be constant, I-V curve is scanned and P_{Ideal} is attained. While P_{MPPT} is calculated for the duration of 4s as shown in Fig. 4.25 and Fig. 4.26.

Table 4.6 indicates that the proposed technique has a dynamic efficiency of 97.3%, which is almost 6.5% superior than the efficiency of P&O. Thus justifying the time response analysis discussed in the previous section that P&O requires more
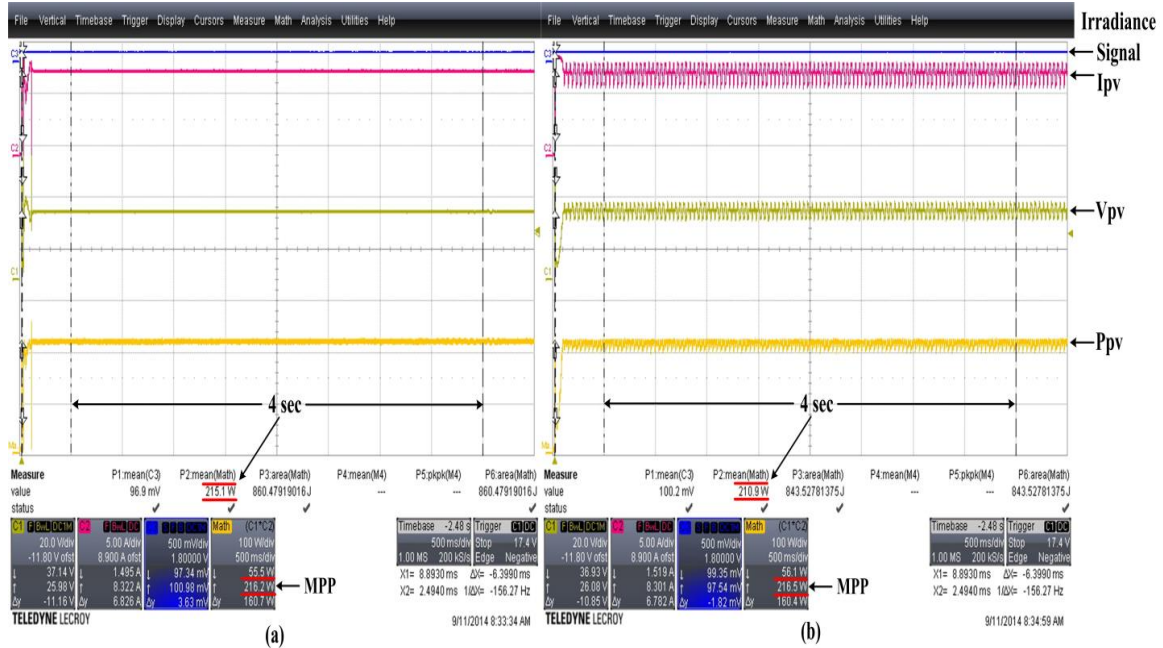

Figure 4.25 – Steady state response of techniques against resistive load
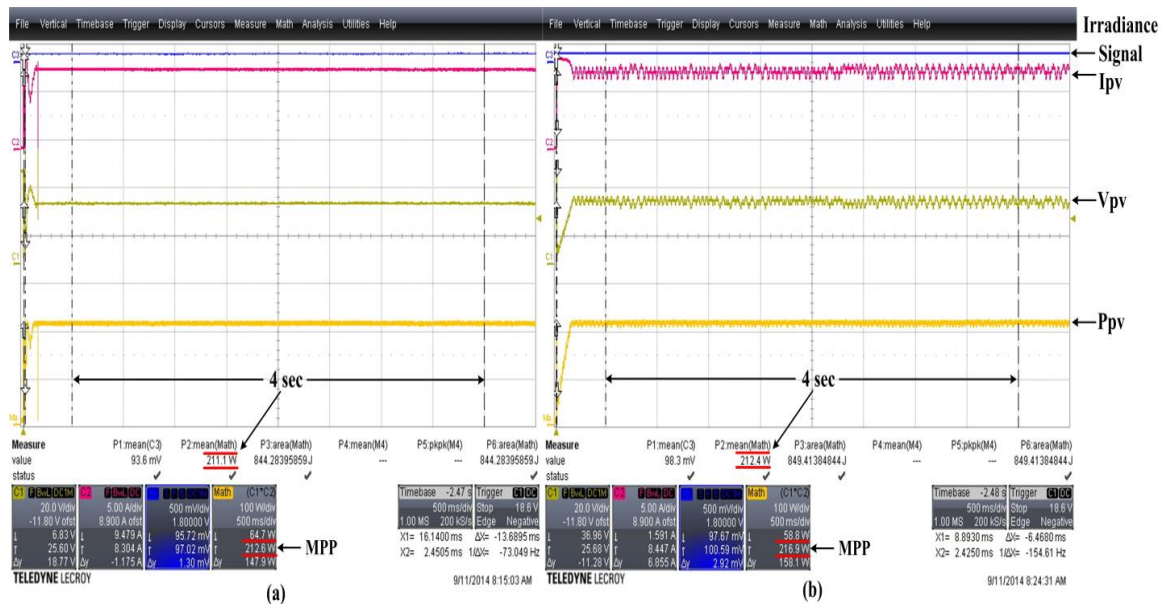

Figure 4.26 – Steady state response of techniques against battery load

samples to reach MPP compared to proposed MPPT. Similarly, the steady state efficiency of the proposed technique is also superior than P&O under both kinds of load as indicated in Table 4.6.

Table 4.6 – Dynamic and steady efficiencies of the techniques

Weather Conditions	Load Type		Efficiency (η_{MPPT})	
	Type	Value	Proposed MPPT	P&O
Dynamic	Resistive	47 Ω	97.3%	90.8%
Steady	Resistive	47 Ω	99.5%	97.4%
Steady	Battery	48 V	99.3%	97.9%